UNIVERSITAT
POLITÈCNICA
DE VALÈNCIA

Role of miR-99a-5p in breast cancer: translating molecular findings into clinical tools

PhD THESIS

Submitted by:

Iris Garrido Cano

PhD supervisors:

Dr. Pilar Eroles Asensio

Prof. Ramón Martínez Máñez

Valencia, October 2021

"Soy de las que piensan que la ciencia tiene una gran belleza. Un científico en su laboratorio no es sólo un técnico: también es un niño colocado ante fenómenos naturales que lo impresionan como un cuento de hadas".

Marie Curie

AGRADECIMIENTOS

Ya desde pequeña soñaba con llegar a ser científica. Recuerdo jugar a mezclar cosas de colores, que era lo que se suponía que se hacía en un laboratorio, y el año en que los Reyes Magos me trajeron un microscopio. Aunque ha pasado mucho tiempo de aquello, hoy sigo teniendo el mismo sueño que entonces y disfrutando de mi trabajo. Tengo claro que he elegido un camino complicado, pero sin duda me compensa. Hoy estoy un paso más cerca de llegar a ser esa científica con la que ya soñaba de pequeña, y eso es algo que no hubiera podido conseguir yo sola. Me siento muy afortunada por rodearme de personas maravillosas que me han apoyado a lo largo de este camino.

En primer lugar, quiero dar las gracias a mis directores, Pilar y Ramón, por haberme dado la oportunidad de trabajar con vosotros. Me abristeis las puertas de vuestros laboratorios y me ofrecisteis la oportunidad de iniciar esta aventura que me ha permitido crecer no solo a nivel profesional sino también a nivel personal. También me gustaría dar las gracias a Juanmi, que aunque llegaste más tarde has sido de gran ayuda. Gracias por confiar en mí y permitir que me siga dedicando a esto que tanto me apasiona.

Y ahora le toca a mi queridísimo Labo 2, que es como una pequeña familia. Anna, ¿quién me iba a decir a mí que acabarías siendo mi equipo unicornio? No empezamos con muy buen pie y sin embargo ahora eres una imprescindible en mi vida. Amiga, ha sido una suerte encontrarte en este camino. Seguiremos sumando muchos momentos. No me cabe duda. My dear Mita, as you say, “thank you from the bottom of my heart”. We have shared this unforgettable adventure full of laughs, cries, good, and bad

moments, and I hope to be together again soon. También quiero agradecer al Doctor Edoard insoportable al que he tenido que aguantar cada día (tu a mí también me has aguantado un pelín pero nada que ver..), a mi Meiri, que está siendo mis manos y también mi cabeza de vez en cuando (espero dejarte un poco más tranquila a partir de ahora pero no prometo nada), a Juanjo, por repartir tranquilidad allá por donde pasa, a Sandra, siempre dispuesta a ayudar con lo que sea, a Ray, el señor del meu poble, y a Bego, que aún nos visitas de vez en cuando porque no puedes vivir sin nosotros. Y por supuesto no me voy a dejar a mi querido Paqui. Eres posiblemente el mayor personaje del planeta pero sé que no importa si tengo el día más horrible del mundo porque siempre vas a estar ahí para sacarme una sonrisa y recordarme lo sexy que eres. Tampoco me puedo olvidar de Guadalupe, siempre dispuesta a escucharme y ayudarme tanto en mis problemas científicos como en la vida. Si alguien merece el premio a la persona con más paciencia del mundo, esa eres tú. Eres mi psicóloga favorita.

Y por otro lado, aunque no he pasado mucho tiempo allí, también me llevo a algunos del 2.6: Ame, gracias por haber sido mi mamá pato, Xente, siempre dispuesto a ayudarme con mis ocurrencias, y Luis, Irene, Bea, Juanfran y Alba, que sois todos unos personajillos con los que espero compartir muchos más momentos. Especialmente te doy las gracias a ti, Alba. Por casualidades acabaste siendo un apoyo fundamental en mi vida. Gracias.

Não posso esquecer a minha estadia no Porto. Professora Carmen, muita obrigada por me dar a oportunidade de viver esta experiência maravilhosa. Muita obrigada aos meus raparigos. Especialmente à Teixas.

Desde o primeiro dia foi uma família para mim. Não és a melhor professora de português mas eu sou uma tuga sem dúvida.

Y además de estas personas que han llegado a mi vida durante esta etapa, también tengo la suerte de tener a los de siempre.

Loli, Inma e Irene, mis bioquímicas favoritas. Es cierto que no lleváis conmigo toda la vida pero es como si siempre hubierais estado. Por vosotras sería capaz de volver Gran Canaria. Espero teneros siempre en mi vida. Os quiero.

A mis chicas, que, aunque he prometido mencionaros en mi discurso del Nobel, os voy a mencionar aquí por si me quedo por el camino. Gracias por estar siempre y para todo. Estela, gracias por amenizarme los días con tus audios de Whatsapp que parecen programas de radio (me dan la vida); Laura, mi matrona favorita, gracias por ser así de especial y por entenderme siempre; Soraya, gracias por ser capaz de sacarme una sonrisa hasta en el peor momento; Amanda, gracias porque, aunque seas una chunga sé que siempre cuento contigo; Sandra, gracias por estar ahí desde que tengo uso de razón. Da igual si hablamos todos los días o si pasa un mes sin tener noticias vuestras. Con vosotras todo está siempre igual. Os quiero.

Y por último y más importante, a mi familia. Gracias a todos y cada uno de vosotros. Aquellos que estáis conmigo y a los que por desgracia ya no están, que me recuerdan lo importante que es disfrutar de cada día de vida.

No puedo no mencionar a Sara, mi primahermanaamiga. No importa si estás a 1 cm, en Australia, o en Qatar, pero siempre estás. Igual de dispuesta a sacar papada en un momento dado, que a diseñarme la portada de una tesis con tu CJVDTLS. Te quiero.

Y para el final me dejo a mis imprescindibles.

Mario, mi compañero de vida. Si alguien ha aguantado la parte negativa de esta tesis, ese has sido tú. Llegar hasta aquí no ha sido fácil. Hemos celebrado resultados y publicaciones, pero también has aguantado esos muchos experimentos que han salido mal, los días en que me he desmotivado pensando que nada tenía sentido, y aquellos en los que me he estresado pensando que no llego a todo. Y ahí estás, siempre confiando en mí más que yo misma, y recordándome que si no salen las cosas no se va a acabar el mundo. Gracias. Me siento muy orgullosa del hogar que hemos construido juntos. Te quiero.

Y Mamá, Papá e Irene, gracias. Gracias por apoyarme siempre sea cual sea mi decisión y por darme las mejores herramientas para afrontar la vida. Si he llegado hasta aquí es sin duda gracias a vosotros. La familia es algo que no se elige y no he podido ser más afortunada con vosotros. Os quiero.

ABSTRACT

This PhD thesis, entitled "Role of miR-99a-5p in breast cancer: translating molecular findings into clinical tools" is focused on the study of the microRNA miR-99a-5p in breast cancer and in determining its potential as a therapeutic target and biomarker for the diagnosis of this disease.

In the first chapter, corresponding to the introduction, a general review of breast cancer is carried out. MicroRNAs are also introduced, as well as their involvement in cancer and their possible application as therapeutic targets and biomarkers. In the second chapter, the general objectives, as well as the specific objectives of each chapter are detailed.

In the third chapter, the microRNA expression profile of a doxorubicin-resistant breast cancer cell line was compared with its parental cell line, leading to the identification of the microRNA miR-99a-5p as the most deregulated between the two of them. Subsequently, by cell proliferation assays, flow cytometry, and western blot, it was confirmed that miR-99a-5p increases drug sensitivity. Through the luciferase reporter gene assay, it was proved that miR-99a-5p directly targets COX-2, which leads to the inhibition of the expression of the ABCG2 protein, widely described to be involved in drug resistance. The inhibition of ABCG2 leads to an increase in intracellular doxorubicin, thus increasing the sensitivity to the drug. This hypothesis was confirmed by PCR, western blot, and flow cytometry. Based on the obtained results, nanodevices based on mesoporous silica nanoparticles were designed for the combined release of miR-99a-5p and doxorubicin in tumors. The ability of the systems to specifically target the CD44 receptor, which is overexpressed in breast cancer tumors, as well as to release the cargo

specifically after internalization, were tested *in vitro*. Furthermore, the efficacy of the nanoparticles to reduce tumor growth and the adverse effects associated with free doxorubicin was confirmed in a murine orthotopic model of breast cancer.

In the fourth chapter, the potential of miR-99a-5p as a biomarker for the diagnosis of breast cancer was evaluated. First, microRNA expression was determined in primary breast cancer tumors and compared with healthy tissues. The results showed that miR-99a-5p is downregulated in breast cancer tissues. Next, to determine the potential of the microRNA as a minimally invasive biomarker, the expression levels of miR-99a-5p in plasma of breast cancer patients and healthy donors were determined. In this case, it was found that miR-99a-5p is at higher concentrations in the plasma of breast cancer patients. These results were validated in an independent cohort. Through the ROC curve analysis, it was confirmed that miR-99a-5p is useful as a non-invasive biomarker for the diagnosis of breast cancer even at early stages.

Based on the findings above, the fifth chapter focus on the design and validation of a biosensor based on nanoporous alumina supports for the detection of miR-99a-5p in plasma. The pores of the alumina plate were loaded with the fluorescent indicator rhodamine B, and oligonucleotides with a sequence complementary to the miR-99a-5p were used as molecular gates able to maintain fluorophores inside the pores. In the presence of miR-99a-5p, the capping oligonucleotide is displaced, leading to the opening of the pores and the release of rhodamine B, which is subsequently optically detected. The specificity and high sensitivity of the biosensor were confirmed. Furthermore, the efficiency of the device to detect breast cancer

even at early stages was confirmed using plasma samples from breast cancer patients and healthy controls.

Finally, chapters five and six present the general discussion and conclusions. In conclusion, this PhD thesis demonstrates that miR-99a-5p is a molecule with potential as a therapeutic target and biomarker for breast cancer, and it could be useful to improve the prognosis of patients. It has been elucidated that one of the mechanisms by which miR-99a-5p is involved in doxorubicin sensitivity is through the regulation of the COX-2/ABCG2 axis. Furthermore, nanoparticles designed for the combined administration of miR-99a-5p and doxorubicin are presented as a tool with great potential for cancer treatment and could be useful for the administration of microRNAs as therapy. Finally, taking advantage of the potential of miR-99a-5p as a diagnostic biomarker, a detection system has been developed and could be a useful tool to improve early detection of breast cancer.

RESUMEN

La presente tesis doctoral, titulada “papel del miR-99a-5p en cáncer de mama: transformando hallazgos moleculares en herramientas clínicas” está centrada en el estudio del microRNA miR-99a-5p en cáncer de mama y en la determinación de su potencial como diana terapéutica y biomarcador para el diagnóstico de dicha enfermedad.

En el primer capítulo, correspondiente a la introducción, se lleva a cabo una revisión general del cáncer de mama. También se presentan los microRNAs, así como su implicación en cáncer y su posible aplicación como dianas terapéuticas y como biomarcadores. A continuación, en el segundo capítulo se presentan los objetivos generales, así como los objetivos específicos de cada capítulo.

En el tercer capítulo se compararon los perfiles de expresión de microRNAs de una línea celular de cáncer de mama resistente a doxorrubicina frente a la línea celular parental, dando lugar a la identificación del microRNA miR-99a-5p como el más desregulado entre ambas. A continuación, mediante ensayos de proliferación celular, citometría de flujo y *western blot, se* confirmó que el miR-99a-5p aumenta la sensibilidad al fármaco. Mediante el ensayo del gen reportero de la luciferasa se confirmó que el miR-99a-5p inhibe la expresión de COX-2 de forma directa, lo que conlleva la inhibición de la expresión de la proteína ABCG2 que está ampliamente descrita por su papel en resistencia a fármacos. La inhibición de ésta última da lugar a un incremento de doxorrubicina intracelular, y por tanto al aumento de la sensibilidad al fármaco. Todo ello fue confirmado mediante PCR, *western blot*, y citometría de flujo. En base a los resultados

obtenidos, se diseñaron nanodispositivos basados en nanopartículas mesoporosas de sílice para la liberación de una combinación de miR-99a-5p y doxorrubicina en los tumores. La capacidad de los sistemas para dirigirse específicamente al receptor CD44, que está sobreexpresado en tumores de cáncer de mama, así como para la liberación su contenido de forma específica tras la internalización, fueron testadas *in vitro*. Además, se confirmó la eficacia de las nanopartículas para reducir el crecimiento tumoral así como los efectos adversos asociados a la doxorrubicina libre en un modelo ortotópico murino de cáncer de mama.

En el cuarto capítulo, se evaluó el potencial del miR-99a-5p como biomarcador para el diagnóstico del cáncer de mama. En primer lugar, se determinó la expresión del microRNA en tumores primarios de cáncer de mama y se compararon con tejidos sanos. Los resultados mostraron que el miR-99a-5p se encuentra infraexpresado en los tejidos cancerosos. A continuación, con el objeto de determinar el potencial del microRNA como biomarcador mínimamente invasivo, se determinaron los niveles de expresión de miR-99a-5p en plasma de pacientes de cáncer de mama y de donantes sanos. En este caso, se encontró que el miR-99a-5p se encuentra a mayor concentración en el plasma de pacientes con cáncer de mama. Estos resultados se validaron en una cohorte independiente. Mediante el análisis en base a curvas ROC se confirmó que el miR-99a-5p es útil como biomarcador no invasivo para el diagnóstico del cáncer de mama incluso en estadíos tempranos de la enfermedad.

En base a los resultados obtenidos, en el quinto capítulo se centra el diseño y validación de un biosensor basado en soportes de alúmina mesoporosa para la detección del miR-99a-5p en plasma. Los poros de una

placa de alúmina mesoporosa se cargaron con el indicador fluorescente rodamina B, y se utilizaron oligonucleótidos complementarios a la secuencia del miR-99a-5p como puertas moleculares capaces de retener los fluoróforos en el interior de los poros. En presencia del miR-99a-5p, el oligonucleótido que actúa como puerta reconoce dicha secuencia y es desplazado, dando lugar a la apertura de los poros de modo que se libera la rodamina B, que es posteriormente detectada ópticamente. Se confirmó la especificidad del biosensor, así como su alta sensibilidad. Además, utilizando muestras de plasma de pacientes de cáncer de mama y controles sanos, se confirmó la eficiencia del dispositivo para detectar cáncer de mama incluso en estadíos tempranos.

Por último, en los capítulos cinco y seis se presentan la discusión general y las conclusiones principales extraídas. En conclusión, esta tesis doctoral demuestra que el miR-99a-5p es una molécula con potencial como diana terapéutica y biomarcador para el cáncer de mama, y podría ser útil para mejorar el pronóstico de los pacientes con dicha enfermedad. Se ha elucidado que uno de los mecanismos por los que el miR-99a-5p está involucrado en sensibilidad a doxorrubicina es mediante la regulación del eje COX-2/ABCG2. Además, las nanopartículas diseñadas para la administración combinada de miR-99a-5p y doxorrubicina se presenta como una herramienta con gran potencial para el tratamiento oncológico, y podría ser útil para la administración de microRNAs como terapia. Por último, aprovechando el potencial del miR-99a-5p como biomarcador diagnóstico, se ha desarrollado un sistema de detección que podría ser una herramienta útil para mejorar la detección temprana del cáncer de mama.

RESUM

La present tesis doctoral, titulada “paper del miR-99a-5p en càncer de mama: transformant descobriments moleculars en eines clíniques” està centrada en l'estudi del microRNA miR-99a-5p en càncer de mama i en la determinació del seu potencial com a diana terapèutica i biomarcador per al diagnòstic d’aquesta malaltia.

En el primer capítol, corresponent a la introducció, es du a terme una revisió general del càncer de mama. També es presenten els microRNAs, així com la seua implicació en càncer i la seua possible aplicació com a dianes terapèutiques i com a biomarcadors. A continuació, en el segon capítol es presenten els objectius generals, així com els objectius específics de cada capítol.

En el tercer capítol es van comparar els perfils d'expressió de microRNAs d'una línia cel·lular de càncer de mama resistent a doxorrubicina amb la seua línia parental, donant lloc a la identificació del microRNA miR-99a-5p com el més desregulat entre ambdues. A continuació, per mitjà d'assajos de proliferació cel·lular, citometría de flux i western blot, es va confirmar que el miR-99a-5p augmenta la sensibilitat al fàrmac. Per mitjà de l'assaig del gen reporter de la luciferasa es va confirmar que el miR-99a-5p inhibeix l'expressió de COX-2 de forma directa, la qual cosa comporta la inhibició de l'expressió de la proteïna ABCG2 que està àmpliament descrita pel seu paper en resistència a fàrmacs. La inhibició de ABCG2 incrementa la doxorrubicina a l'interior de les cèl·lules, i per tant dona lloc a l'augment de la sensibilitat al fàrmac. Tot això va ser confirmat per mitjà de PCR, western blot¸y citometría de flux. Basant-se en els resultats obtinguts, es van

dissenyar nanodispositius basats en nanopartícules mesoporoses de sílice per a l'alliberament d'una combinació de miR-99a-5p i doxorrubicina en els tumors. La capacitat dels sistemes per a dirigir-se específicament al receptor CD44, que està sobreexpressat en tumors de càncer de mama, així com per a l'alliberament el seu contingut de forma específica després de la internalització, van ser testades *in vitro*. A més, es va confirmar la seua eficàcia per a reduir el creixement tumoral així com els efectes adversos associats a la doxorrubicina lliure en un model ortotòpic murí de càncer de mama.

En el quart capítol, es va avaluar el potencial del miR-99a-5p com a biomarcador per al diagnòstic del càncer de mama. En primer lloc, es va determinar l'expressió del microRNA en tumors primaris de càncer de mama i es van comparar amb teixits sans. Els resultats van mostrar que el miR-99a-5p es troba infraexpressat en els teixits cancerosos. A continuació, amb l'objectiu de determinar el potencial del microRNA com a biomarcador mínimament invasiu, es van determinar els nivells d'expressió de miR-99a-5p en plasma de pacients de càncer de mama i de donants sans. En aquest cas, es va veure que el miR-99a-5p es troba a major concentració en el plasma de pacients amb càncer de mama. Aquestos resultats es van validar en una cohort independent. Per mitjà de l'anàlisi basant-se en corbes ROC es va confirmar que el miR-99a-5p és útil com a biomarcador no invasiu per al diagnòstic del càncer de mama inclús en estadis primerencs de la malaltia.

Basant-se en els resultats obtinguts, el centra en el disseny i validació d'un biosensor basat en suports d'alúmina nanoporosa per la detecció del miR-99a-5p en plasma. Els porus d'una placa d'alúmina es van carregar amb l'indicador fluorescent rodamina B, i es van utilitzar oligonucleòtids

complementaris a la seqüència del miR-99a-5p com a portes moleculars amb la capacitat de retindre els fluoròfors a l'interior dels porus. En presència del miR-99a-5p, l'oligonucleòtid que actua com a porta reconeix dita seqüència i és desplaçat, donant lloc a l'obertura dels porus de manera que s'allibera la rodamina B, que serà posteriorment detectada òpticament. Es va confirmar l'especificitat del biosensor, així com la seua alta sensibilitat. A més, utilitzant mostres de plasma de pacients de càncer de mama i controls sans, es va confirmar l'eficiència del dispositiu per a detectar càncer de mama inclús en estadis primerencs.

Finalment, en els capítols sis i set es presenten la discussió general i les conclusions principals. En conclusió, aquesta tesi doctoral demostra que el miR-99a-5p és una molècula amb potencial com a diana terapèutica i biomarcador per al càncer de mama, i podria ser útil per a millorar el pronòstic dels pacients amb dita malaltia. S'ha elucidat que un dels mecanismes pels quals el miR-99a-5p està involucrat en sensibilitat a doxorrubicina és per mitjà de la regulació de l'eix COX-2/ABCG2. A més, les nanopartícules dissenyades per a l'administració combinada de miR-99a-5p i doxorrubicina es presenta com una ferramenta amb gran potencial per al tractament oncològic, i podria ser útil per a l'administració de microRNAs com a teràpia. Finalment, aprofitant el potencial del miR-99a-5p com a biomarcador diagnòstic, s'ha desenvolupat un sistema de detecció que podria ser una ferramenta útil per a millorar la detecció primerenca del càncer de mama.

PUBLICATIONS

Results obtained from this PhD Thesis and other contributions have resulted in the following scientific publications:

- Garrido-Cano, I.; Candela-Noguera, V.; Herrera, G.; Cejalvo, J.M.; Lluch, A.; Marcos, M.D.; Sancenon, F.; Eroles, P.; Martínez-Máñez, R. Biocompatibility and Internalization Assessment of Bare and Functionalised Mesoporous Silica Nanoparticles. *Microporous Mesoporous Mater.* 2021;310:110593.

- Garrido-Cano, I.; Constâncio, V.; Adam-Artigues, A.; Lameirinhas, A.; Simón, S.; Ortega, B.; Martínez, M.T.; Hernando, C.; Bermejo, B.; Lluch, A.; et al. Circulating MiR-99a-5p Expression in Plasma: A Potential Biomarker for Early Diagnosis of Breast Cancer. *Int. J. Mol. Sci.* 2020;21(19):7427.

- Garrido-Cano, I.; Pla, L.; Santiago-Felipe, S.; Simón, S.; Ortega, B.; Bermejo, B.; Lluch, A.; Cejalvo, J.M.; Eroles, P.; Martínez-Máñez, R. Nanoporous Anodic Alumina-Based Sensor for MiR-99a-5p Detection as an Effective Early Breast Cancer Diagnostic Tool. *ACS Sensors.* 2021;6(3):1022–1029.

- Garrido-Cano, I.; Pattanayak, B.; Adam-Artigues, A.; Lameirinhas, A.; Torres-Ruiz, S.; Tormo, E.; Cervera, R.; Eroles, P. MicroRNAs as a Clue to Overcome Breast Cancer Treatment Resistance. *Cancer Metastasis Rev.* 2021**;**

- Adam-Artigues, A.; Garrido-Cano, I.; Simón, S.; Ortega, B.; Moragón, S.; Lameirinhas, A.; Constâncio, V.; Salta, S.; Burgués, O.; Bermejo, B.; et al. Circulating MiR-30b-5p Levels in Plasma as a Novel Potential Biomarker for Early Detection of Breast Cancer. *ESMO Open.* 2021;6(1):100039.

- Adam-Artigues, A.; Garrido-Cano, I.; Carbonell-Asins, J.A.; Lameirinhas, A.; Simón, S.; Ortega-Morillo, B.; Martínez, M.T.; Hernando, C.; Constâncio, V.; Burgues, O.; et al. Identification of a Two-Microrna Signature in Plasma as a Novel Biomarker for Very Early Diagnosis of Breast Cancer. *Cancers (Basel).* 2021;13(11):2848.

- Hernando, C.; Ortega-Morillo, B.; Tapia, M.; Moragón, S.; Martínez, M.T.; Eroles, P.; Garrido-Cano, I.; Adam-Artigues, A.; Lluch, A.; Bermejo, B.; et al. Oral Selective Estrogen Receptor Degraders (SERDs) as a Novel Breast Cancer Therapy: Present and Future from a Clinical Perspective. *Int. J. Mol. Sci.* 2021;22(15):7812.

- Pattanayak, B.; Garrido-Cano, I.; Adam-Artigues, A.; Tormo, E.; Pineda, B.; Cabello, P.; Alonso, E.; Bermejo, B.; Hernando, C.; Martínez, M.T.; et al. MicroRNA-33b Suppresses Epithelial–Mesenchymal Transition Repressing the MYC–EZH2 Pathway in HER2+ Breast Carcinoma. *Front. Oncol.* 2020;10:1661.

ABBREVIATIONS AND ACRONYMS

ABC	ATP-binding cassette
ABCG2	ATP Binding Cassette Subfamily G Member 2
ACN	Acetonitrile
AGO2	Argonaute 2
ALT	Alanine transaminase
APTES	3-aminopropyl)triethoxysilane
ASR	Age-standardized rates
AST	Aspartate aminotransferase
ATCC	American Type Culture Collection
ATR	Attenuated total reflectance
ATR	Attenuated total reflectance
AUC	Area Under the Curve
BC	Breast cancer
BCRP	Breast cancer resistance protein
BCSCs	Breast cancer stem cells
BET	Brunauer−Emmett−Teller
BJH	Barrett−Joyner−Halenda
BUN	Blood urea nitrogen
cDNA	Coding DNA
CDS	Coding sequence
COX-2	Cyclooxygenase-2
CRE	Creatinine
CTAB	Cetyltrimethylammonium bromide
DFS	Disease-free survival

DLS	Dynamic light scattering
DNA	Deoxyribonucleic acid
DPBS	Dulbecco's Phosphate Buffered
DRFS	Distant-relapse free survival
EDX	Energy-dispersive X-ray spectroscopy
EMT	Epithelial-to-mesenchymal transition
EPR	Enhanced permeability and retention
ER	Estrogen Receptor
EDTA	Ethylenediaminetetraacetic acid
FBS	Fetal bovine serum
FESEM	Field emission scanning electron microscopy
FTIR	Fourier-transform infrared
GEO	Gene Expression Omnibus
H&E	Hematoxylin & eosin
HA	Hyaluronic acid
HDL	High-density lipoprotein (HDL)
HER2	Human epidermal growth factor receptor 2
HR	Hormone receptors
ICP-MS	Inductively coupled plasma mass spectroscopy
IDC	Invasive ductal carcinoma
ILC	Invasive lobular carcinoma
LOD	Limit of detection
MFI	Mean fluorescence intensity
MHC-β	Myosin heavy chain β
miRISC	miRNA-induced silencing complex
miRNAs	microRNAs

mRNAs	Messenger RNAs
MSNs	Mesoporous silica nanoparticles
MVB	Multivesicular bodies.
NAA	Nanoporous anodic alumina
NC	Negative control
NCBI	National Center for Biotechnology Information
NPM-1	Nucleophosmin-1
OS	Overall survival
PEI	Polyethyleneimine
PR	Progesterone receptor
pre-miRNA	Precursor miRNA
pri-miRNA	Primary miRNA transcripts
PTFE	Polytetrafluoroethylene
PXRD	Powder X-ray diffraction
qRT-PCR	Quantitative real-time PCR
RES	Reticuloendothelial system
RISC	RNA-induced silencing complex
RNA	Ribonucleic acid
ROC	Receiver-operating characteristic
saRNAs	Small activating RNAs
SD	Standard deviation
SEM	Standard error of the mean
siCOX	COX-2 silencer
siRNAs	Short interfering RNAs
TCGA	The Cancer Genome Atlas
TEM	Transmission electron microscopy

TEOS	Tetraethylorthosilicate
TGA	Thermogravimetric analysis
TLRs	Toll-like receptors
TMAH	Tetramethylammonium hydroxide solution
TNBC	Triple-negative breast cancer
TRIS	Tris(hydroxymethyl)aminomethane
UTR	Untranslated regions
γH2AX	Phosphorylated H2AX at Ser-139 residue

TABLE OF CONTENTS

CHAPTER 1 | General introduction 7
1.1 Breast cancer 9
1.1.1 Epidemiology 9
1.1.2 Risk factors 13
1.1.3 Breast cancer screening 14
1.1.4 Breast cancer classification 15
1.1.5 Treatment 18
1.2 MicroRNAs 21
1.2.1 Biogenesis 21
1.2.2 Target regulation 24
1.2.3 miRNAs in cancer 25
1.2.3.1 Transcriptional control of miRNAs 27
1.2.3.2 Genetic alterations of miRNA genes 29
1.2.3.3 Alterations in miRNAs biogenesis machinery 30
1.2.4 miRNA-based therapies 31
1.2.4.1 Viral vectors for miRNAs delivery 33
1.2.4.2 Nanoparticles for miRNAs delivery 33
1.2.5 miRNAs as biomarkers 37
CHAPTER 2 | Objectives 43
CHAPTER 3 | miR-99a-as therapeutic target 47
3.1 Abstract 51
3.2 Introduction 52
3.3 Materials and methods 53
3.3.1 Cell culture 53
3.3.2 miRNA and mRNA arrays, and data analysis 54
3.3.3 RNA extraction, reverse transcription, and quantitative real-time PCR 54
3.3.4 Patient's data acquisition and analysis 55
3.3.5 Cell transfection 55
3.3.6 Apoptosis analysis 56
3.3.7 IC_{50} determination 56

3.3.8 miRNA-target prediction 56
3.3.9 Western blot 57
3.3.10 Luciferase reporter assay 57
3.3.11 Doxorubicin intracellular accumulation analysis 57
3.3.12 ABCG2 activity analysis 58
3.3.13 Synthesis of mesoporous silica nanoparticles 58
3.3.14 Characterization of nanoparticles 59
3.3.15 Cargo release studies 60
3.3.16 CD44 expression evaluation by flow cytometry 60
3.3.17 Nanoparticles' uptake and competition assay 61
3.3.18 *In vivo* experiments 61
3.3.19 Silicon biodistribution analysis 62
3.3.20 Immunohistochemistry 62
3.3.21 Statistical analyses 62
3.4 Results 63
3.4.1 miR-99a-5p is downregulated in doxorubicin-resistant breast cancer cells 63
3.4.2 miR-99a-5p overexpression associates with better clinical prognosis in breast cancer patients 64
3.4.3 miR-99a-5p regulates doxorubicin response *in vitro* 67
3.4.4 miR-99a-5p regulates doxorubicin sensitivity by directly targeting COX-2 69
3.4.5 ABCG2 is a downstream target of miR-99a-5p and COX-2 73
3.4.6 Nanoparticles targeting breast tumors for co-delivery of doxorubicin and miR-99a-5p 76
3.4.7 Anti-tumor activity of co-delivered doxorubicin and miR-99a-5p by NP-dox-miR99a in *in vivo* model 80
3.4.8 Nanoformulation protects from doxorubicin-induced cardiotoxicity 82
3.5 Discussion 84
3.6 Conclusion 88
3.7 Bibliography 90
3.8 Supporting information 95
CHAPTER 4 | miR-99a-5p as biomarker 107
4.1 Abstract 111

4.2 Introduction 112
4.3 Materials and methods 114
4.3.1 Clinical samples 114
4.3.2 RNA Extraction from tissue and plasma 115
4.3.3 cDNA synthesis 115
4.3.4 miRNA expression analysis 116
4.3.5 TCGA database validation 116
4.3.6 Statistical analysis 117
4.4 Results 117
4.4.1. Study design to develop a novel miRNA biomarker 117
4.4.2. miR-99a-5p expression in tissue 118
4.4.2.1 Cohort #1: Discovery cohort 118
4.4.3 miR-99a-5p expression in plasma 121
4.4.3.1 Cohort #2: Testing cohort 121
4.4.3.2 Cohort #3: Validation cohort 124
4.3.4. miR-99a-5p as a biomarker for early BC detection 125
4.5 Discussion 127
4.6 Conclusions 131
4.7 Bibliography 132
CHAPTER 5 | Biosensor for detection of circulating miR-99a-5p 139
5.1 Abstract 143
5.2 Introduction 144
5.3 Materials and methods 146
5.3.1 General techniques 146
5.3.2 Chemicals 146
5.3.3 Synthesis of solids 147
5.3.4 Cargo quantification 147
5.3.5 Detection protocol 148
5.3.6 Amplification assay 148
5.3.7 Selectivity assessment 148
5.3.8 Determination of sensitivity of miR-99a-5p in real competitive media 149
5.3.9 Validation in clinical samples 149
5.3.10 Ethical committee 150
5.3.11 Statistical analysis 150

5.4 Results and discussion..... 150
5.4.1 Design, synthesis, and characterization of the functional nanodevice 150
5.4.2 Controlled delivery studies 153
5.4.3 Validation in clinical samples 156
5.5 Conclusions 160
5.6 Bibliography 162
CHAPTER 6 | General discussion..... 167
CHAPTER 7 | Conclusions..... 173

CHAPTER 1 |

General introduction

1.1 Breast cancer

1.1.1 Epidemiology

Breast cancer (BC) is the most commonly diagnosed type of cancer and the fifth cause of cancer-related death worldwide. In 2020, 2,261,419 patients were diagnosed with BC, and 684,996 died as a consequence. Female BC accounts for 11.7% of diagnosed cancers in the total population, being the most commonly diagnosed cancer. In women, BC represents approximately one in four diagnosed cancers (24.5%) (**Figure 1**) [1]. Conversely, in men, BC is considered a rare disease that accounts for less than 1% of all diagnosed BC cases [2].

[1]Sung, H.; Ferlay, J.; Siegel, R.L.; Laversanne, M.; Soerjomataram, I.; Jemal, A.; Bray, F. Global Cancer Statistics 2020: GLOBOCAN Estimates of Incidence and Mortality Worldwide for 36 Cancers in 185 Countries. *CA.* Cancer *J. Clin.* 2021;71(3):209–249.

[2]Korde, L.A.; Zujewski, J.A.; Kamin, L.; Giordano, S.; Domchek, S.; Anderson, W.F.; Bartlett, J.M.S.; Gelmon, K.; Nahleh, Z.; Bergh, J.; et al. Multidisciplinary Meeting on Male Breast Cancer: Summary and Research Recommendations. *J Clin Oncol.* 2010;28:2114–2122.

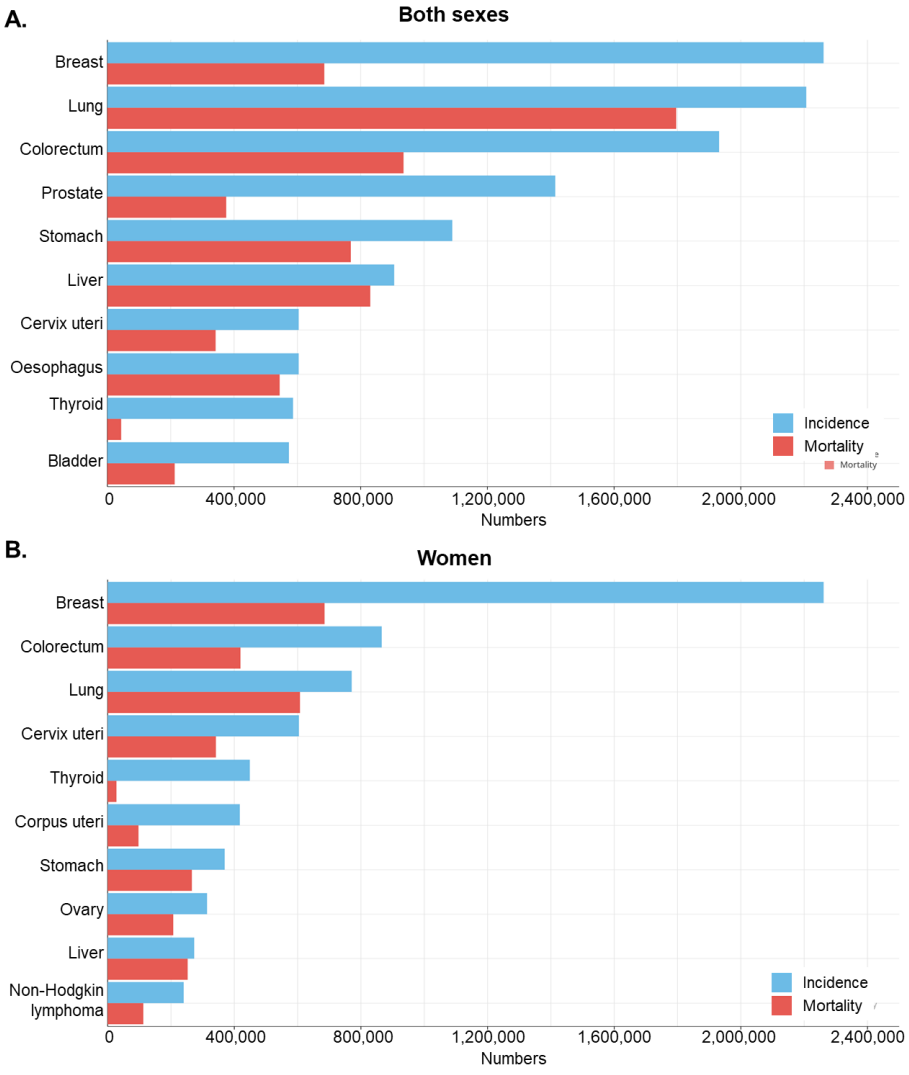

Figure 1. Estimated number of incident cases and deaths for the top 10 most common cancers among both sexes (A), and women (B) in 2020, worldwide. Source: Globocan 2020.

BC incidence rates are higher in transitioned (55.9 per 100,000) than in transitioning countries (29.7 per 100,000) (**Figure 2A**). These differences are attributed to multiple factors such as lifestyle or hormonal factors, although increased detection through mammographic screening in transitioned countries also contributes to these discrepancies [1]. Besides, according to GLOBOCAN prediction tool, the incidence of BC will increase by 41% in 2040, which is attributed to screening programs as well as to changes in lifestyle [3,4].

Regarding mortality, BC caused 685,000 deaths in 2020, being the fifth cause of cancer-related death for the whole population (6.9%), and the first cause for women (15.5%) (**Figure 1**). Contrary to incidence, mortality rates are lower in transitioned countries (12.8 per 100,000) than in transitioning countries (15.0 per 100,000), as a consequence of lack of screening programs, diagnosis at late stages, and poor access to treatments (**Figure 2B**) [1,3]. In this context, it is important to highlight the importance of diagnosis at early stages to improve the outcome of BC patients, which is evidenced by the 98% 5-year overall survival (OS) of patients diagnosed at stage I, and

[3]Heer, E.; Harper, A.; Escandor, N.; Sung, H.; McCormack, V.; Fidler-Benaoudia, M.M. Global Burden and Trends in Premenopausal and Postmenopausal Breast Cancer: A Population-Based Study. Lancet Glob. Heal. 2020;8(8):e1027–e1037.

[4]Ferlay, J.; Laversanne, M.; Ervik, M.; Lam, F.; Colombet, M.; Mery, L.; Piñeros, M.; Znaor, A.; Soerjomataram, I.; Bray, F. Global Cancer Observatory: Cancer Tomorrow Available online: https://gco.iarc.fr/tomorrow (accessed on 1 August 2021)

decreases to 92% for stage II, 75% for stage III, and 27% for stage IV (metastatic disease) [5,6].

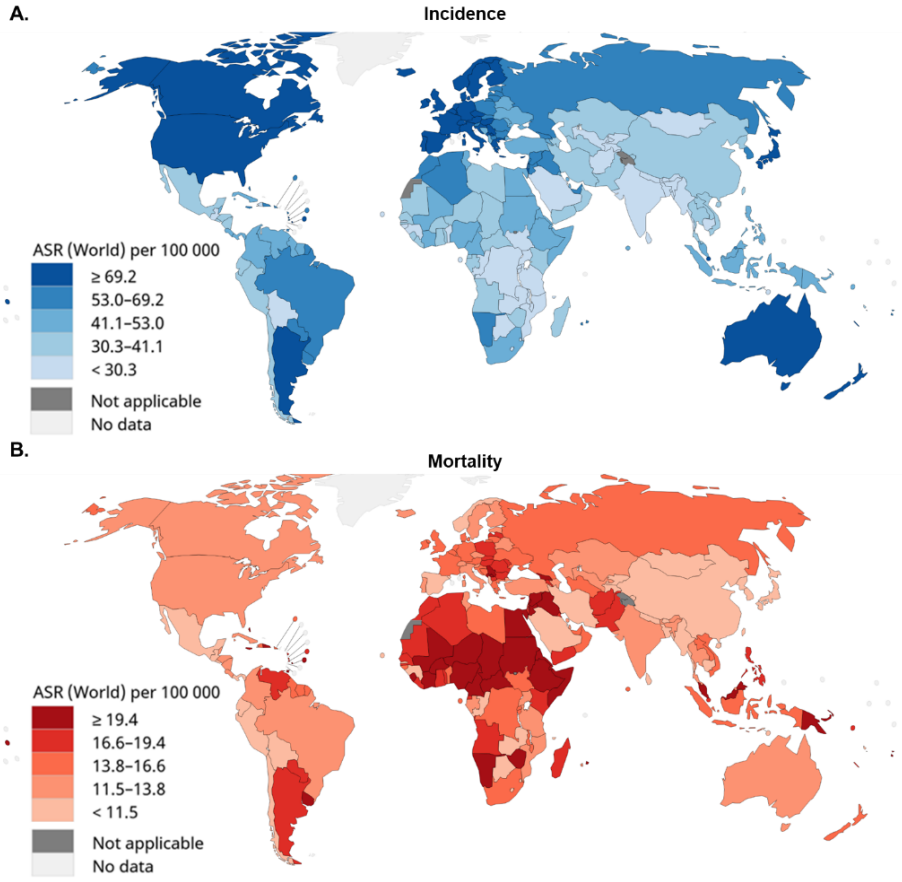

Figure 2. Female breast cancer (A) incidence and (B) mortality age-standardized rates (ASR) by country in 2020. Source: Globocan 2020.

[5] Miller, K.D.; Nogueira, L.; Mariotto, A.B.; Rowland, J.H.; Yabroff, K.R.; Alfano, C.M.; Jemal, A.; Kramer, J.L.; Siegel, R.L. Cancer Treatment and Survivorship Statistics, 2019. *CA. Cancer J. Clin.* 2019;69(5):363–385.

[6] DeSantis, C.E.; Ma, J.; Gaudet, M.M.; Newman, L.A.; Miller, K.D.; Goding Sauer, A.; Jemal, A.; Siegel, R.L. Breast Cancer Statistics, 2019. *CA. Cancer J. Clin.* 2019;69(6):438–451.

1.1.2 Risk factors

Only around 10% of BC cases are attributed to genetic factors such as mutations in *BRCA1* or *BRCA2* [7]. Mutations in these genes involved in DNA repair increase the risk of BC and also other types of cancer such as ovarian or pancreatic cancer [8]. Regarding BC, around 5-10% of cases are associated with *BRCA1/2* mutations, which increase BC risk to 45-65% by age of 70 [9].

The vast majority of BC cases are attributed to lifestyle-associated risk factors such as obesity, smoking, and alcohol consumption. Reproductive patterns such as nulliparity or older age at first pregnancy are also risk factors. Besides, early menarche, late menopause, and hormone replacement therapy after menopause increase the lifetime exposure to hormones, thereby increasing the risk of BC. In fact, a decrease in BC incidence was observed after the reduction of hormone replacement therapy. Contrarily, prolonged breastfeeding and physical activity associate with a reduced risk of BC [8,10,11].

[7]Loibl, S.; Poortmans, P.; Morrow, M.; Denkert, C.; Curigliano, G. Breast Cancer. *Lancet.* 2021;397(10286):1750–1769.

[8]Winters, S.; Martin, C.; Murphy, D.; Shokar, N.K. Breast Cancer Epidemiology, Prevention, and Screening. In *Progress in Molecular Biology and Translational Science*; Lakshmanaswamy, R., Ed.; Academic Press, 2017; Vol. 151, pp. 1–32.

[9]Owens, D.; Davidson, K.; Krist, A.; Barry, M.; Cabana, M.; Caughey, A.; Doubeni, C.; Epling, J.; Kubik, M.; Landefeld, C.; et al. Risk Assessment, Genetic Counseling, and Genetic Testing for BRCA-Related Cancer: US Preventive Services Task Force Recommendation Statement. *JAMA.* 2019;322(7):652–665.

[10]Coughlin, S.S. Epidemiology of Breast Cancer in Women. In *Breast Cancer Metastasis and Drug Resistance*; Ahmad, A., Ed.; Springer International Publishing: Cham, 2019; pp. 9–29.

[11]Danaei, G.; Vander Hoorn, S.; Lopez, A.D.; Murray, C.J.L.; Ezzati, M. Causes of Cancer in the World: Comparative Risk Assessment of Nine Behavioural and Environmental Risk Factors. *Lancet.* 2005;366(9499):1784–1793.

1.1.3 Breast cancer screening

The aim of BC screening is to detect asymptomatic early-stage BC, in order to diminish the mortality rates. Most countries of the European Union are involved in mammography-based BC screening programs, which have shown to be effective in reducing BC mortality. These are carried out following the recommendations from the World Health Organization, which recommends mammography screening every two years in women aged between 50 and 69 years. In women with a family history of BC, screening is carried out every year since younger ages [1,12,13].

Mammographic screening presents some limitations such as false-negative results, the risk of radiation-induced BC, and false-positive results that lead to overdiagnosis and overtreatment. Besides, the detection sensitivity is low in women with dense breast tissue. To overcome these limitations, other screening techniques such as magnetic resonance imaging are available for the high-risk population but are not used in screening programs [12,13]. Therefore, it is important to develop new diagnostic tools able to detect BC at early stages.

[12]Cardoso, F.; Kyriakides, S.; Ohno, S.; Penault-Llorca, F.; Poortmans, P.; Rubio, I.T.; Zackrisson, S.; Senkus, E. Early Breast Cancer: ESMO Clinical Practice Guidelines for Diagnosis, Treatment and Follow-up. *Ann. Oncol.* 2019;30:1194–1220.

[13]Lauby-Secretan, B.; Scoccianti, C.; Loomis, D.; Benbrahim-Tallaa, L.; Bouvard, V.; Bianchini, F.; Straif, K. Breast-Cancer Screening — Viewpoint of the IARC Working Group. *N. Engl. J. Med.* 2015;372(24):2353–2358.

1.1.4 Breast cancer classification

There are several histological tumor types of BC. The most common is the invasive ductal carcinoma (IDC), which represents 70-75% of patients, followed by invasive lobular carcinoma (ILC, 12-15%). There are other 18 types of BC that include mixed carcinomas or other invasive carcinomas that affect a minority of patients (0.5-5%) [13,14].

Besides, BC tumors are classified by molecular subtype, which defines the therapeutic options and prognosis of the disease. Molecular classification of BC began in 2000 when Perou *et al.* identified four "intrinsic molecular subtypes" of BC by gene expression profiling: luminal, HER-2 enriched, Basal-like, and Normal-like [15]. Subsequent studies carried out by Sorlie *et al.* led to the identification of the subgroups luminal A and luminal B, which were previously considered as luminal, thereby improving the molecular classification [16]. Further additional studies led to the discovery of additional "intrinsic subtypes" such as claudin-low [17].

[14]Ullah, M.F. Breast Cancer: Current Perspectives on the Disease Status. In *Breast Cancer Metastasis and Drug Resistance*; Springer, Cham, 2019; Vol. 1152, pp. 51–64.

[15]Perou, C.M.; Sørlie, T.; Eisen, M.B.; Rijn, M. van de; Jeffrey, S.S.; Rees, C.A.; Pollack, J.R.; Ross, D.T.; Johnsen, H.; Akslen, L.A.; et al. Molecular Portraits of Human Breast Tumours. *Nature.* 2000;406(6797):747–752.

[16]Sørlie, T.; Tibshirani, R.; Parker, J.; Hastie, T.; Marron, J.S.; Nobel, A.; Deng, S.; Johnsen, H.; Pesich, R.; Geisler, S.; et al. Repeated Observation of Breast Tumor Subtypes in Independent Gene Data Sets. *PNAS.* 2003;100(14):8423.

[17]Prat, A.; Parker, J.; Karginova, O.; Fan, C.; Livasy, C.; Herschkowitz, J.; He, X.; Perou, C. Phenotypic and Molecular Characterization of the Claudin-Low Intrinsic Subtype of Breast Cancer. *Breast cancer Res.* 2010;12(5):R68.

The importance of the molecular classification lies in its value to predict response to therapies and outcome of patients, which is determined by the "intrinsic subtype" [18,19]. Based on these findings, Parker *et al.* developed a signature based on the expression of 50 genes (PAM50) that allows classifying tumors into the main "intrinsic subtypes" (luminal A, luminal B, HER2-enriched, or basal-like) and to predict prognosis and outcomes [20]. The application of gene expression profiling of breast tumors has some limitations such as technical complexity, amount of sample, and high cost, which makes difficult its applicability in clinical practice [21]. Therefore, in the attempt to translate these findings into clinical practice, the expression of estrogen receptor (ER), progesterone receptor (PR), overexpression of human epidermal growth factor receptor 2 (HER2, also known as ERBB2), and Ki-67 can be defined by immunohistochemistry to approximate the molecular classification. Hence, four subtypes can be found: luminal A (ER+, PR+/-, HER2-, Ki-67 low), luminal B (ER+, PR+/-, HER2+/-, Ki-67 high), HER-2 enriched (ER-, PR-, HER2+, Ki-67 high), and triple-negative

[18]Hu, Z.; Fan, C.; Oh, D.S.; Marron, J.; He, X.; Qaqish, B.F.; Livasy, C.; Carey, L.A.; Reynolds, E.; Dressler, L.; et al. The Molecular Portraits of Breast Tumors Are Conserved across Microarray Platforms. BMC Genomics. 2006;7:96.

[19]Prat, A.; Pineda, E.; Adamo, B.; Galván, P.; Fernández, A.; Gaba, L.; Díez, M.; Viladot, M.; Arance, A.; Muñoz, M. Clinical Implications of the Intrinsic Molecular Subtypes of Breast Cancer. *The Breast.* 2015;24:S26–S35.

[20]Parker, J.S.; Mullins, M.; Cheang, M.C.U.; Leung, S.; Voduc, D.; Vickery, T.; Davies, S.; Fauron, C.; He, X.; Hu, Z.; et al. Supervised Risk Predictor of Breast Cancer Based on Intrinsic Subtypes. *J. Clin. Oncol.* 2009;27(8):1160–1167.

[21]Guiu, S.; Michiels, S.; André, F.; Cortes, J.; Denkert, C.; Leo, A. Di; Hennessy, B.T.; Sorlie, T.; Sotiriou, C.; Turner, N.; et al. Molecular Subclasses of Breast Cancer: How Do We Define Them? The IMPAKT 2012 Working Group Statement. *Ann. Oncol.* 2012;23(12):2997–3006.

(ER-, PR-, HER2-, Ki-67 high) (**Table 1**) [22,23,24,25]. The immunohistochemical and molecular classification overlap in most cases, but presents some limitations, as approximately 30% of BC subtypes classified by immunohistochemistry do not correspond to PAM50 intrinsic subtypes. In fact, 86% of triple-negative BC (TNBC) tumors classified by immunohistochemistry correspond to basal-like gene expression-based classification, and the concordance of luminal A, luminal B, luminal B HER2 positive, and HER2-enriched are 62%, 51%, 46%, 66%, respectively [20,22]. Despite these differences, the immunohistochemical classification still determines the treatment choice for each patient.

Table 1. Immunohistochemical classification of BC subtypes.

Subtype	ER	PR	HER2	Ki-67
Luminal A	+	+/-	-	<14%
Luminal B	+	+/-	+/-	≥14%
HER2-enriched	-	-	+	≥14%
Triple-negative	-	-	-	≥14%

[22]Harbeck, N.; Penault-Llorca, F.; Cortes, J.; Gnant, M.; Houssami, N.; Poortmans, P.; Ruddy, K.; Tsang, J.; Cardoso, F. Breast Cancer. *Nat. Rev. Dis. Prim.* 2019;5(1):66.

[23]Edén, P.; Ritz, C.; Rose, C.; Fernö, M.; Peterson, C. "Good Old" Clinical Markers Have Similar Power in Breast Cancer Prognosis as Microarray Gene Expression Profilers. *Eur. J. Cancer.* 2004;40(12):1837–1841.

[24]Cheang, M.C.U.; Chia, S.K.; Voduc, D.; Gao, D.; Leung, S.; Snider, J.; Watson, M.; Davies, S.; Bernard, P.S.; Parker, J.S.; et al. Ki67 Index, HER2 Status, and Prognosis of Patients With Luminal B Breast Cancer. *J. Natl. Cancer Inst.* 2009;101(10):750.

[25]Goldhirsch, A.; Wood, W.C.; Coates, A.S.; Gelber, R.D.; Thürlimann, B.; Senn, H.-J. Strategies for Subtypes—Dealing with the Diversity of Breast Cancer: Highlights of the St Gallen International Expert Consensus on the Primary Therapy of Early Breast Cancer 2011. *Ann. Oncol.* 2011;22(8):1747.

1.1.5 Treatment

The main objective of BC treatment is to eliminate the tumor and to prevent the recurrence of BC patients [26]. To accomplish these objectives, local and systemic treatments can be used alone or in combination.

On the one hand, local treatments include surgery and radiotherapy. In most cases, the surgery consists of breast-conserving surgery but in some cases, mastectomy is recommended. Postoperative radiotherapy is commonly used to reduce the risk of recurrence. Besides, regional lymph nodes are evaluated, as can predict long-term outcomes of patients. When metastasis is found in regional lymph nodes, local treatment can be applied in axillary lymph nodes [13,27].

On the other hand, systemic treatments comprise endocrine therapy, targeted therapies, and chemotherapy, that can be administered to BC patients before surgery (neoadjuvant), after surgery (adjuvant), or both of them. The treatment choice is determined by the subtype of BC, and the individual risk of relapse is determined by the tumor burden.

There are several therapeutical strategies based on endocrine therapy, which are administered to patients with tumors expressing hormone receptors (HR). Selective ER modulators such as tamoxifen, and selective ER degraders such as fulvestrant target the ER, thus inhibiting its activity. Besides, aromatase inhibitors such as letrozole, anastrozole, and

[26]Waks, A.G.; Winer, E.P. Breast Cancer Treatment: A Review. *JAMA.* 2019;321(3):288–300.
[27]Ruddy, K.J.; Ganz, P.A. Treatment of Nonmetastatic Breast Cancer. *JAMA.* 2019;321(17):1716–1717.

exemestane inhibit estrogen biosynthesis, thus decreasing circulating estrogen levels. Typically, adjuvant endocrine therapy is maintained during 5-10 years in HR+ patients and has been demonstrated to reduce the recurrence rate by 50%. Furthermore, new endocrine therapies are being studied to increase clinical efficacy [14,27,28].

Furthermore, nowadays, we have genomic platforms to define the risk of relapse in luminal BC such as Oncotype DX, Mammaprint, Prosigna, Breast Cancer Index, or EndoPredict. The use of these gene signatures in combination with clinicopathological characteristics is helpful to determine the need for chemotherapy [13]. Among the different combinations of chemotherapeutic agents that have been tested, the regimes containing anthracyclines (doxorubicin or epirubicin) and taxanes are the most effective for patients with a high risk of recurrence [13,27].

Regarding HER2-positive tumors, the development of HER2-targeted therapies dramatically improved the outcomes of these patients. Trastuzumab was the first approved anti-HER2 therapy, that in combination with chemotherapy demonstrated to have a positive impact on disease-free survival (DFS) and OS in patients with HER2 positive BC [13,27,29].

[28]Hernando, C.; Ortega-Morillo, B.; Tapia, M.; Moragón, S.; Martínez, M.T.; Eroles, P.; Garrido-Cano, I.; Adam-Artigues, A.; Lluch, A.; Bermejo, B.; et al. Oral Selective Estrogen Receptor Degraders (SERDs) as a Novel Breast Cancer Therapy: Present and Future from a Clinical Perspective. *Int. J. Mol. Sci.* 2021;22(15):7812.

[29]Slamon, D.; Leyland-Jones, B.; Shak, S.; Fuchs, H.; Paton, V.; Bajamonde, A.; Fleming, T.; Eiermann, W.; Wolter, J.; Pegram, M.; et al. Use of Chemotherapy plus a Monoclonal Antibody against HER2 for Metastatic Breast Cancer That Overexpresses HER2. *N. Engl. J. Med.* 2001;344(11):783–792.

Nevertheless, cytotoxic chemotherapy is the only systemic option effective for triple-negative tumors [13].

Metastatic BC and inoperable locally advanced BC are considered incurable diseases. Treatment in these patients aims to increase the OS while maintaining a high quality of life. Even if local therapies can be useful in some cases, therapeutic regimes are mainly based on systemic treatments that include the options described previously, as well as other drugs recently approved. Some examples are CDK4/6, PIK3CA, and mTOR inhibitors that are frequently used to delay the development of endocrine resistance in luminal patients, PARP inhibitors which are used in *BRCA* mutated patients, immunotherapy that has shown efficacy in PD-L1 positive TNBC, and new antibody-drug conjugates such as Trastuzumab-Deruxtecan [23,27,30]. In this context, it is urgent to develop new therapeutic strategies for triple-negative metastatic patients. Despite last advances in BC therapy have improved the outcomes of patients, the median OS for this subset of patients is approximately 1 year, while luminal and HER2-positive metastatic patients have a median OS of 4-5 years [27]. Hence, further advances in diagnosis and treatment are necessary to improve BC patients' outcomes.

[30]Cardoso, F.; Paluch-Shimon, S.; Senkus, E.; Curigliano, G.; Aapro, M.S.; André, F.; Barrios, C.H.; Bergh, J.; Bhattacharyya, G.S.; Biganzoli, L.; et al. 5th ESO-ESMO International Consensus Guidelines for Advanced Breast Cancer (ABC 5). *Ann. Oncol.* 2020;31(12):1623–1649.

1.2 MicroRNAs

microRNAs (miRNAs) are small single-stranded non-coding ribonucleic acids (RNAs) of approximately 20 nucleotides that regulate gene expression and are implicated in a wide variety of physiological processes including cell development, differentiation, and apoptosis, but are also involved in pathological processes such as cardiovascular diseases, neurodegeneration, autoimmune diseases, and cancer [31,32].

The first miRNA was found in *Caenorhabditis elegans* in 1993. Since that discovery, numerous miRNAs have been found in vertebrates and invertebrates, and nowadays more than 2,600 mature miRNAs have been identified in humans [33].

1.2.1 Biogenesis

In mammals, most miRNA genes (70%) are located in introns and can either share promoter with the host gene or have their own, whereas intergenic miRNAs are independently regulated. miRNAs' biogenesis starts in the nucleus, where genes encoding miRNAs are transcribed into primary miRNA transcripts (pri-miRNA) by RNA polymerase II, although can be transcribed by RNA polymerase III in some cases. Then, pri-miRNAs containing a 5' methylated cap and a 3' polyadenylated tail are cleaved by a

[31]Peng, Y.; Croce, C.M. The Role of MicroRNAs in Human Cancer. *Signal Transduct. Target. Ther.* 2016;1:15004.

[32]Loh, H.Y.; Norman, B.P.; Lai, K.S.; Rahman, N.M.A.N.A.; Alitheen, N.B.M.; Osman, M.A. The Regulatory Role of MicroRNAs in Breast Cancer. *Int. J. Mol. Sci.* 2019;20(19):4940.

[33]Kozomara, A.; Birgaoanu, M.; Griffiths-Jones, S. MiRBase: From MicroRNA Sequences to Function. *Nucleic Acids Res.* 2019;47(D1):D155–D162.

protein complex formed by the Drosha Ribonuclease III and the DGCR8 Microprocessor Complex Subunit that lead to the precursor miRNA (pre-miRNA) that have 60-70 nucleotides in length and a hairpin loop structure. After processing, pre-miRNAs are actively exported to the cytoplasm by the Exportin-5, which is RanGTP-dependent. Once in the cytoplasm, pre-miRNAs are processed by the ribonuclease III Dicer to give rise to miRNA duplexes containing two strands of approximately 20 nucleotides that are unwound by RNA helicases. Generally, one of the strands is degraded while the remaining strand associates with Argonaute 2 (AGO2) protein in the miRNA-induced silencing complex (miRISC), and guides the complex to target mRNAs. However, the dominant mature miRNA can vary between tissues or developmental stages and may be influenced by the availability of target mRNAs (**Figure 3**) [34,35,36].

[34]Finnegan, E.F.; Pasquinelli, A.E. MicroRNA Biogenesis: Regulating the Regulators. Crit. Rev. Biochem. Mol. Biol. 2013;48(1):68.

[35]Krol, J.; Loedige, I.; Filipowicz, W. The Widespread Regulation of MicroRNA Biogenesis, Function and Decay. Nat. Rev. Genet. 2010;11:597–610.

[36]Saliminejad, K.; Khorshid, H.R.K.; Fard, S.S.; Ghaffari, S.H. An Overview of MicroRNAs : Biology, Functions, Therapeutics, and Analysis Methods. J. Cell. Physiol. 2019;234:5451–5465.

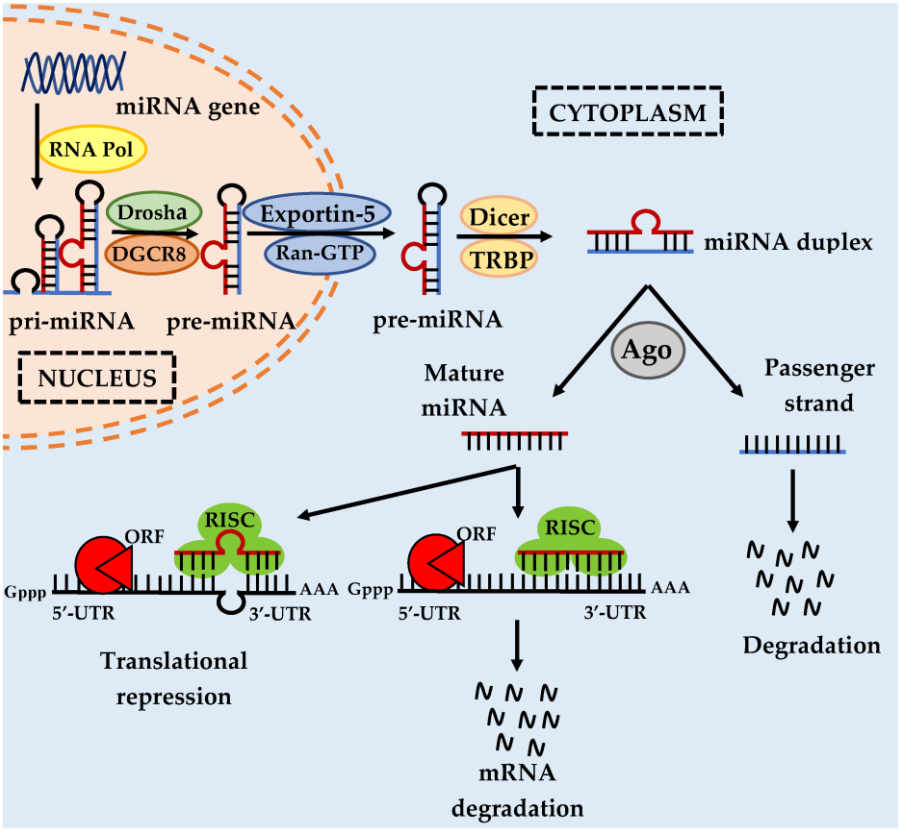

Figure 3. miRNA biogenesis. miRNA genes are transcribed by RNA polymerase (RNA pol) to produce pri-miRNAs that will be processed by Drosha/DGCR8 leading to pre-miRNAs. Following transportation by Exportin-5 from nucleus to cytoplasm, pre-miRNAs are processed by Dicer/TRBP to give rise to miRNA duplex. Mature miRNA can bind target mRNAs and will induce their degradation or translational repression depending on the complementarity between sequences. Reproduced with permission from *Mol. Cell. Pharmacol.* 2010;2(5):213–219 [37].

[37]Bhardwaj, A.; Singh, S.; Singh, A.P. MicroRNA-Based Cancer Therapeutics: Big Hope from Small RNAs. *Mol. Cell. Pharmacol.* 2010;2(5):213–219.

1.2.2 Target regulation

The miRISC complex binds target mRNAs through base pairing by miRNA complementarity. There is an imperfect match between the miRNA seed sequence of 6-8 nucleotides and the mRNA. Typically, target recognition occurs in the 3' untranslated regions (UTR) of mRNAs, although in some cases have been described to target the 5'UTR, or the coding sequence (CDS). Therefore, each miRNA may regulate numerous targets, and each mRNA may be targeted by several miRNAs, thus creating complex regulatory networks [38]. Accordingly, it is estimated that half of the genome is regulated by miRNAs [35].

miRNAs lead to gene silencing by target degradation or translational repression, which will be determined depending on the miRNA-mRNA complementarity. When there is high complementarity, mRNAs are degraded by members of the Argonaute family of proteins with nuclease activity. Otherwise, if there is imperfect pairing, targets are not degraded but protein translation is inhibited by physically blocking the RNA polymerase binding site [39,40].

Despite the traditional regulatory role of miRNAs described above, several authors reported that miRNAs may act as positive regulators of the translation of target mRNAs. Activator miRNAs are known as small activating

[38]Hayes, J.; Peruzzi, P.P.; Lawler, S. MicroRNAs in Cancer: Biomarkers, Functions and Therapy. *Trends Mol. Med.* 2014;20(8):460–469.

[39]Terrinoni, A.; Calabrese, C.; Basso, D.; Aita, A.; Caporali, S.; Plebani, M.; Bernardini, S. The Circulating MiRNAs as Diagnostic and Prognostic Markers. *Clin. Chem. Lab. Med.* 2019;57(7):932–953.

[40]Fridrichova, I.; Zmetakova, I. MicroRNAs Contribute to Breast Cancer Invasiveness. *Cells.* 2019;8(11):1361.

RNAs (saRNAs), that can bind to target promoters and increase the affinity of RNA Polymerase II by these regions, thus increasing the expression of the target gene [41]. An example is miR-6734, which positively regulates the expression of the tumor suppressor p21 in colon cancer cells [42]. Besides, miRNAs have been described by several authors to be ligands of Toll-like receptors (TLRs) and may activate TLR-mediated tumor growth and metastasis [32].

1.2.3 miRNAs in cancer

As previously mentioned, each miRNA can regulate many targets involved in different biological processes. Therefore, changes in miRNAs expression have been associated with numerous pathological processes including cancer.

The implication of miRNAs in cancer was first demonstrated in a study carried out by Calin *et al.* in 2002. Authors found *miR-15a* and *miR-16-1* deleted or downregulated in most chronic lymphocytic leukemia patients, suggesting their role as tumor suppressors [43]. Since that discovery, numerous authors have demonstrated the role of miRNAs in cancer through

[41]Rahman, M.M.; Brane, A.C.; Tollefsbol, T.O. MicroRNAs and Epigenetics Strategies to Reverse Breast Cancer. Cells. 2019;8:1214.

[42]Kang, M.R.; Park, K.H.; Yang, J.-O.; Lee, C.W.; Oh, S.J.; Yun, J.; Lee, M.Y.; Han, S.-B.; Kang, J.S. MiR-6734 Up-Regulates P21 Gene Expression and Induces Cell Cycle Arrest and Apoptosis in Colon Cancer Cells. PLoS One. 2016;11(8):e0160961.

[43]Calin, G.A.; Dumitru, C.D.; Shimizu, M.; Bichi, R.; Zupo, S.; Noch, E.; Aldler, H.; Rattan, S.; Keating, M.; Rai, K.; et al. Frequent Deletions and Down-Regulation of Micro- RNA Genes MiR15 and MiR16 at 13q14 in Chronic Lymphocytic Leukemia. Proc. Natl. Acad. Sci. U. S. A. 2002;99(24):15529.

regulating the expression of target mRNAs involved in hallmarks of cancer such as cell proliferation, invasion, or apoptosis [39].

miRNAs playing a role in cancer can be classified as oncogenic or tumor suppressor miRNAs. Oncogenic miRNAs use to be upregulated in tumors and target tumor suppressor genes, while tumor suppressor miRNAs are usually downregulated in tumors and target oncogenes (**Figure 4**) [33].

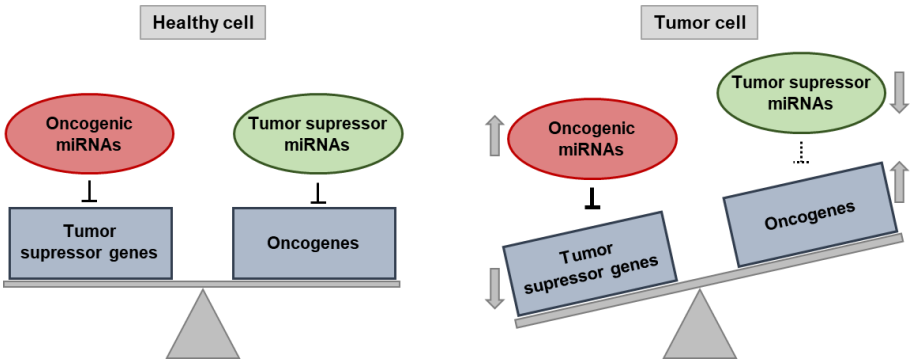

Figure 4. miRNAs can be classified in tumor suppressor miRNAs and oncogenic miRNAs. In healthy cells (left), there is a balanced expression of miRNAs, tumor suppressor genes, and oncogenes. In tumor cells (right), upregulation of oncogenic miRNAs downregulate tumor suppressor genes, and downregulation of tumor suppressor miRNAs lead to an increased expression of oncogenes, thus contributing to tumorigenesis.

An example of tumor suppressor miRNAs is the miR-200 family, found downregulated in numerous types of cancer including BC. This family of miRNAs suppresses the epithelial-to-mesenchymal transition (EMT), involved in metastasis and drug resistance. By contrast, miR-21 is an oncogenic miRNA involved in apoptosis and metastasis regulation and is

frequently upregulated in different cancers such as BC, hepatocellular carcinoma, ovarian cancer, or prostate cancer [44]. Intriguingly, some miRNAs may have tissue-specific roles so may act as oncogenic or tumor suppressor miRNAs depending on the cancer type [41]. An example is miR-498, which is considered an oncogenic miRNA in breast and prostate cancers, and a tumor suppressor miRNA in liver cancer [33].

Several alterations are found in tumors, leading to abnormal miRNAs expression levels:

1.2.3.1 Transcriptional control of miRNAs

Expression of miRNA genes is regulated by numerous transcriptional repressors or activators. Therefore, deregulation of tumor-related transcription factors may trigger alterations in miRNAs expression (**Figure 5**). An example is the MYC oncogene, which induces the expression of the miR-17/92 cluster, that targets E2F1, thus giving rise to increased proliferation. Another example is the tumor suppressor p53, which induces the expression of the tumor suppressor miR-34. p53 and miR-34 have been found downregulated in 60-80% of patients with ovarian cancer [32,45,46].

[44]Rupaimoole, R.; Slack, F.J. MicroRNA Therapeutics: Towards a New Era for the Management of Cancer and Other Diseases. *Nat. Rev. Drug Discov.* 2017;16:203–221.

[45]Lin, S.; Gregory, R.I. MicroRNA Biogenesis Pathways in Cancer. *Nat. Rev. Cancer.* 2015;15(6):321–333.

[46]Leva, G. Di; Garofalo, M.; Croce, C.M. MicroRNAs in Cancer. *Annu. Rev. Pathol.* 2014;9:287–314.

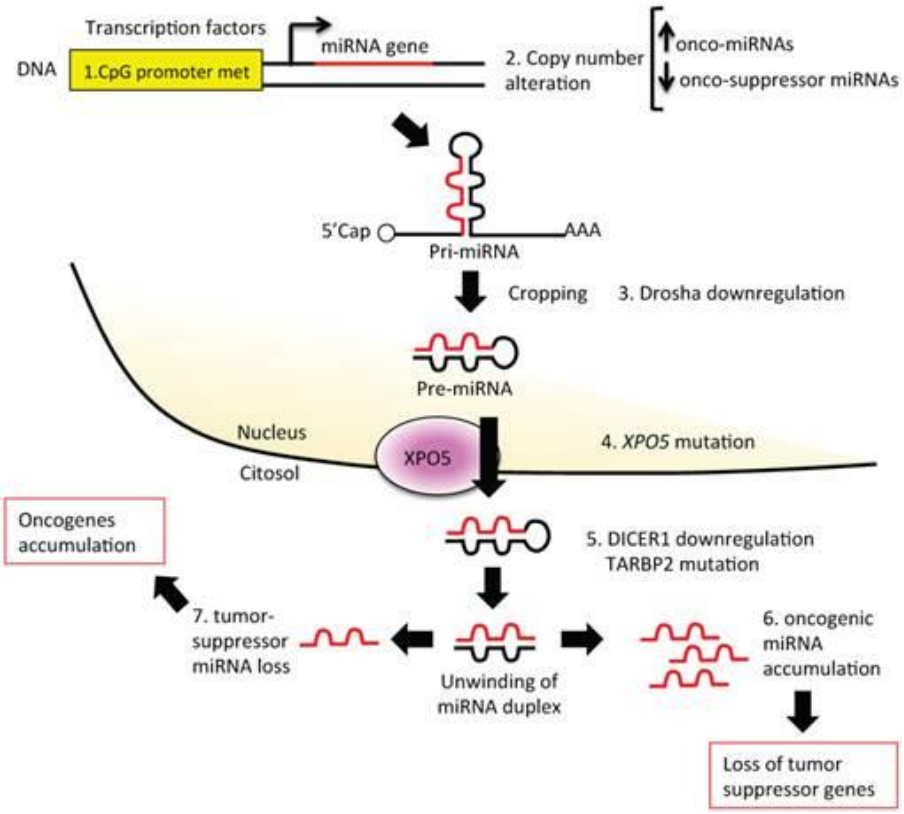

Figure 5. Alterations leading to abnormal expression of miRNAs in cancer cells. Transcriptional and genetic alterations and impairment of the biosynthesis machinery result in downregulation of tumor suppressor genes and upregulation of oncogenes. Adapted with permission from *Theranostics*. 2015; 5(10): 1122–1143 [47].

[47]Bertoli, G.; Cava, C.; Castiglioni, I. Micrornas: New Biomarkers for Diagnosis, Prognosis, Therapy Prediction and Therapeutic Tools for Breast Cancer. *Theranostics.* 2015;5(10):1122–1143.

Besides, miRNA genes are usually associated with CpG islands that are regulated by methylation. Several authors have demonstrated that DNA methylation and histone acetylation may modulate the expression of miRNAs (**Figure 5**) [46,47]. Indeed, Lujambio *et al.* demonstrated that treatment of cancer cells with DNA demethylating agents increases the expression of several tumor suppressor miRNAs [48].

1.2.3.2 Genetic alterations of miRNA genes

Genetic alterations underlie the abnormal expression of numerous miRNAs involved in cancer (**Figure 5**). Copy number variations, single-base mutations, deletions, translocations, or amplifications are usual in malignant cells. One example is the previously mentioned deletion of the *miR-15a*/*miR-16-1* cluster that is commonly found in B-cell chronic lymphocytic leukemia patients, as described by Calin *et al.* [44]. Besides, Zhang *et al.* studied DNA copy number alterations in miRNA genes in different types of cancer. Results from BC revealed that 72.8% of miRNA genes are located in regions with copy number alterations [49]. Other alterations such as SNPs, deletions, or duplications may modify the structure of the pre-miRNA, thus impeding its correct processing [39].

[48]Lujambio, A.; Calin, G.A.; Villanueva, A.; Ropero, S.; Sánchez-Céspedes, M.; Blanco, D.; Montuenga, L.M.; Rossi, S.; Nicoloso, M.S.; Faller, W.J.; et al. A MicroRNA DNA Methylation Signature for Human Cancer Metastasis. *PNAS.* 2008;105(36):13561.

[49]Zhang, L.; Huang, J.; Yang, N.; Greshock, J.; Megraw, M.S.; Giannakakis, A.; Liang, S.; Naylor, T.L.; Barchetti, A.; Ward, M.R.; et al. MicroRNAs Exhibit High Frequency Genomic Alterations in Human Cancer. *PNAS*. 2006;103(24):9141.

1.2.3.3 Alterations in miRNAs biogenesis machinery

Proteins involved in miRNAs biogenesis play an essential role in mature miRNAs synthesis. Consequently, alterations in these molecules may cause abnormal expression of miRNAs (**Figure 5**). Despite that miRNAs can act as oncogenic or tumor suppressors, several studies have shown that miRNAs are usually downregulated in tumoral tissues when compared to healthy tissues. This could be a consequence of the impairment of miRNA biogenesis in cancer cells [39].

Drosha and Dicer have been found downregulated in several types of cancer and associated with advanced stages, poor outcome, and cancer progression [47, 50]. Regarding BC, decreased expression of Dicer and Drosha is found in approximately 50% of BC patients, and reduced levels associate with high-grade BC, shorter DFS, and shorter distant relapse-free survival (DRFS) [46,51].

The Exportin-5 and its cofactor Ran-GTP mediate the transport of miRNAs to the cytoplasm, where will be processed to give mature miRNAs. Mutations in Exportin-5 have been identified in several types of cancer and lead to the accumulation of pre-miRNAs in the nucleus and downregulation of mature miRNAs [47]. Melo *et al.* found that Exportin-5 mutations occur frequently in tumors with microsatellite instability leading to entrapment of pre-miRNAs in the nucleus and that its restoration has tumor suppressor

[50]Iliou, M.S.; Silva-Diz, V. da; Carmona, F.J.; Ramalho-Carvalho, J.; Heyn, H.; Villanueva, A.; Muñoz, P.; Esteller, M. Impaired DICER1 Function Promotes Stemness and Metastasis in Colon Cancer. *Oncogene.* 2014;33(30):4003–4015.

[51]Yan, M.; Huang, H.-Y.; Wang, T.; Wan, Y.; Cui, S.-D.; Liu, Z.; Fan, Q.-X. Dysregulated Expression of Dicer and Drosha in Breast Cancer. *Pathol. Oncol. Res.* 2012;18:343–348.

features *in vitro* and *in vivo* [52]. Similar results were found in hepatocellular carcinoma, where defective Exportin-5 phosphorylation was shown to induce the impairment of Exportin-5, and the downregulation of mature miRNAs as consequence [53].

Another example is the abnormal expression of Argonaute proteins, which has been found in Wilms' tumors and melanoma, affecting the activity of the miRISC complex [32].

1.2.4 miRNA-based therapies

Despite advances in BC treatment, more effective therapies are needed. Given that miRNAs regulate multiple targets involved in processes such as tumor progression and treatment response, these molecules have emerged as a promising strategy to treat cancer. miRNA-based therapies aim to inhibit oncogenic miRNAs or to restore the expression of tumor suppressor miRNAs. To achieve it, oncogenic miRNAs can be inhibited through complementary RNAs (anti-miRNAs), and tumor suppressor miRNAs can be replaced by miRNA mimics. Among their applications, miRNAs and anti-miRNAs can enhance the efficacy of other approved therapies such as cytotoxic agents.

[52]Melo, S.A.; Moutinho, C.; Ropero, S.; Calin, G.A.; Rossi, S.; Spizzo, R.; Fernandez, A.F.; Davalos, V.; Villanueva, A.; Montoya, G.; et al. A Genetic Defect in Exportin-5 Traps Precursor MicroRNAs in the Nucleus of Cancer Cells. *Cancer Cell.* 2010;18(4):303–315.

[53]Sun, H.-L.; Cui, R.; Zhou, J.; Teng, K.; Hsiao, Y.-H.; Nakanishi, K.; Fassan, M.; Luo, Z.; Shi, G.; Tili, E.; et al. ERK Activation Globally Downregulates MiRNAs through Phosphorylating Exportin-5. *Cancer Cell.* 2016;30(5):736.

As miRNAs and anti-miRNAs are easily degraded by blood nucleases, chemical modifications such as methylation, locked nucleic acids, 2'-OH group modification, or phosphorothioate-like groups can be included to increase nuclease resistance [54]. Hence, their half-life in the bloodstream increases from minutes to several hours [55]. Despite the increased stability, chemically modified miRNAs and anti-miRNAs still present important limitations to be used as therapeutic agents. Once in circulation, miRNAs are cleared by the reticuloendothelial system (RES), kidney, and liver. Moreover, miRNAs have to reach tumors, where cannot be efficiently internalized by tumor cells due to their negative charge. Besides, after internalization, miRNAs can be easily degraded in late endosomes/lysosomes. Furthermore, miRNAs lead to immune-dependent toxic effects and neurotoxicity through TLRs [56,56,57].

To overcome these limitations, local delivery of miRNAs allows increased efficiency and reduced toxicity when compared to systemic delivery, but is not possible for inaccessible tumors or metastatic patients [57]. Therefore, viral vectors and nanoparticles are being studied for systemic miRNAs delivery.

[54]Mollaei, H.; Safaralizadeh, R.; Rostami, Z. MicroRNA Replacement Therapy in Cancer. *J. Cell. Physiol.* 2019;234(8):12369–12384.

[55]Ganju, A.; Khan, S.; Hafeez, B.B.; Behrman, S.W.; Yallapu, M.M.; Chauhan, S.C.; Jaggi, M. MiRNA Nanotherapeutics for Cancer. *Drug Discov. Today.* 2017;22(2):424–432.

[56]Chen, Y.; Gao, D.-Y.; Huang, L. In Vivo Delivery of MiRNAs for Cancer Therapy: Challenges and Strategies. *Adv. Drug Deliv.* Rev. 2015;81:128–141.

[57]Lee, S.W.L.; Paoletti, C.; Campisi, M.; Osaki, T.; Adriani, G.; Kamm, R.D.; Mattu, C.; Chiono, V. MicroRNA Delivery through Nanoparticles. *J. Control. Release.* 2019;313:80–95.

1.2.4.1 Viral vectors for miRNAs delivery

Viral vectors can be targeted to tumor cells to deliver vectors into cells that will express the encoded miRNAs. Lentiviral vectors integrate their genome into recipient cells, which can induce insertional mutagenesis. Therefore, non-integrative virus such as adenovirus and adeno-associated virus are preferred. Despite these systems can efficiently deliver miRNAs, also present some limitations such as induced immune-related adverse effects and the difficulty to scale up their manufacturing [55,57].

1.2.4.2 Nanoparticles for miRNAs delivery

Nanoparticles have been raised as safe miRNA delivery systems that present advantages such as efficient transport of miRNAs, and the possibility to be targeted to tumors by modifying their surface with specific ligands or antibodies, thus reducing the side effects (**Figure 6**) [55,58].

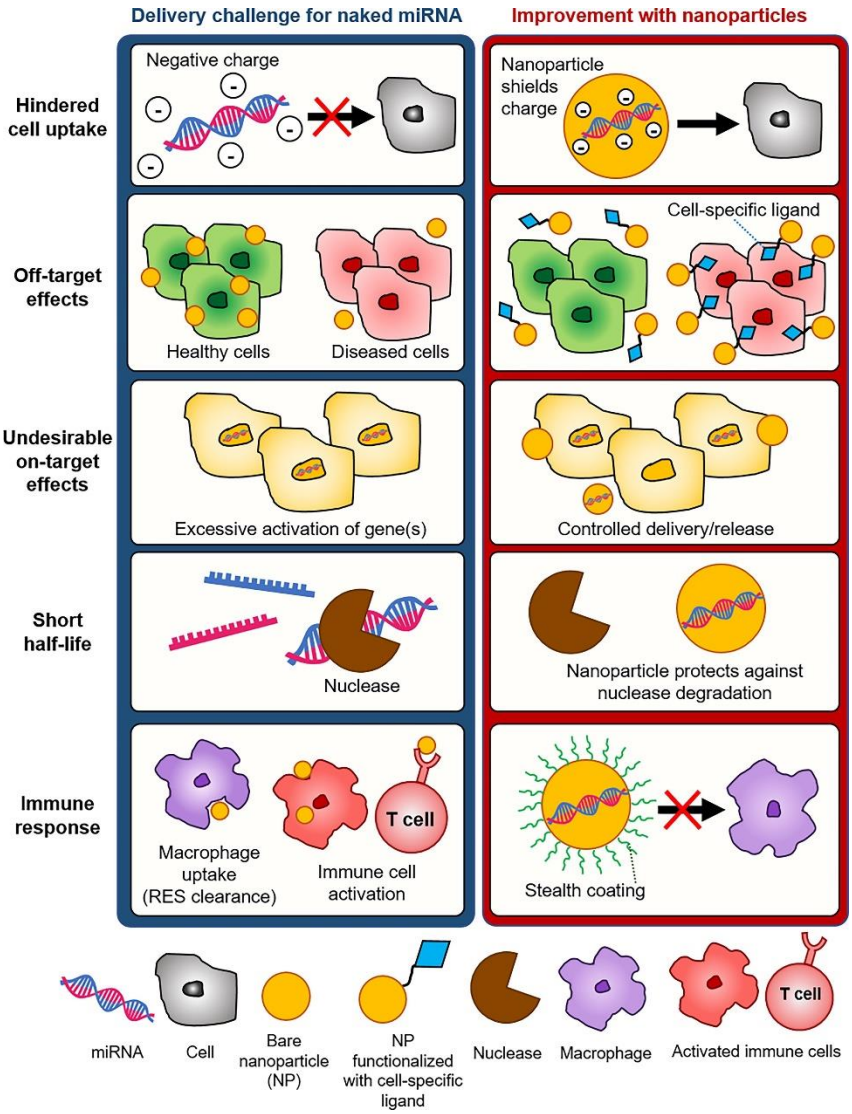

Figure 6. Nanoparticle-based delivery of miRNAs for cancer therapy allows efficient uptake by cells, specific controlled delivery in tumor cells that decreases off-target and on-target effects, increased half-life of miRNAs, and prevention of undesired immune response. Reproduced with permission from *J. Control. Release.* 2019;313:80–95 [58].

Nanosystems can be classified in inorganic, polymeric, and lipid-based nanoparticles. Among them, mesoporous silica nanoparticles (MSNs) have gained attention for cancer therapy due to their unique properties. MSNs are solid materials with an ordered porous structure (mesopores). These biocompatible materials have large pore volume with tunable size, great surface area, and chemical and thermal stability. The high density of silanols at their surface allows their functionalization with molecules acting as "molecular gates" able to trigger a controlled release of their content in response to specific stimuli such as pH, light, ultrasounds, temperature, or magnetic fields. Besides, antibodies or specific ligands may also be included in the surface to target a specific cell type. Despite the active targeting through surface molecules, MSNs have been shown to passively accumulate in tumors. This is given by the enhanced permeability and retention (EPR) effect, which is characteristic of tumors due to a defective vasculature and lymphatic drainage, which enhance the passive accumulation of nanoparticles (**Figure 7**)[56,58,59].

[58]Cha, W.; Fan, R.; Miao, Y.; Zhou, Y.; Qin, C.; Shan, X.; Wan, X.; Li, J. Mesoporous Silica Nanoparticles as Carriers for Intracellular Delivery of Nucleic Acids and Subsequent Therapeutic Applications. *Molecules.* 2017;22(5):782.

[59]Manzano, M.; Vallet-Regí, M. Mesoporous Silica Nanoparticles for Drug Delivery. *Adv. Funct. Mater.* 2020;30(2):1902634.

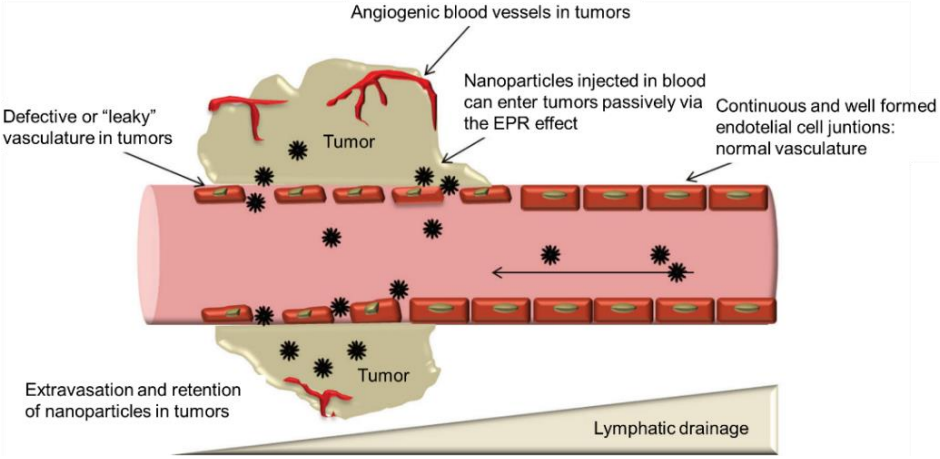

Figure 7. Passive targeting of nanoparticles through the EPR effect. Adapted with permission from *Front. Pharmacol.* 2014; 5: 77 [60].

The ability of nanoparticles to specifically target tumors and to deliver their cargo on-demand make them good candidates to develop effective anticancer therapies. Nucleic acids including miRNAs can be efficiently transported by MSNs, which will protect them from degradation until reaching tumoural tissue. Also, to avoid their degradation in endosomes/lysosomes, it is possible to design nanodevices able to escape from these organelles, thus delivering miRNAs in the cytoplasm where will be effective. Besides, MSNs give the possibility to design systems for combined delivery of miRNAs and clinically used drugs to increase the efficacy of actual treatments [56,60,61].

[60]Jhaveri, A.M.; Torchilin, V.P. Multifunctional Polymeric Micelles for Delivery of Drugs and SiRNA. *Front. Pharmacol.* 2014;5:77.

[61]Watermann, A.; Brieger, J. Mesoporous Silica Nanoparticles as Drug Delivery Vehicles in Cancer. *Nanomaterials.* 2017;7(7):189.

1.2.5 miRNAs as biomarkers

As detailed before (*1.3 BC screening*), current diagnostic tools present some limitations. Besides, early detection of BC has been shown to improve the outcomes of BC patients [5,6]. Therefore, new diagnostic tools able to detect BC even at early stages are needed to increase the OS of BC patients. In this context, miRNAs have emerged as potential biomarkers.

Despite their role in cells, miRNAs can be also found in different body fluids such as blood, saliva, urine, and tears. Extracellular miRNAs can be passively released from apoptotic or necrotic cells, or actively secreted in exosomes, microvesicles, apoptotic bodies, or bound to lipoproteins (HDL) or RNA binding proteins (AGO2 and nucleophosmin-1,) [62]. Evidences are suggesting the role of actively secreted miRNAs in cell-to-cell communication, whereas circulating vesicle-free miRNAs do not have a particular function and represent the majority of the extracellular miRNAs (**Figure 8**) [37].

[62]Cheng, G. Circulating MiRNAs: Roles in Cancer Diagnosis, Prognosis and Therapy. *Adv. Drug Deliv. Rev.* 2015;81:75–93.

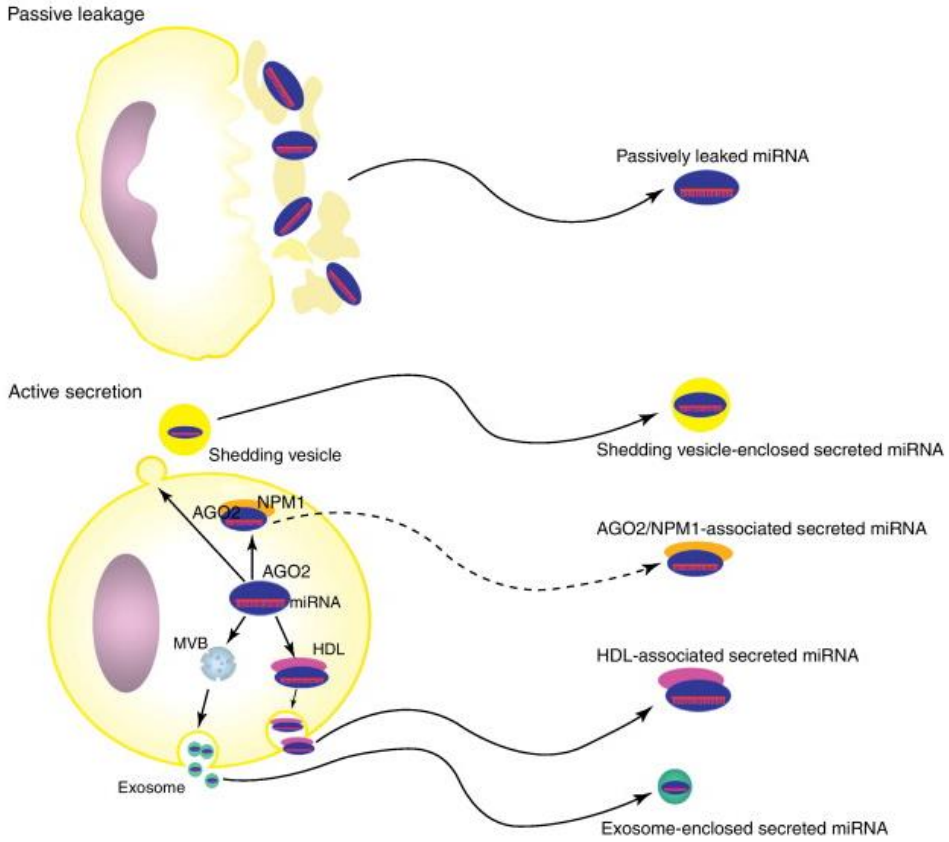

Figure 8. Origin of circulating miRNAs. miRNAs can be passively released from apoptotic and necrotic cells, or actively secreted via vesicles (exosomes and microvesicles) or associated with the high-density lipoprotein (HDL), or other RNA-binding proteins such as AGO2 or nucleophosmin-1 (NPM-1). MVB, multivesicular bodies. Adapted from *Trends Cell Biol.* 2012; 22(3): 125–132 [63].

[63]Chen, X.; Liang, H.; Zhang, J.; Zen, K.; Zhang, C.-Y. Secreted MicroRNAs: A New Form of Intercellular Communication. *Trends Cell Biol.* 2012;22(3):125–132.

Circulating miRNAs present some properties that reinforce their applicability as biomarkers such as their stability and resistance to storage. Besides, circulating miRNAs can be obtained by minimally invasive techniques and easily determined through several techniques such as quantitative real-time PCR (qRT-PCR) or microarray [39,64]. Thus, there are numerous examples of circulating miRNAs with potential as cancer biomarkers. Plasma and serum are the most used body fluids to measure circulating miRNAs, as can be easily obtained with minimally invasive procedures and have a high amount of miRNAs [65]. Many authors described the differential expression between cancer patients and healthy individuals, as well as their potential as early diagnostic and prognostic biomarkers [65,66]. An example is the four miRNA signature described by Sahlberg *et al.*, which can predict relapse and OS of TNBC patients [67]. Besides, circulating miRNAs can be useful as predictive biomarkers for treatment response, as evidenced by McGuire *et al*. that demonstrated the role of circulating miR-21, miR-195, and miR-145 to predict neoadjuvant chemotherapy response [68]. Interestingly, several clinical trials aim to validate the applicability of

[64]Kashyap, D.; Kaur, H. Cell-Free MiRNAs as Non-Invasive Biomarkers in Breast Cancer: Significance in Early Diagnosis and Metastasis Prediction. Life Sci. 2020;246:117417.

[65]Hamam, R.; Hamam, D.; Alsaleh, K.A.; Kassem, M.; Zaher, W.; Alfayez, M.; Aldahmash, A.; Alajez, N.M. Circulating MicroRNAs in Breast Cancer: Novel Diagnostic and Prognostic Biomarkers. Cell Death Dis. 2017;8(9):e3045.

[66]Grimaldi, A.M.; Incoronato, M. Clinical Translatability of "Identified" Circulating Mirnas for Diagnosing Breast Cancer: Overview and Update. Cancers (Basel). 2019;11(7):901.

[67]Sahlberg, K.K.; Bottai, G.; Naume, B.; Burwinkel, B.; Calin, G.A.; Børresen-Dale, A.-L.; Santarpia, L. A Serum MicroRNA Signature Predicts Tumor Relapse and Survival in Triple-Negative Breast Cancer Patients. Clin. Cancer Res. 2015;21(5):1207–1214.

[68]McGuire, A.; Casey, M.-C.; Waldron, R.M.; Heneghan, H.; Kalinina, O.; Holian, E.; McDermott, A.; Lowery, A.J.; Newell, J.; Dwyer, R.M.; et al. Prospective Assessment of Systemic MicroRNAs as Markers of Response to Neoadjuvant Chemotherapy in Breast Cancer. Cancers (Basel). 2020;12(7):1820.

circulating miRNAs as cancer biomarkers. As an example, circulating miR-125a-5p and miRNA143-3p are being evaluated as diagnostic and prognostic biomarkers of BC (NCT04778202). Hence, miRNAs are potential diagnostic, prognostic, and predictive biomarkers for BC and could be useful in the clinical management of BC patients.

CHAPTER 2 |

Objectives

The present PhD thesis aims to deepen the knowledge of miRNAs involved in cancer. More specifically, this study is focused on the study of the role of miR-99a-5p in breast cancer, as well as its applicability as a therapeutic target and biomarker.

The specific objectives referred to each chapter are:

1. To study the implication of miR-99a-5p in doxorubicin resistance and its potential as a therapeutic target for breast cancer treatment.
2. To study the applicability of miR-99a-5p as a diagnostic biomarker for breast cancer diagnosis.
3. To develop a system for the detection of circulating miR-99a-5p as a potential breast cancer diagnosis tool.

CHAPTER 3 |

miR-99a-as therapeutic target

miR-99a-5p modulates doxorubicin resistance in breast cancer via COX-2/ABCG2 axis: from the discovery to *in vivo* studies using nanoparticles as carriers.

Iris Garrido-Cano[a,b], Anna Adam-Artigues[a], Ana Catarina Trigo Lameirinhas[a], Juan F. Blandez[b,c,d,e], Vicente Candela-Noguera[c], Federico Rojo[f,g], Sandra Zazo[g], Juan Madoz-Gúrpide[g], Ana Lluch[a,f,h,i], Felix Sancenón[b,c,d,e], Juan Miguel Cejalvo[a,f,h], Ramón Martínez-Máñez[b,c,d,e], Pilar Eroles[a,f,i]

[a]Biomedical Research Institute INCLIVA, 46010 Valencia, Spain.

[b]CIBER de Bioingeniería, Biomateriales y Nanomedicina (CIBER-BBN), 28029 Madrid, Spain,

[c]Instituto Interuniversitario de Investigación de Reconocimiento Molecular y Desarrollo Tecnológico (IDM), Universitat Politècnica de València, Universitat de València, 46010 Valencia, Spain.

[d]Unidad Mixta UPV-CIPF de Investigación en Mecanismos de Enfermedades y Nanomedicina, 46022 Valencia, Spain.

[e]Unidad Mixta de Investigación en Nanomedicina y Sensores. Universitat Politècnica de València, IIS La Fe, 46026 Valencia, Spain

[f]Centro de Investigación Biomédica en Red de Cáncer (CIBERONC), 46010 Valencia, Spain. Universitat de València, Valencia, Spain.

[g]Department of Pathology, Instituto de Investigación Sanitaria de la Fundación Jiménez Díaz, 28015 Madrid, Spain

[h]Clinical Oncology Department, Hospital Clínico Universitario de Valencia, 46010 Valencia, Spain.

[i]Universitat de València, 46010 Valencia, Spain

Submitted

3.1 Abstract

BACKGROUND

Despite the advances in breast cancer targeted therapies, cytotoxic chemotherapy is still widely used alone or in combination with other drugs. Around 20-30% of breast cancer patients develop metastasis after treatment as a consequence of drug resistance. In this context, microRNAs have emerged as potential therapeutic targets to overcome therapy resistance.

METHODS

microRNA expression profile of *wild type* and acquired doxorubicin-resistant MDA-MB-231 (MDA-MB-231R) cell lines were compared by microRNA array analysis, thus identifying miR-99a-5p downregulated in MDA-MB-231R cells. The correlation between miR-99a-5p expression and breast cancer patients' distant relapse-free survival and overall survival was evaluated *in silico*. Potential targets were identified from mRNA array of MDA-MB-231R and MDA-MB-231 and evaluated by luciferase reporter gene assays. The effect of microRNA and genes modulation were evaluated by IC_{50} determination, qRT-PCR, western blot, and flow cytometry. Besides, mesoporous silica nanoparticles-based nanodevices containing a combination of miR-99a-5p and doxorubicin and coated with polyethyleneimine and hyaluronic acid were designed and tested *in vitro* and in a murine orthotopic breast cancer model.

RESULTS

miR-99a-5p was found downregulated in breast cancer cells with acquired resistance to doxorubicin and correlates with poor clinical

outcomes in patients. Functional studies demonstrated that overexpression of miR-99a-5p increases sensitivity to doxorubicin through direct inhibition of COX-2, which induces downregulation of ABCG2. To translate this finding, we developed a nanodevice based on mesoporous silica nanoparticles for specific co-delivery of miR-99a-5p and doxorubicin into breast tumors. We confirmed the efficacy of the nanodevice to reduce tumor growth, cellular proliferation, and doxorubicin-induced cardiotoxicity in an *in vivo* model.

CONCLUSION

Altogether, our findings demonstrate that miR-99a-5p is a novel tumor suppressor that increases sensitivity to doxorubicin through the regulation of COX-2 and ABCG2. Our results suggest that a combination of miR-99a-5p and doxorubicin is a potential therapeutic strategy to increase chemotherapy efficacy in breast cancer.

3.2 Introduction

Breast cancer (BC) is the most commonly diagnosed cancer and the fifth cause of cancer-related death worldwide [1]. Classically, BC tumors have been classified according to the expression of estrogen receptor (ER), progesterone receptor (PR), and human epidermal growth factor receptor 2 (HER2), which determines the prognosis of patients and their treatment. Several targeted therapies are available for luminal or HER2-positive BC patients who express one or more of these biomarkers. However, cytotoxic chemotherapy is the only option for triple-negative BC (TNBC) patients that lack expression of ER, PR, and HER2. Chemotherapy is also given in combination with other cytotoxic drugs as well as with endocrine and anti-HER2 therapies to treat luminal and HER2-positive patients [2,3]. Despite the

improvement in BC treatment during the last years, around 20-30% of patients relapse with metastatic disease as a consequence of resistance to therapies [4]. Once metastatic recurrence occurs, the 5-year survival rate is approximately 25% [5].

Regarding chemotherapy resistance, microRNAs (miRNAs) have gained attention in recent years. These are epigenetic regulators that inhibit the translation of target mRNAs through binding their 3'UTR region and are dysregulated in most types of cancer including BC, where can present oncogenic or suppressor functions and modulate processes such as proliferation, metastasis, or drug sensitivity [6,7].

This work aimed to elucidate the molecular mechanisms underlying resistance to the widely used cytotoxic drug doxorubicin. Herein, we describe the role of miR-99a-5p in doxorubicin response and its molecular mechanism of action. Furthermore, we developed a nanoparticle-based delivery system to simultaneously provide miR-99a-5p and doxorubicin and tested its efficacy in an *in vivo* BC model.

3.3 Materials and methods

3.3.1 Cell culture

MDA-MB-231, MDA-MB-468, HEK293T, and OE19 cells were obtained from American Type Culture Collection (ATCC). MDA-MB-231R cells with acquired resistance to doxorubicin were provided by Dr. Federico Rojo (Fundación Jiménez Díaz, Madrid). MDA-MB-231, MDA-MB-231R, MDA-MB-468, and HEK293T were cultured in DMEM/F-12 medium (Gibco) supplemented with 10% (v/v) fetal bovine serum (FBS) (Gibco) and 1% (v/v)

penicillin-streptomycin (10,000 U/mL) (Gibco), and OE19 were cultured in RPMI (Gibco) supplemented with 10% (v/v) FBS, 1% L-glutamine (Gibco) and 1% (v/v) penicillin-streptomycin (10,000 U/mL) (Gibco). All cell lines were maintained at 37°C in a humidified atmosphere containing 5% CO_2.

3.3.2 miRNA and mRNA arrays, and data analysis

miRNA and mRNA expression profiles were determined using Affymetrix GeneChip miRNA 4.0 and Clariom S human arrays, respectively. Background subtraction and normalization were performed. Two-fold or larger change was set as a threshold of significant difference. Expression differences were calculated with the Affymetrix Transcriptome Analysis Console using One-Way Between-Subject ANOVA (unpaired) test.

3.3.3 RNA extraction, reverse transcription, and quantitative real-time PCR

Total RNA was extracted from cells using Trizol reagent (Invitrogen). Retrotranscription was carried out using TaqMan MicroRNA Reverse Transcription Kit (Thermo Fisher Scientific) for miRNAs analysis, or High-Capacity cDNA Reverse Transcription Kit (Thermo Fisher Scientific) for genes analysis. miR-99a-5p (ID: 000435), *COX*-2 (Hs00153133_m1), *ABCG2* (Hs01053790_m1), and *MKI67* (Hs04260396_g1) were analyzed by quantitative real-time PCR (qRT-PCR) using Taqman Assays (Thermo Fisher Scientific). RNU43 (ID: 001095) and *GAPDH* (Hs03929097_g1) were used to normalize the expression of miRNAs and genes, respectively. For cardiotoxicity assessment, *myh7* (Mm00600555_m1) and *gapdh* (Mm99999915_g1) Taqman Assays (Thermo Fisher Scientific) were used. Relative expression was calculated using the $2^{-\Delta\Delta Ct}$ method.

3.3.4 Patient's data acquisition and analysis

The miRNA expression data of GSE22216 is available in the repository Gene Expression Omnibus (GEO, https://www.ncbi.nlm.nih.gov/geo/) of the National Center for Biotechnology Information (NCBI). miRNA expression was determined in 210 tumor samples from BC patients by using the Illumina Human v1 MicroRNA expression BeadChip. Raw data of microarray was analyzed using the online tool GEO2R (https://www.ncbi.nlm.nih.gov/geo/geo2r/). Samples were divided into disease-free or patients who experienced distant relapse, and differential expression data was obtained. An FDR adjusted *p*-value < 0.05 was considered significant.

The correlation of miR-99a-5p expression in BC primary tumor tissue with overall survival (OS) was analyzed in METABRIC and TCGA datasets using the Kaplan-Meier Plotter tool (https://kmplot.com/analysis/)[8]. The samples were split into two groups according to the expression of miR-99a-5p (auto-selected best cut-off). The log-rank *p*-value and hazard ratio with the 95% confidence intervals were calculated.

3.3.5 Cell transfection

Cell transfections were carried out using Lipofectamine 2000 (Invitrogen) according to manufacturer's protocol. miR-99a-5p mimic (MC10719), scramble miRNA (4464058), COX-2 short interfering RNAs (siRNAs) (s11474 and s11472), and siRNA negative control (4390843), were purchased from Invitrogen and transfected at 50 nM. The transfection efficiency was assessed by qRT-PCR at 72 hours.

3.3.6 Apoptosis analysis

8×10^3 transfected cells were seeded in 96-well plates and treated with doxorubicin 0.5 µM (Pfizer) for 48 hours. Untreated cells were included as a control. After treatment, cells were stained with FITC annexin V (Immunostep) as recommended by the manufacturer. Samples were acquired using BD LSRFortessa (BD Biosciences), and data were analyzed using FlowJo V10 (FlowJo, LLC).

3.3.7 IC_{50} determination

8×10^3 transfected cells were seeded in 96-well plates and treated with increasing concentrations of doxorubicin (Pfizer) for 48 hours. Untreated cells were included as a control. Cell proliferation was assessed using WST-1 assay (Abcam). Optical density was measured at 450 nm with background correction at 650 nm using the microplate reader Spectra Max Plus (Molecular Devices).

3.3.8 miRNA-target prediction

The tool miRWalk 2.0 (http://zmf.umm.uni-heidelberg.de/apps/zmf/mirwalk2/) was used to predict targets of miR-99a-5p. 3'UTR with a minimum seed length of 7 nucleotides and $p < 0.05$ were identified. Twelve dataset algorithms were included: miRWalk, MicroT4, miRanda, miRBridge, miRDB, miRMap, miRNAMap, PICTAR2, PITA, RNA22, RNAhybrid, and Targetscan.

3.3.9 Western blot

96 hours after transfection, cells were collected, lysed, and sonicated in RIPA buffer with protease and phosphatase inhibitors (ThermoFisher Scientific). Proteins were separated by SDS-PAGE, and transferred to a nitrocellulose membrane (Bio-Rad). After blocking, membranes were incubated with primary antibodies to γH2AX (9718, Cell Signaling), cleaved PARP (5625, Cell Signaling), GAPDH (ab8245, Abcam), COX-2 (35-8200, ThermoFisher Scientific), ABCG2 (4477, Cell Signaling), or CD44 (3570, Cell Signaling) and secondary antibodies anti-mouse (7076, Cell Signaling) or anti-rabbit (7074, Cell Signaling). Proteins were detected using Pierce ECL Western Blotting Substrate or SuperSignal West Femto Maximum Sensitivity Substrate (ThermoFisher Scientific) in ImageQuant Las 4000 (GE Healthcare).

3.3.10 Luciferase reporter assay

The COX-2 3'UTR (NM_000963.2) and ABCG2 3'UTR (NM_004827.2) were cloned into pEZX-MT06 vectors (Genecopoeia). HEK293T cells were co-transfected with miR-99a-5p or scrambled control (100 nM) and a vector containing 3'UTR or pEZX-MT06 control vector (5 ng/µL). After 24 hours, cells were lysed and luciferase activity was determined by using the Luc-Pair Duo-Luciferase Assay Kit 2.0 (Genecopoeia) in a LUMIstar Omega (BMG Labtech). Relative luciferase activity was calculated relative to scrambled miRNA.

3.3.11 Doxorubicin intracellular accumulation analysis

72 hours after transfection, cells were incubated with doxorubicin 5 µM for 3 hours at 37°C. Then, cells were washed and intracellular accumulation was evaluated by fluorescence microscopy (DMI3000, Leica).

Mean fluorescence intensity (MFI) per cell was analyzed using Image J Software (version 1.51h, NIH) and normalized as a percentage of the negative control. A minimum of 400 cells were analyzed for each condition.

3.3.12 ABCG2 activity analysis

The activity of ABCG2 was evaluated by determining the efflux of Pheophorbide A. Cells were incubated with 10 µM Pheophorbide A for 30 minutes at 37°C. MFI was determined by flow cytometry in BD LSRFortessa X-20 (BD Biosciences, USA) at 640 nm (excitation)/670-730 nm (emission) at initial time (MFI_0) and after 90 minutes of incubation in Dulbecco's Phosphate Buffered (DPBS) at 37°C (MFI_{90}). Data were processed using FlowJo V10 (FlowJo, LLC). Pheophorbide efflux was expressed as a percentage of MFI_0.

3.3.13 Synthesis of mesoporous silica nanoparticles

Cetyltrimethylammonium bromide (CTAB, 1 g, 2.74 x 10^{-3} mol, Sigma) was dissolved in 480 mL of deionized water. Aqueous NaOH (3.5 mL, 2 M in deionized water, Sigma) was added and the temperature was adjusted to 80°C. The silica source tetraethylorthosilicate (TEOS, 5 mL, 2.57 × 10^{-2} mol, Sigma) was then added to the surfactant solution. The mixture was stirred for 2 hours at 80°C to obtain a white precipitate (as-synthesized MSNs), which was isolated by centrifugation (10,000 xg, 20 minutes), washed with deionized water until reaching neutral pH, and dried at 60°C. As-synthesized MSNs were calcined at 550°C using an oxidant atmosphere for 5 hours to remove the CTAB template, obtaining the surfactant-free final MSNs.

For doxorubicin loading, 300 mg of MSNs were suspended in 10 mL of a water solution of doxorubicin (Carbosynth, 15 mg/mL) and stirred for 24

hours at room temperature. The suspension was centrifuged (10,000 xg, 20 minutes) to recover nanoparticles and the loaded solid was dried. 70 mg of the loaded solid were resuspended in a mixture of 5 mL of PBS 41x, and 50 mg of branched polyethyleneimine (PEI, Mw= 25KDa, Sigma), and stirred for 3 hours at room temperature. After that, solids were isolated by centrifugation (10,000 xg, 20 minutes), resuspended in a water solution of miR-99a-5p (3.5 mL, 10 μM), and stirred. To obtain control nanoparticles, miRNA was not added in this step. After 30 minutes, a water suspension of HA was added to the mixture (3.5 mL, 0.5 mg/mL, Sigma). The mixture was stirred for 3 hours at room temperature and the resulting solid was recovered by centrifugation (10,000 xg, 20 minutes), washed several times with water, and dried. NP-dox-miR99a and NP-dox were obtained. Unloaded MSN scaffolds were employed to obtain blank NPs and NP-miR99a.

3.3.14 Characterization of nanoparticles

Transmission electron microscopy (TEM) images were taken at 200 kV in a JEOL JEM-1010 (JEOL Europe SAS) microscope equipped with an X-ray detector. Powder X-ray diffraction (PXRD) patterns were obtained by a diffractometer using Cu-Kα radiation (D8 Advance, Philips). Porosity of materials was assessed by N_2 adsorption-desorption isotherms recorded with a Micromeritics ASAP 2010 automate desorption analyzer (Micromeritics Instrument Corporation). Samples were degassed at 120 °C in vacuum overnight. Pore size was determined following the Barret-Joyner-Halenda (BJH) method. The specific surface areas were determined from the adsorption data in the low pressures range using the Brunauer-Emmett-Teller (BET) model. Thermogravimetric analyses (TGA) were performed using TGA/SDTA 851e (Mettler Toledo), in an oxidant atmosphere (air, 80 mL/min)

with a heating program consisting of a heating rate of 10°C/minute from 25°C to 100°C, an isothermal heating step at 100°C for 60 minutes, a heating rate of 10°C/minute 100°C to 1000°C, and an isothermal heating step at this final temperature for 30 minutes. Dynamic light scattering (DLS) measurements were carried out in a Malvern Zetasizer Nano ZS. Fourier-transform infrared (FTIR) measurements in the 4000–400 cm^{-1} rang were taken by a Nicolet 6700 (Thermo scientific).

3.3.15 Cargo release studies

1 mg of NP-dox-miR99a were suspended in 1 mL of deionized water and divided into two aliquots of 0.5 mL. Then, either 1 mL of lysosomal extract (obtained from rabbit liver by using LYSISO1, Sigma) or 1 mL of PBS was added. The obtained suspension was stirred for 3 hours, and during this period some aliquots of 150 µL were collected at scheduled times and centrifuged at 13,000 rpm for 2 minutes. The supernatant was analyzed to monitor the cargo release by determining the emission band of doxorubicin centered at 557 nm (λexc = 480 nm) in a JASCO FP-8300 spectrophotometer.

3.3.16 CD44 expression evaluation by flow cytometry

1 x 10^6 MDA-MB-231 and OE19 cells were incubated with phycoerythrin-conjugated monoclonal antibody against human CD44 (550989, BD Biosciences) according to manufacturer's instructions for 30 minutes. An isotype control (555749, BD Biosciences) was used as negative control. Cells were washed and analyzed using flow cytometer BD LSRFortessa (BD Biosciences).

3.3.17 Nanoparticles' uptake and competition assay

5 x 10^4 cells were seeded in cover glass slides (Ibidi GMBH) and treated with NP-dox-miR99 (25 µg/mL) for 15 minutes, washed with PBS, and fixed with 4% paraformaldehyde. Nuclei were stained with DAPI (4',6-diamidino-2-phenylindole, 5 µg/ml). Cellular uptake was evaluated by confocal microscopy (TCS SP2, Leica). For competition assay, MDA-MB-231 cells were treated with HA (5 mg/ml) for 30 minutes and washed with PBS before adding NP-dox-miR99. MFI per cell was determined using Image J Software (version 1.51h, NIH) and normalized to MDA-MB-231. A minimum of 200 cells per condition were analyzed.

3.3.18 *In vivo* experiments

1.6 x 10^6 MDA-MB-231 cells were injected into the mammary fat pad of 6- to 8-week-old female BALB/C nude mice (Charles River Laboratories). Once tumors were palpable, mice were randomly divided into 6 groups of 10 animals and treated separately with PBS, 10 mg/kg of nanoparticles, or 1.6 mg/kg of free doxorubicin three times per week for one month. Tumors were measured two times per week and tumor volume was calculated as $(D x d^2)/2$, where D and d are the longest and the shortest diameters, respectively. Relative tumor volume was calculated. Mice were sacrificed two days after the last treatment, or when they met the institutional euthanasia criteria for tumor size or overall health condition. Tumor, kidney, lungs, spleen, and liver were collected and frozen at -80°C. Serum samples were also obtained for aspartate aminotransferase (AST), alanine transaminase (ALT), creatinine (CRE), and urea (URE) determination. All experiments were approved by the Institutional Review Board of INCLIVA (2020/VSC/PEA/0131).

3.3.19 Silicon biodistribution analysis

For silicon (Si) detection, tissues were weighted and digested into 1 mL of tetramethylammonium hydroxide solution (TMAH, 25% (v:v) in water, Sigma) in polytetrafluoroethylene (PTFE) vials at 80°C for 2 hours in a digestion unit Bloc digest 20 (Selecta). Then, samples were diluted in Milli-Q water (1:10), filtered with 0.45 µm Nylon filters, and kept in polystyrene tubes. Si determination was performed by inductively coupled plasma mass spectroscopy (ICP-MS) in an Agilent 7900 in H2 mode.

3.3.20 Immunohistochemistry

Automated immunohistochemical staining of Ki-67 was performed using BenchMark XT (Ventana) with UltraView Universal DAB Detection Kit (0526980600, Roche) and Ki-67 antibody (790-4286, Roche).

3.3.21 Statistical analyses

All statistical analyses were performed using the GraphPad Prism 6.0. Student's t-test was conducted to compare two groups. Data in abnormal distribution were analysed by Mann-Whitney U Test. $p < 0.05$ was considered statistically significant.

3.4 Results

3.4.1 miR-99a-5p is downregulated in doxorubicin-resistant breast cancer cells

To explore the key miRNAs involved in resistance to doxorubicin, the miRNAs expression profile of MDA-MB-231R cells with acquired resistance to doxorubicin, and their parental cell line MDA-MB-231 were compared. We found 11 significantly dysregulated miRNAs with a fold change higher than 2. Among them, miR-99a-5p was identified as the most differentially expressed miRNA. It was upregulated in sensitive cells with a fold change of 17.83 (p=0.0273) compared to MDA-MB-231R (**Figure 1A, B**). Furthermore, miR-99a-5p determination by qRT-PCR in MDA-MB-231R and MDA-MB-231 confirmed its downregulation in doxorubicin-resistant cells (**Figure 1C**).

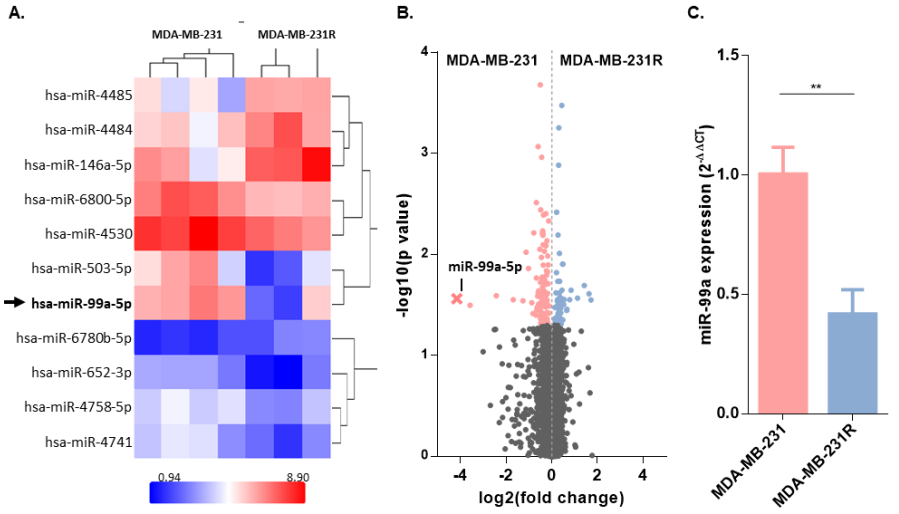

Figure 1. miR-99a-5p is downregulated in doxorubicin-resistant cells. A. Heat map and hierarchical clustering of miRNAs that are differentially expressed between MDA-MB-231 and MDA-MB-231R. Expression of miRNAs was analyzed by Affymetrix GeneChip miRNA 4.0. Cut-off ± 2 fold change was applied. miRNAs are represented in rows and samples are represented in columns. B. Volcano plot representing array results. Red dots represent miRNAs significantly upregulated in MDA-MB-231, blue dots represent miRNAs significantly upregulated in MDA-MB-231R, and cross symbol represents miR-99a-5p. C. miR-99a-5p expression in MDA-MB-231 and MDA-MB-231R by qRT-PCR. Mean ± SD. $^{**}p < 0.01$.

3.4.2 miR-99a-5p overexpression associates with better clinical prognosis in breast cancer patients

In a previous study, we determined that miR-99a-5p is downregulated in BC tissues when compared to healthy breast tissues [9]. Based on this,

herein we examined the association between its expression and distant-relapse free survival (DRFS) in a dataset containing miRNAs expression data from 210 breast tumors (GSE22216) [10] to determine the clinical relevance of miR-99a-5p expression levels in BC. Significantly dysregulated miRNAs between patients who experienced distant relapse (n=79) and patients free of progression (n=131) were identified (**Figure 2A**). Among them, miR-99a-5p was found upregulated in disease-free patients (fold change = 1.7238; p = 0.0193). In addition, low miR-99a-5p expression was significantly associated with shorter DRFS ($p < 0.0037$; **Figure 2B**). To further validate the correlation of miR-99a-5p with clinical outcome, its association with OS of BC patients was assessed in METABRIC (n=1262) and TCGA (n=1062) cohorts, confirming that low expression significantly associates with poor prognosis, which is consistent with the previous results (**Figure 2C, D**).

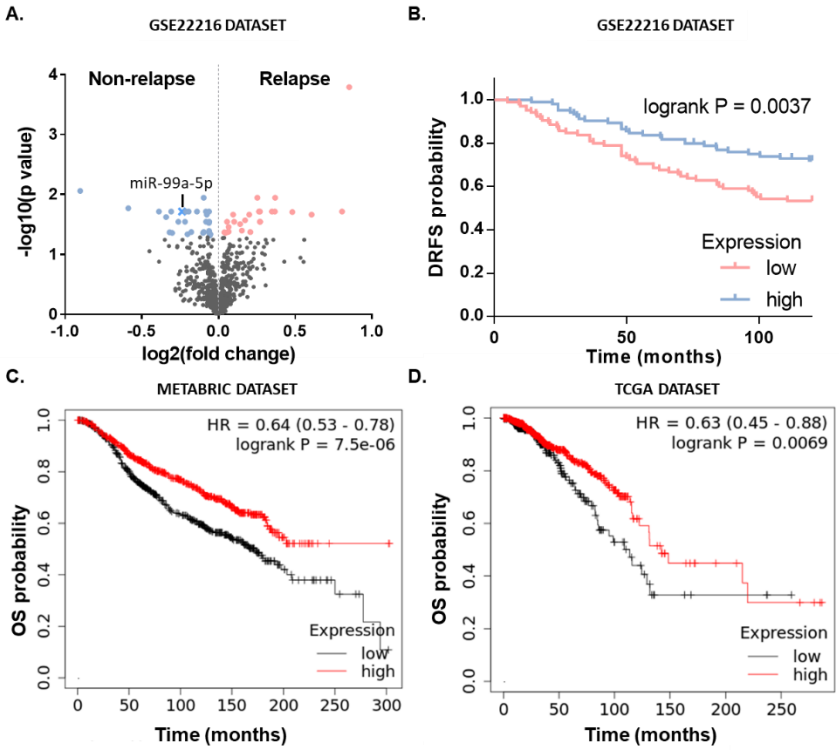

Figure 2. High miR-99a-5p levels are associated with better clinical prognosis in BC patients. A. Expression of miRNAs was analyzed in 210 tumor samples from BC patients by Illumina Human v1 MicroRNA expression BeadChip (GSE22216). Volcano plot representing array results. Red dots represent miRNAs significantly upregulated in patients who experienced distant relapse, blue dots represent miRNAs significantly upregulated in samples from patients free of progression, and cross symbol represents miR-99a-5p. B. DRFS Kaplan–Meier plot based on the expression of miR-99a-5p in GSE22216. Patients were divided into high (blue) or low (red) miR-99a-5p expression by median. Log-rank test *p*-value is shown. C, D. OS Kaplan–Meier plot based on the expression of miR-99a in METABRIC (C), and TCGA (D) datasets. Patients were divided into high (red) or low (black) expression by the optimal cut-off. Log-rank test P-values are shown; HR, hazard ratio.

3.4.3 miR-99a-5p regulates doxorubicin response *in vitro*

To test the hypothesis that miR-99a-5p has a role in regulating doxorubicin sensitivity, we investigated the effect of miR-99a-5p overexpression in cytotoxicity induced by doxorubicin in MDA-MB-231 and MDA-MB-231R cells transfected with scrambled miRNA or miR-99a-5p. Overexpression of miR-99a-5p significantly decreased doxorubicin IC_{50} value in both MDA-MB-231 ($p = 0.0007$) and MDA-MB-231R ($p < 0.0001$) cell lines (**Figure 3A**). Besides, apoptosis analysis revealed that miR-99a-5p alone does not affect apoptosis, but significantly increases the doxorubicin-induced apoptosis in MDA-MB-231 and MDA-MB-231R cells (**Figure 3B, C**). Furthermore, the effect of miR-99a-5p on doxorubicin-induced DNA damage and apoptosis was also assessed by western blot. Our results confirmed that miR-99a-5p increases doxorubicin-induced cleaved PARP, which is a marker of apoptosis. Besides, levels of phosphorylation of histone H2AX in Ser139 (γH2AX) (indicators of DNA damage) displayed an increment in cells overexpressing miR-99a-5p upon treatment with doxorubicin (**Figure 3D**). Overall, our data suggest that miR-99a-5p sensitizes BC cells to doxorubicin.

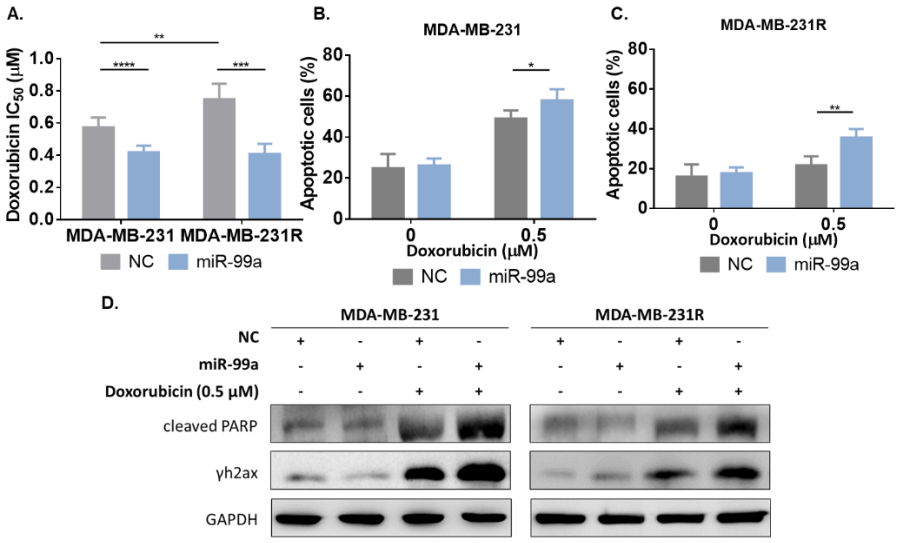

Figure 3. Overexpression of miR-99a-5p increases doxorubicin sensitivity. MDA-MB-231 and MDA-MB-231R were transfected with scrambled miRNA (NC) or miR-99a-5p (miR-99a). A. WST-1 assay was performed to determine the doxorubicin IC_{50} value after 48 hours. Mean ± SD B,C. MDA-MB-231 (B) and MDA-MB-231R (C) cells were treated with 0.5 μM doxorubicin for 48 hours and apoptosis was evaluated by flow cytometry after FITC Annexin V staining. Untreated cells were included as a control. Mean±SD. D. Doxorubicin induction of PARP cleavage and H2AX phosphorylation of the Ser-139 (γH2AX) (0.5 μM, 48 hours), measured by western blot. *$p < 0.05$; **$p < 0.01$, ***$p < 0.001$, ****$p < 0.0001$.

3.4.4 miR-99a-5p regulates doxorubicin sensitivity by directly targeting COX-2

To shed the light on the molecular mechanism by which miR-99a-5p sensitizes cells to doxorubicin, a microarray was performed to compare the mRNA expression profile of MDA-MB-231R and MDA-MB-231. To find potential targets of miR-99a-5p, the mRNAs significantly upregulated in MDA-MB-231R cells with a fold change higher than two were selected (**Figure 4A**) and compared with the resulting predicted targets of miR-99a-5p from miRWALK2.0 software to identify potential targets of miR-99a-5p that are upregulated in MDA-MB-231R cells (Supplementary Table S1). We identified *COX-2* (cyclooxygenase-2, also known as *PTGS2*) as the potential target with the highest differential expression between cell lines (fold change=4.94; *p*=0.0013) (**Figure 4B**). Furthermore, the upregulation of COX-2 in MDA-MB-231R was confirmed by western blot (**Figure 4C**).

COX-2 is a protein widely known for its role in inflammation, but it has also been described to be involved in tumorigenesis and drug resistance [11]. Based on our results, we hypothesized that miR-99a-5p could modulate sensitivity to doxorubicin through COX-2 regulation. To address this hypothesis, we first confirmed that miR-99a-5p overexpression inhibits *COX-2* in MDA-MB-231 cells at mRNA and protein levels (**Figure 5A, B**). Second, we investigated whether *COX-2* is a direct target of miR-99a-5p. The interaction between the miRNA and the 3'UTR region of its potential target was assessed by the luciferase reporter gene assay. Co-transfection of miR-99a-5p and the plasmid containing the luciferase reporter gene driven by the human COX-2 3'UTR region suppressed the expression of the reporter gene when compared to cells co-transfected with the plasmid and scrambled

miRNA (**Figure 5C**). When the reporter plasmid was replaced by a control plasmid, no effect of miR-99a-5p was observed, thus confirming that miR-99a-5p directly interacts with the COX-2 3'UTR.

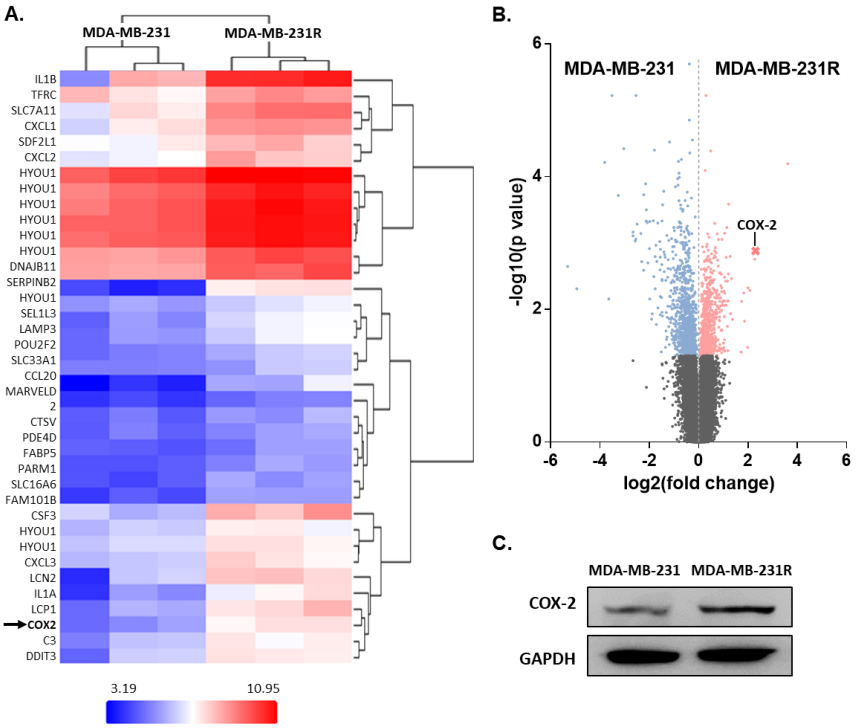

Figure 4. COX-2 is upregulated in doxorubicin-resistant cells. A. Heat map and hierarchical clustering of mRNAs that are differentially expressed between MDA-MB-231R and MDA-MB-231. Expression of mRNAs was analyzed by Affymetrix Clariom S array. Cut-off ± 2-fold change was applied. B. Volcano plot representing array results. Red dots represent mRNAs significantly upregulated in MDA-MB-231R, blue dots represent mRNAs significantly upregulated in MDA-MB-231, and cross symbol represents COX-2. C. COX-2 protein expression in MDA-MB-231 and MDA-MB-231R determined by western blot.

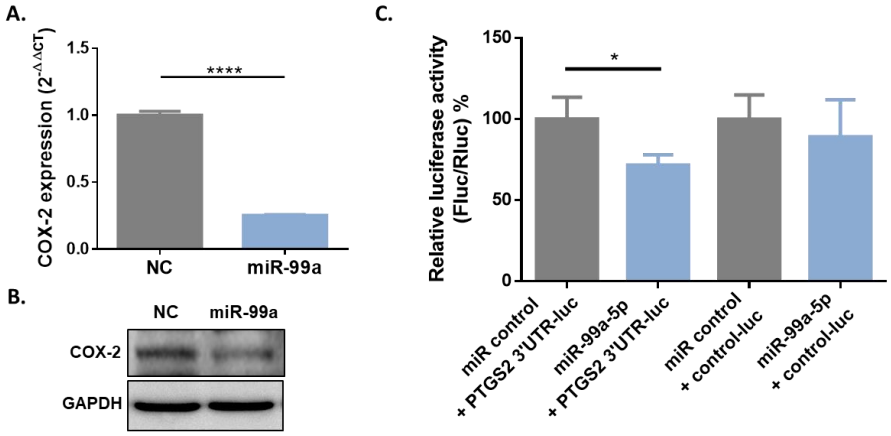

Figure 5. miR-99a-5p directly targets COX-2. MDA-MB-231 cells were transfected with miRNA (NC) or miR-99a-5p mimics (miR-99a), and expression levels of COX-2 were evaluated by qRT-PCR (A), and western blot (B). C. Luciferase activity assays of HEK293T cells co-transfected with miR-99a-5p or scrambled control and the luciferase vector containing 3'UTR of COX-2 or control luciferase vector. Mean ± SD. *$p < 0.05$; ****$p < 0.0001$.

Third, to assess the role of COX-2 as a mediator of the miR-99a-5p's effect on doxorubicin sensitivity, it was inhibited in MDA-MB-231 cells by two siRNAs, and cells were treated with doxorubicin. Doxorubicin IC_{50} values were significantly reduced in MDA-MB-231 cells with COX-2 knockdown compared to the parental cell line (**Figure 6A**). Moreover, a significant increase in apoptosis in COX-2-depleted cell lines after doxorubicin treatment was confirmed by flow cytometry (**Figure 6B**). In addition, apoptosis and DNA damage assessed by western blot showed that COX-2 inhibition induced an increment in cleaved PARP and γH2AX levels (**Figure 6C**). Therefore, our results confirm that COX-2 downregulation sensitizes BC cells to doxorubicin.

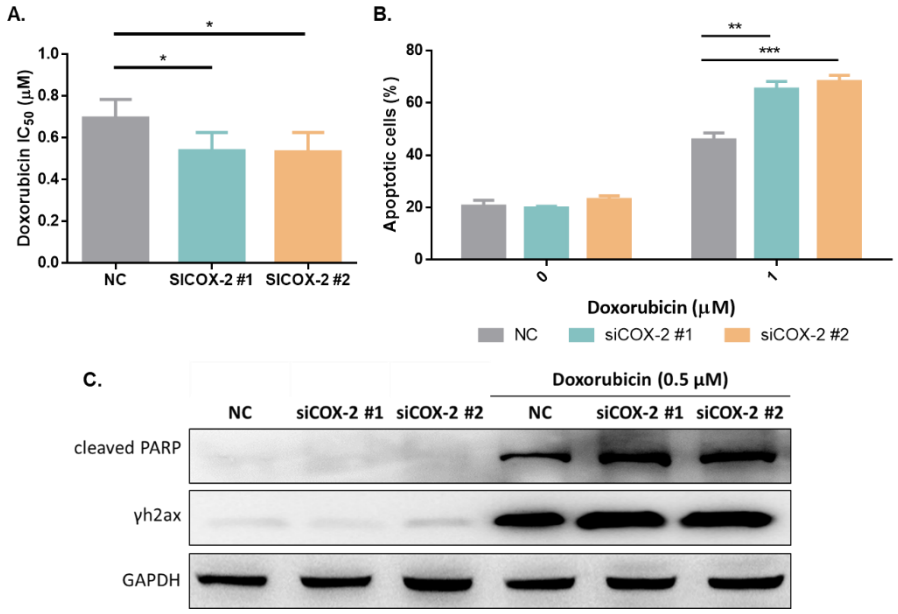

Figure 6. silencing of COX-2 increases sensitivity to doxorubicin. MDA-MB-231 cells were transfected with silencer negative control (NC) or the COX-2 siRNAs siCOX-2 #1 and siCOX-2 #2. (A) WST-1 assay was performed to determine the doxorubicin IC_{50} value (NC: 0.70 µM, siCOX-2#1: 0.54 µM, siCOX-2#2: 0.53 µM). (B) Cells were treated with 0.5 µM doxorubicin for 48 hours and apoptosis was evaluated by flow cytometry after FITC Annexin V staining. Untreated cells were included as a control. Mean±SD. (C) Induction of PARP cleavage and γH2AX by doxorubicin (0.5 µM, 48 hours), measured by western blot. *$p < 0.05$, **$p < 0.01$; ***$p < 0.001$.

3.4.5 ABCG2 is a downstream target of miR-99a-5p and COX-2

ABCG2 is an ATP-binding cassette (ABC) transporter involved in doxorubicin efflux [12]. Previous works suggested that COX-2 may regulate ABCG2 expression in BC cells [13]. Due to this fact, we hypothesized that ABCG2 could be a downstream target of miR-99a-5p through COX-2. Therefore, we investigated the effect of miR-99a-5p modulation in ABCG2 expression and activity in MDA-MB-231 cells. First, we showed that the miRNA downregulates the expression of ABCG2 at mRNA and protein levels (**Figure 7A, B**). To further confirm our hypothesis, the activity of ABCG2 was evaluated by determining the efflux of the ABCG2 specific substrate pheophorbide A by flow cytometry. In MDA-MB-231 cells overexpressing miR-99a-5p, the pheophorbide A efflux was significantly inhibited to near 1% compared to the 15 % observed in negative control cells **(Figure 7C**). Besides, to confirm the implication of ABCG2 in drug response, doxorubicin intracellular accumulation was also examined by fluorescence microscopy. As expected, cells overexpressing miR-99a-5p presented a significantly higher accumulation of doxorubicin compared to control (**Figure 7D, E**).

Despite ABCG2 3'UTR was listed as a predicted target of miR-99a-5p by miRwalk 2.0, luciferase reporter gene assay showed that there is no interaction between miR-99a-5p and 3'UTR of ABCG2 (**Supplementary Figure S1**). Hence, miR-99a-5p may inhibit ABCG2 expression by an indirect mechanism.

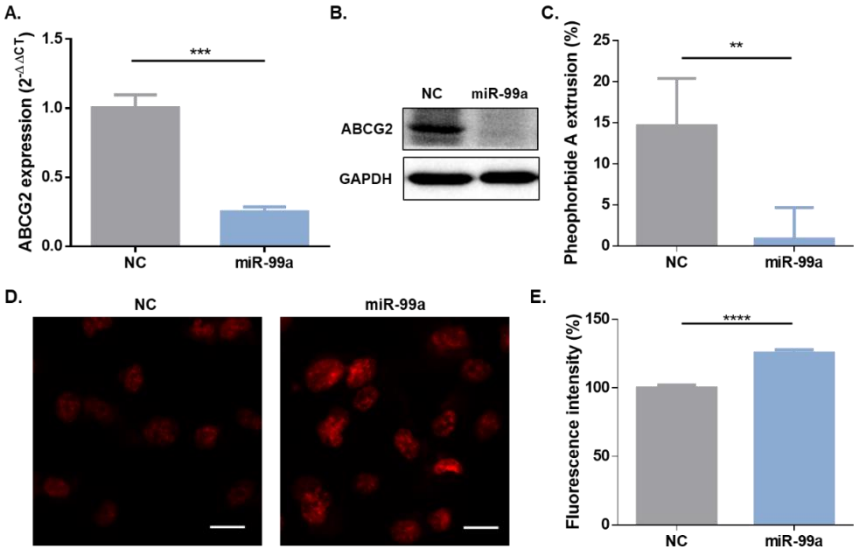

Figure 7. miR-99a-5p inhibits ABCG2 expression. Expression levels of ABCG2 were measured by qRT-PCR (Mean±SD) (A) and western blot (B) upon transfection of scrambled miRNA (NC) or miR-99a-5p mimics (miR-99a) into MDA-MB-231 cells. C. The percentage of pheophorbide A efflux was measured by flow cytometry to evaluate ABCG2 activity. Mean±SD. D, E. After transfection, MDA-MB-231 cells were incubated with doxorubicin 5 µM for 3 hours at 37°C and intracellular accumulation was evaluated by fluorescence microscopy. Representative images (scale bar 20 µm) (D) and graph bar representation of mean fluorescence intensity of doxorubicin (mean±SEM) (E) are shown. $^{**}p < 0.01$; $^{***}p < 0.001$; $^{****}p < 0.0001$.

Therefore, we explored the role of COX-2 as a link between miR-99a-5p and ABCG2. We investigated whether depletion of COX-2 influences ABCG2 expression and activity in MDA-MB-231 cells. Our results confirmed that siRNA-mediated knockdown of COX-2 downregulates ABCG2 at mRNA and protein levels (**Figure 8A, B**). Regarding ABCG2 activity, pheophorbide A

efflux was significantly reduced from approximately 20% in negative control cells until less than 5% in COX-2 knockdown cells (**Figure 8C**). As expected, we confirmed that inhibition of COX-2 increases significantly the intracellular accumulation of doxorubicin (**Figure 8D, E**). Besides, we confirmed the upregulation of ABCG2 in MDA-MB-231R cells (**Supplementary Figure S2**). Collectively, these data suggest that miR-99a-5p increases sensitivity to doxorubicin in part by modulation of ABCG2 through COX-2.

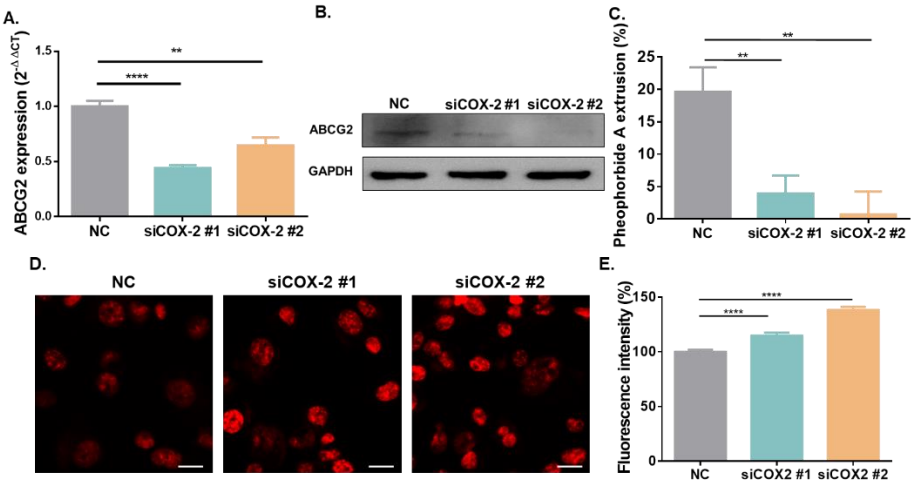

Figure 8. COX-2 regulates ABCG2. Expression levels of ABCG2 were measured by qRT-PCR (A) and western blot (B) upon transfection of scrambled siRNA (NC), and two siRNAs targeting COX-2 (siCOX #1 and siCOX-2 #2) into MDA-MB-231 cells. C. The percentage of pheophorbide A efflux was measured by flow cytometry to evaluate ABCG2 activity. Mean±SD. D. After transfection, MDA-MB-231 cells were incubated with doxorubicin 5 µM for 3 hours at 37°C and intracellular accumulation was evaluated by fluorescence microscopy. Representative images (Scale bar 20 µm) (D) and graph bar representation of mean fluorescence intensity of doxorubicin (mean±SEM) (E) are shown. ** $p < 0.01$; **** $p < 0.0001$.

3.4.6 Nanoparticles targeting breast tumors for co-delivery of doxorubicin and miR-99a-5p

Despite the potential of miR-99a-5p to enhance the efficacy of doxorubicin, miRNAs cannot easily be used as therapeutic strategies, as can be degraded by serum nucleases, and cannot easily enter into cytoplasm due to their physicochemical properties. Therefore, we designed a nanodevice based on MSNs to deliver a combination of miR-99a-5p and doxorubicin to tumor cells. The designed nanodevices consist of MSNs loaded with doxorubicin and capped with three consecutive layers of polyethyleneimine (PEI), miR-99a-5p, and hyaluronic acid (HA) (NP-dox-miR-99a). Empty nanoparticles (control NP), nanoparticles containing miR-99a-5p but not loaded with doxorubicin (NP-miR99a), and nanoparticles containing doxorubicin but not miR-99a-5p (NP-dox) were evaluated as controls. To ensure the efficient controlled delivery of cargo molecules, PEI was included, as this molecule acts as a "proton sponge" and ensures the lysosomal escape, necessary to ensure the delivery of the miRNA into the cytoplasm. Moreover, nanoparticles were coated with HA, which has a dual role. On the one hand, is a biocompatible molecule that will act as a cap inhibiting the release of doxorubicin and miR-99a-5p outside the cell. On the other hand, it will target the HA receptor CD44 that plays an important role in BC drug resistance (**Figure 9, Supplementary Figure S3**)[14].

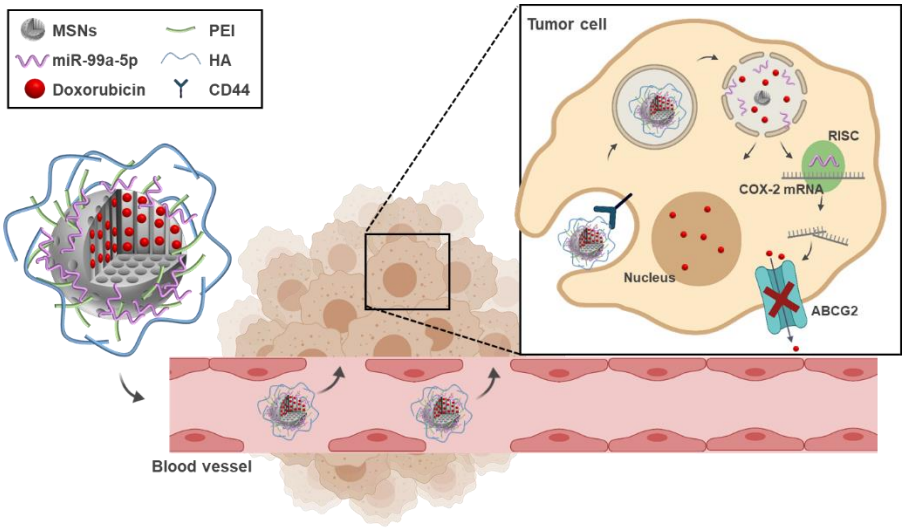

Figure 9: After intravenous injection, NP-dox-miR99a will passively target tumors by EPR effect, where HA will target CD44 receptor. After cellular uptake, PEI induces disruption of lysosomal membranes, thereby delivering the content of nanoparticles into the cytoplasm. Created with BioRender.com.

The synthesized nanoparticles were characterized by PXRD and N_2 adsorption-desorption isotherms (**Supplementary Figures S4-S5**). TEM images show the ordered pore structure before and after treatments and a spherical morphology for the nanoparticles with a diameter of ca. 100 nm (**Supplementary Figure S6**), which was confirmed by determining the nanoparticles' hydrodynamic ratio by DLS (**Supplementary Table S2**). Besides, attenuated total reflectance (ATR) spectra, TGA, and ζ potential were determined to confirm the loading and functionalization of nanoparticles (**Supplementary Figure S7-S8, Supplementary Table S3**). From TGA analysis, we could determine that ca. 70 mg of doxorubicin were encapsulated per gram of nanoparticles (**Supplementary Figure S8**).

Due to the presence of PEI and HA, we hypothesized that nanoparticles would deliver their content in a controlled manner in lysosomes. We confirmed that the NP-dox-miR99a deliver doxorubicin in presence of lysosomal extract, whereas doxorubicin delivery in PBS was very low (15% of the maximum doxorubicin release after 120 min) (**Figure 10A**). This result suggests that nanoparticles will deliver their content after being uptaken by cells, avoiding the delivery of doxorubicin and miRNA in an unspecific manner.

The capacity of the designed nanoparticles to target the CD44 receptor was assessed by two different approaches. On the one hand, nanoparticles uptake by MDA-MB-231 cells with a high expression of CD44 was compared to the uptake of OE19 cancer cells, which have a negligible expression of CD44 (**Supplementary Figure S9**). On the other hand, a competition assay was carried out with the MDA-MB-231 cell line, in which the cells were treated with HA before treatment with nanoparticles, and uptake was compared with control cells. After incubating the cells with the NP-dox-miR99a nanoparticles, their internalization was examined by confocal microscopy, as doxorubicin emits red fluorescence. After 15 minutes incubation, the cytoplasmic red fluorescence in MDA-MB-231 cells evidenced the successful uptake. By contrast, uptake by OE19 and HA-pretreated MDA-MB-231 cells was significantly lower (OE19: ca. 26% of control, $p < 0.0001$; HA-MDA-MB-231: 29% of control, $p < 0.0001$) (**Figure 10B, C**). Our results confirmed the ability of synthesized nanoparticles to specifically target the CD44 receptor.

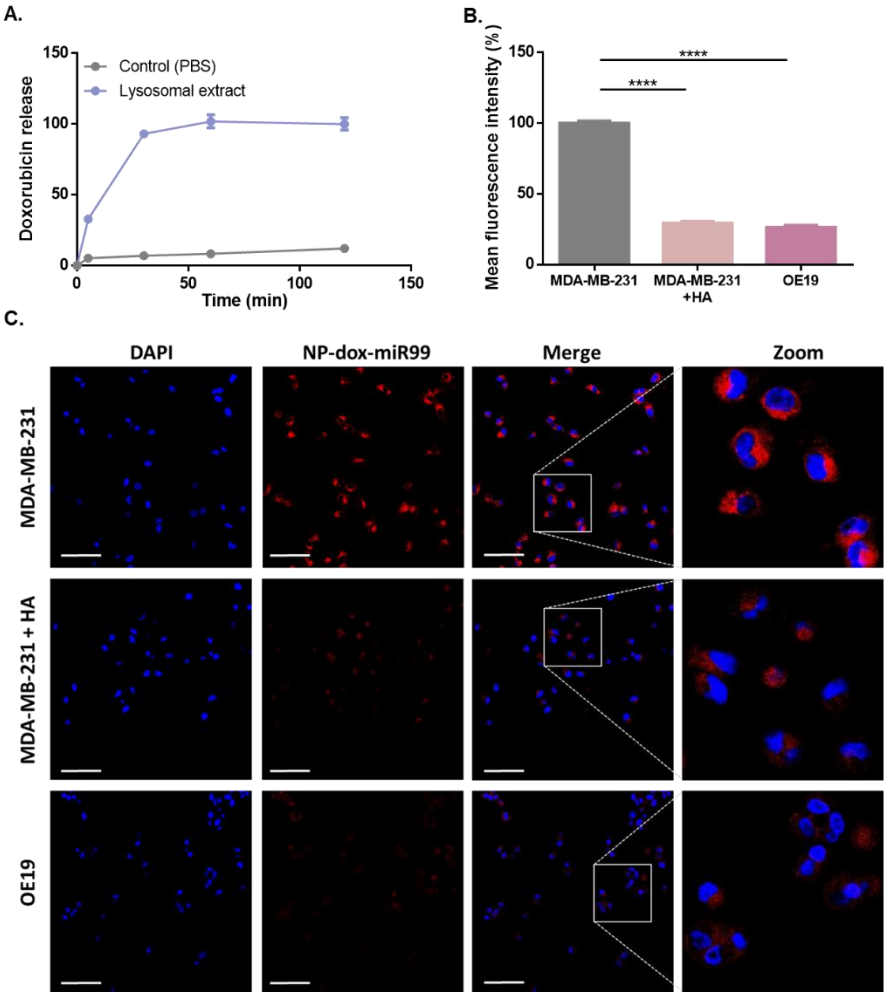

Figure 10: Characterization of NP-dox-miR99a. A. Cargo release study of the NP-dox-miR99a. Doxorubicin release in PBS (grey) or lysosomal extract (blue) at room temperature at the indicated time points. B. Internalization of NP-dox-miR99a in MDA-MB-231, MDA-MB-231 pretreated with HA (5mg/ml) for 30 minutes (MDA-MB-231+ HA), and OE19 cells after 15 minutes exposure to nanoparticles (25µg/mL). Mean red fluorescent intensity (mean ±SEM). ****$p < 0.0001$. C. Representative confocal microscopy images. Scale bars: 75 µm.

3.4.7 Anti-tumor activity of co-delivered doxorubicin and miR-99a-5p by NP-dox-miR99a in an *in vivo* model

We next examined the *in vivo* efficacy of the designed nanodevices in a murine orthotopic xenograft model of BC. Tumour–bearing mice were treated with PBS (vehicle), control NP, NP-miR99a, NP-dox, or NP-dox-miR99a. After one month of treatment, NP-dox-miR99a induced the highest tumor growth inhibition (**Figure 11A**). As shown, control-NP and NP-mir99a had no statistical differences with untreated animals, and the NP-dox showed a significant but moderate capacity to inhibit tumor growth. At endpoint, the tumor volume inhibition rates for NP-dox, and NP-dox-miR99a were 36.27% ($p = 0.02$), and 59.49% ($p < 0.0001$), respectively (**Figure 11B**). Consistently, the NP-dox-miR99a are the most effective in reducing proliferation of tumor cells, as evidenced by immunohistochemical staining and mRNA expression of Ki-67 in tumor sections (**Figure 11C, D**) and Ki-67 expression quantification by qRT-PCR (**Figure 11D**).

To validate the functional effect of miR-99a-5p, we determined the expression levels of their targets COX-2 and ABCG2 in tumor tissue. Consistent with an efficient miR-99a-5p delivery into tumor cells, *COX-2* and *ABCG2* were found downregulated in tumors treated with NP-dox-miR99a when compared to controls (**Figure 11E, F**).

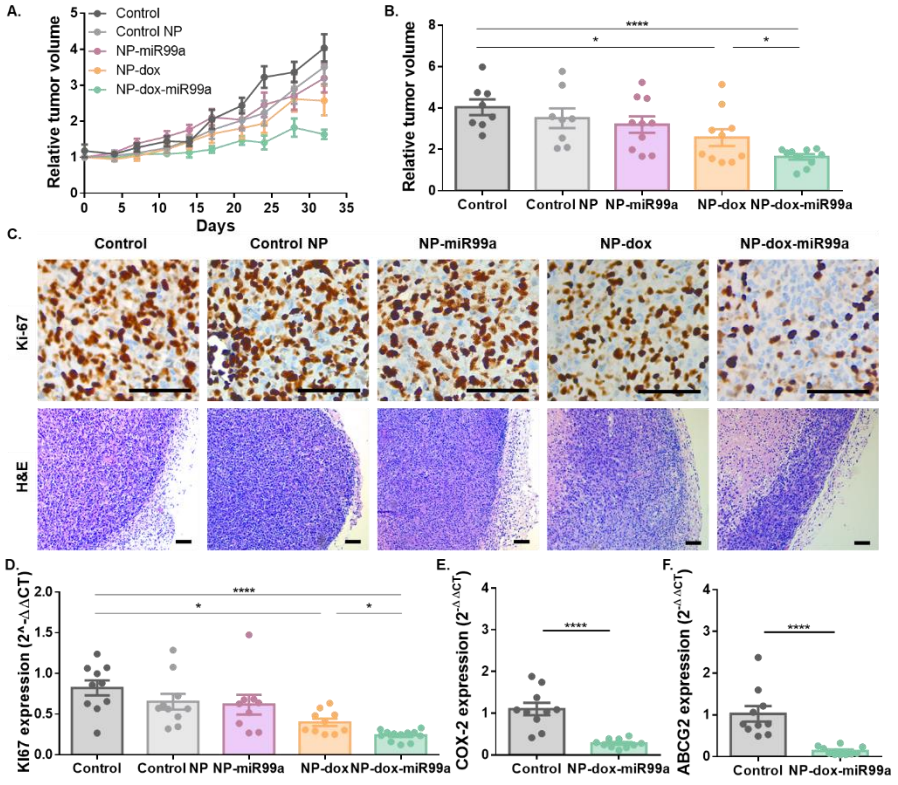

Figure 11. *In vivo* efficacy of NP-dox-miR99a. A, B. MDA-MB-231 were injected into the mammary fat pad of BALB/C mice. When the tumor size reached approximately 50 mm^3, mice (n=10 per group) were treated 3 times per week with 10 mg/kg of nanoparticles for one month. Tumor growth curve (A) and final tumor volume (B). C. Representative images of immunohistochemical staining of Ki-67 and H&E staining of paraffin-embedded xenograft sections. Scale bar: 100 µm. D-F. Ki-67 (D), COX-2 (E), and ABCG2 (F) expression in xenografts determined by qRT- PCR.

We next examined the biodistribution of NP-dox-miR99a. 48 hours after the last dose, the tumors and major organs were harvested for biodistribution quantification. Silicon levels determined by ICP-MS confirmed the ability of nanoparticles to target tumors and were also found in kidney, lungs, spleen, and liver (**Supplementary Figure S10**). The safety of the designed nanodevices was confirmed as they had no impact on body weight (**Supplementary Figure S11**), and hepatic and renal functions (**Supplementary Figure S12**).

Altogether, our results demonstrate that nanoparticles loaded with a combination of doxorubicin and miR-99a-5p are a biocompatible and effective strategy to treat breast cancer.

3.4.8 Nanoformulation protects from doxorubicin-induced cardiotoxicity

Cardiotoxicity is among the most severe adverse effects induced by doxorubicin [15]. In this context, nanoparticles impede the delivery of loaded doxorubicin upon their internalization in the targeted tissue, thus decreasing the required chemotherapy dose, and decreasing its side effects. In this scenario, we hypothesized that cardiotoxic effects could be reduced by treating breast tumors with NP-dox-miR99a in comparison to free doxorubicin. To investigate this, we treated a group of mice with 1.6 mg/kg of free doxorubicin 3 times per week based on previous works [16,17] in parallel to those treated with NP-dox-miR99a. The equivalent dose of administered doxorubicin in nanoparticles was ca. 0.7 mg/kg. First, we observed that to obtain a similar tumor growth inhibition (**Supplementary Figure S13**), the dose of doxorubicin loaded into the NP-dox-mir99a was ca. 44% of free drug dose, thus evidencing the ability of nanoparticles to

diminish the required dose of doxorubicin. Besides, higher levels of the marker of cardiac atrophy myosin heavy chain β (MHC-β, *myh7*), and the presence of cytoplasmic vacuoles in cardiac tissue evidenced that free doxorubicin induces cardiotoxicity, whereas NP-dox-miR99a did not have any effect when compared to control group (**Figure 12**) [18–20].

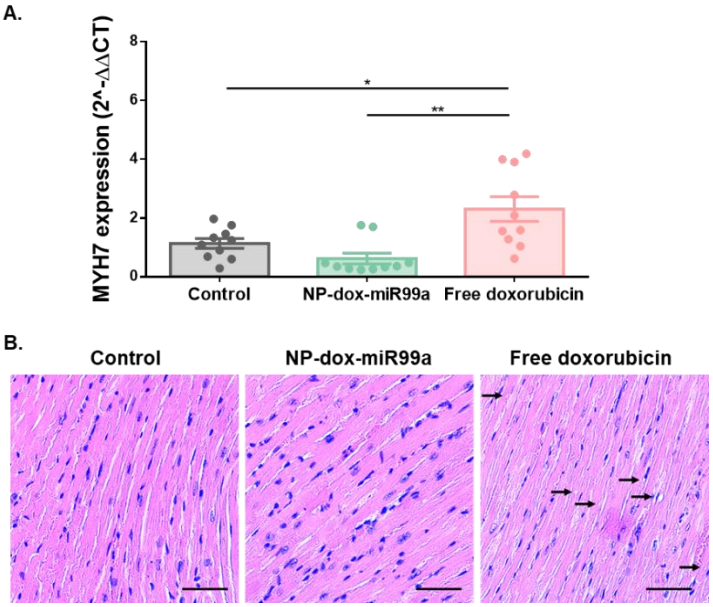

Figure 12. Nanoformulation protects from doxorubicin-induced cardiotoxicity. A. *myh7* expression in heart tissue determined by qRT-PCR. B. Representative images of H&E staining of paraffin-embedded heart tissue. Scale bar: 50 µm. Arrows indicate cytoplasmic lysosomes. Data are presented as mean±SEM *$p < 0.05$; **$p < 0.01$; ****$p < 0.0001$.

3.5 Discussion

In the present study, we identified miR-99a-5p as the most dysregulated miRNA in doxorubicin-resistant cells by using a miRNA expression profiling approach. Numerous authors studied the role of miR-99a-5p in cancer [21]. We previously found that miR-99a-5p is downregulated in BC when compared to healthy breast tissues, and its detection in plasma allows to identify BC at early stages [9,22]. In the context of BC, a tumor-suppressive role has been previously attributed to miR-99a-5p through regulating multiple targets such as *FGFR3* [23], *MTOR* [24,25], *CDC25A* [26], *HOXA1* [27], or *IGF1R* [28]. Regarding drug resistance, Mueller *et al.* showed that miR-99a-5p enhances the sensitivity to radiation therapy through its target SNF2H in breast and prostate cancer cells [29]. In the same trend, Yin *et al.* demonstrated that miR-99a-5p also increases sensitivity to radiation in non-small cell lung cancer by targeting mTOR [30]. By contrast, Zhang *et al.* described that miR-99a-5p may induce cisplatin resistance in gastric cancer through targeting CAPNS1 [31]. As far as we know, our study is the first to demonstrate the role of miR-99a-5p in doxorubicin response in cancer.

We further found a positive correlation between the expression levels of miR-99a-5p and DRFS and OS in BC patients. Response to neoadjuvant chemotherapy is a prognostic factor in BC, showing an inverse correlation with DRFS and OS [32]. Therefore, we hypothesized that the observed correlation could be a consequence of a better response to chemotherapy in those patients with tumors expressing high levels of miR-99a-5p.

To identify the molecular mechanism underlying the role of miR-99a-5p in doxorubicin response, an mRNA array was performed and potential miRNA targets were identified. *COX-2* appeared as the potential target with the highest overexpression in doxorubicin-resistant cells, and we demonstrated that miR-99a-5p inhibits its expression by directly targeting its 3'UTR. According to our hypothesis, we confirmed that silencing of COX-2 increased sensitivity to doxorubicin.

COX-2 has been widely described to be implicated in inflammation. Moreover, it has been found upregulated in many tumor types, where the overexpression has been related to tumorigenesis, treatment resistance, and worse prognosis in patients [11,33]. In fact, COX-2 has been involved in the generation and maintenance of BC stem cells (BCSCs) [34–36]. In line with this, the combination of doxorubicin plus celecoxib (a COX-2 inhibitor) increases the antitumoral effect in breast and cervix cancer [37–40]. Although the mechanism is unclear, several researchers have stated that celecoxib decreases ABCG2 activity, while COX-2 upregulation has the opposite effect [13]. In addition, a positive correlation between *COX-2* and *ABCG2* expression has been found in non-small cell lung cancer and non-Hodgkin's lymphomas patients [41,42]. ABCG2 (also known as BC resistance protein, BCRP), is a transporter involved in drug resistance through the extrusion of anticancer agents such as doxorubicin from cells [12,43]. We confirmed that miR-99a-5p overexpression decreases COX-2 levels and induces downregulation of ABCG2 at mRNA and protein levels, giving rise to a decrease of its activity and an increment of intracellular doxorubicin accumulation as consequence. Thus, our work unrevealed a new mechanism of BC doxorubicin resistance based on the action of miR-99a-5p regulating

COX-2 and ABCG2. Since doxorubicin treatment is more effective in cells that overexpress miR-99a-5p, the combined administration of both, miRNA and chemotherapy, would possibly improve the response of BC cells to doxorubicin treatment alone.

The use of miRNAs as therapeutic agents *in vivo* presents some challenges such as their instability in body fluids due to the presence of endonucleases. Moreover, once internalized by cells, miRNAs will reach the lysosomes where will be degraded. In this context, nanoparticles are useful tools for miRNA delivery, as can avoid miRNA degradation, ensure their delivery to the cytosol, and can also be functionalized to target specific cells [44,45]. Among the different types of nanoparticles, MSNs are promising candidates due to their unique properties such as large surface area and pore volume, biocompatibility, and stability [46,47]. Herein, we have designed a nanodevice based on MSNs to deliver a combination of miR-99a-5p and doxorubicin to tumor cells. A potential limitation of MSNs as carriers of miRNAs is the endosomal entrapment, where their biological function will be impaired because of degradation [48]. Due to this fact, PEI was included in nanoparticles. PEI is protonated once exposed to acidic pH, inducing a "proton sponge" effect giving rise to the scape of the nanoparticles from endosomes/lysosomes to the cytoplasm [49,50]. Furthermore, nanoparticles were coated with HA, which is a biocompatible molecule that reduces the adsorption of proteins to the surface of nanodevices as well as their immunogenicity and is also able to target the CD44 receptor [14]. CD44 is a transmembrane glycoprotein that binds HA and has been described to be involved in tumor progression. Besides, its variant CD44v isoform is overexpressed in tumors and presents a higher affinity for HA than the

standard CD44 isoform [51]. Interestingly, CD44 is overexpressed in BCSCs [52], and the elimination of this population that is known to overexpress ABCG2 is a priority to increase the efficacy of therapies [53–55]. Based on these facts, we coated our nanodevices with HA. In addition to the active targeting, our nanoparticles are in the range size of 20-400 nm, thus can passively target tumors *in vivo* due to the enhanced permeability and retention (EPR) effect, given by the enhanced vascular permeability in combination with an impaired lymphatic function. Therefore, MSNs can easily enter into tumors, where are retained [56,57].

Nanoparticles were synthesized and their characterization confirmed the loading of cargos. The *in vitro* experiments confirmed that the opening of the pores and delivery of encapsulated drugs is triggered in lysosomal extract but not in PBS. Moreover, the specific targeting of CD44 by the nanoparticles was also demonstrated. The potential of the nanodevices to treat BC was tested in an orthotopic xenograft mice model. Our results demonstrated that NP-dox-miR99a exhibits the highest effect on tumor growth inhibition, reduction of proliferation of tumoral cells, and efficient inhibition of miR-99a-5p' targets, when compared with nanoparticles lacking doxorubicin or miR-99a-5p. After 48 hours of treatment, a significant accumulation of nanoparticles was found in tumors. We also found nanoparticles' presence in lung, spleen, kidney, and liver. Besides, similar biodistribution results of MSNs have been found by other authors [58]. Nonetheless, the safety of the nanoparticles was also confirmed since no impact on hepatic and renal functions and body weight was observed. Moreover, our results evidence that nanocarriers may enhance the therapeutic effect of doxorubicin and decrease the *in vivo* toxicity. In fact,

NP-dox-miR99a reduces the needed dose of free doxorubicin by more than 50%, thus decreasing its cardiotoxic effects.

The data above support the use of therapeutic strategies based on the combined delivery of chemotherapy and biologically active molecules by using nanodevices for the treatment of cancer. The designed system has the ability to deliver the cargo to specific populations of cells in a controlled manner. To get clinically relevant combinatorial treatments, further studies are needed in order to expand the knowledge of cancer drug resistance mechanisms and to increase the therapeutic target candidates. Besides, the improvement of devices design and delivery performance is also guaranteed.

3.6 Conclusion

Overall, we demonstrated that miR-99a-5p is significantly downregulated in doxorubicin-resistant cells, and its expression positively correlated to better clinical outcomes in BC patients. We also found that miR-99a-5p increases sensitivity to doxorubicin through downregulation of COX-2 and ABCG2. In the attempt to translate our finding, we developed a multifunctional nanocarrier to deliver a combination of miR-99a-5p and doxorubicin as a new strategy to treat BC. This system presents several advantages including tumor targeting, efficient delivery of miRNA, high tumor growth inhibition, and no toxicity *in vivo*. Besides, the proposed system allows improving chemotherapy efficacy while reducing side effects. The developed nanosystem is a promising strategy to increase the efficacy of the currently available therapies. Our findings suggest that miR-99a-5p has potential clinical value for BC treatment, and encourage to continue

exploring MSN-based nanocarriers and codelivery of miRNAs and chemotherapeutic agents as a strategy to treat cancer.

Author Contributions

I.G.-C.: Conceptualization, methodology, data analysis, writing—original draft preparation. A.A.-A., A.L.(Ana Lameirinhas), J.F.B., V.C.-N., F.R., S.Z., J.M-G.: Methodology, data analysis. A.L. (Ana Lluch): Conceptualization, funding acquisition. F.S.: data acquisition and analysis. J.M.C., P.E, R.M.-M.: Supervision, conceptualization, writing—reviewing and editing, funding acquisition. *Corresponding authors.

Funding

This work was supported by Spanish Government (PI18/01219, PI21/01351, and RTI2018-100910-B-C41), CIBER-BBN (CB07/01/2012), and CIBERONC (CB16/12/00481). I.G.-C. was funded by Generalitat Valenciana (ACIF/2016/030), A.A. and A.L. were funded by Asociación Española Contra el Cancer. J.F.B., was funded by Instituto de Salud Carlos III and the European Social Fund for the financial support “Sara Borrell” (CD19/00038), V.C.-N., was funded by Ministerio de Ciencia e Innovación (FPU grant), and J.M.C. was funded by Sociedad Española de Oncología Médica (Río Hortega-SEOM).

Conflicts of Interest

The authors declare no conflict of interest.

3.7 Bibliography

1. Sung, H.; Ferlay, J.; Siegel, R.L.; Laversanne, M.; Soerjomataram, I.; Jemal, A.; Bray, F. Global Cancer Statistics 2020: GLOBOCAN Estimates of Incidence and Mortality Worldwide for 36 Cancers in 185 Countries. *CA. Cancer J. Clin.* 2021;71(3):209–249.

2. Harbeck, N.; Penault-Llorca, F.; Cortes, J.; Gnant, M.; Houssami, N.; Poortmans, P.; Ruddy, K.; Tsang, J.; Cardoso, F. Breast Cancer. *Nat. Rev. Dis. Prim.* 2019;5(1):66.

3. Waks, A.G.; Winer, E.P. Breast Cancer Treatment: A Review. *JAMA*. 2019;321(3):288–300.

4. Tevaarwerk, A.J.; Gray, R.J.; Schneider, B.P.; Smith, M. Lou; Wagner, L.I.; Fetting, J.H.; Davidson, N.; Goldstein, L.J.; Miller, K.D.; Sparano, J.A. Survival in Patients with Metastatic Recurrent Breast Cancer after Adjuvant Chemotherapy: Little Evidence of Improvement over the Past 30 Years. *Cancer*. 2013;119(6):1140–1148.

5. Cardoso, F.; Paluch-Shimon, S.; Senkus, E.; Curigliano, G.; Aapro, M.S.; André, F.; Barrios, C.H.; Bergh, J.; Bhattacharyya, G.S.; Biganzoli, L.; et al. 5th ESO-ESMO International Consensus Guidelines for Advanced Breast Cancer (ABC 5). *Ann. Oncol.* 2020;31(12):1623–1649.

6. Si, W.; Shen, J.; Zheng, H.; Fan, W. The Role and Mechanisms of Action of MicroRNAs in Cancer Drug Resistance. *Clin. Epigenetics*. 2019;11:25.

7. Loh, H.Y.; Norman, B.P.; Lai, K.S.; Rahman, N.M.A.N.A.; Alitheen, N.B.M.; Osman, M.A. The Regulatory Role of MicroRNAs in Breast Cancer. *Int. J. Mol. Sci.* 2019;20(19):4940.

8. Nagy, Á.; Munkácsy, G.; Győrffy, B. Pancancer Survival Analysis of Cancer Hallmark Genes. *Sci. Rep.* 2021;11(1):.

9. Garrido-Cano, I.; Constância, V.; Adam-Artigues, A.; Lameirinhas, A.; Simón, S.; Ortega, B.; Martínez, M.T.; Hernando, C.; Bermejo, B.; Lluch, A.; et al. Circulating MiR-99a-5p Expression in Plasma: A Potential Biomarker for Early Diagnosis of Breast Cancer. *Int. J. Mol. Sci.* 2020;21(19):7427.

10. Buffa, F.M.; Camps, C.; Winchester, L.; Snell, C.E.; Gee, H.E.; Sheldon, H.; Taylor, M.; Harris, A.L.; Ragoussis, J. MicroRNA-Associated Progression Pathways and Potential Therapeutic Targets Identified by Integrated MRNA and MicroRNA Expression Profiling in Breast Cancer. *Cancer Res.* 2011;71(17):5635–5645.

11. Hashemi Goradel, N.; Najafi, M.; Salehi, E.; Farhood, B.; Mortezaee, K. Cyclooxygenase-2 in Cancer: A Review. *J. Cell. Physiol.* 2019;234(5):5683–5699.

12. Fletcher, J.I.; Williams, R.T.; Henderson, M.J.; Norris, M.D.; Haber, M. ABC Transporters as Mediators of Drug Resistance and Contributors to Cancer Cell Biology. *Drug Resist. Updat.* 2016**;**26:1–9.

13. Kalalinia, F.; Elahian, F.; Behravan, J. Potential Role of Cyclooxygenase-2 on the Regulation of the Drug Efflux Transporter ABCG2 in Breast Cancer Cell Lines. *J. Cancer Res. Clin. Oncol.* 2011**;**137(2):321–330.

14. Luo, Z.; Dai, Y.; Gao, H. Development and Application of Hyaluronic Acid in Tumor Targeting Drug Delivery. *Acta Pharm. Sin. B*. 2019**;**9(6):1099–1112.

15. Ferreira de Souza, T.; Quinaglia A.C. Silva, T.; Osorio Costa, F.; Shah, R.; Neilan, T.G.; Velloso, L.; Nadruz, W.; Brenelli, F.; Sposito, A.C.; Matos-Souza, J.R.; et al. Anthracycline Therapy Is Associated With Cardiomyocyte Atrophy and Preclinical Manifestations of Heart Disease. *JACC Cardiovasc. Imaging*. 2018**;**11(8):1045–1055.

16. Chougule, M.B.; Patel, A.R.; Jackson, T.; Singh, M. Antitumor Activity of Noscapine in Combination with Doxorubicin in Triple Negative Breast Cancer. *PLoS One*. 2011**;**6(3):e17733.

17. Ottewell, P.D.; Mönkkönen, H.; Jones, M.; Lefley, D. V.; Coleman, R.E.; Holen, I. Antitumor Effects of Doxorubicin Followed by Zoledronic Acid in a Mouse Model of Breast Cancer. *JNCI J. Natl. Cancer Inst.* 2008**;**100(16):1167–1178.

18. Willis, M.S.; Parry, T.L.; Brown, D.I.; Mota, R.I.; Huang, W.; Beak, J.Y.; Sola, M.; Zhou, C.; Hicks, S.T.; Caughey, M.C.; et al. Doxorubicin Exposure Causes Subacute Cardiac Atrophy Dependent on the Striated Muscle-Specific Ubiquitin Ligase MuRF1. *Circ. Hear. Fail.* 2019**;**12(3):e005234.

19. Baskin, K.K.; Taegtmeyer, H. Taking Pressure off the Heart: The Ins and Outs of Atrophic Remodelling. *Cardiovasc. Res.* 2011**;**90(2):243–250.

20. Guo, R.; Hua, Y.; Ren, J.; Bornfeldt, K.E.; Nair, S. Cardiomyocyte-Specific Disruption of Cathepsin K Protects against Doxorubicin-Induced Cardiotoxicity. *Cell Death Dis.* 2018**;**9(6):692.

21. Eniafe, J.; Jiang, S. MicroRNA-99 Family in Cancer and Immunity. *Wiley Interdiscip. Rev. RNA*. 2021**;**12(3):e1635.

22. Garrido-Cano, I.; Pla, L.; Santiago-Felipe, S.; Simón, S.; Ortega, B.; Bermejo, B.; Lluch, A.; Cejalvo, J.M.; Eroles, P.; Martínez-Máñez, R. Nanoporous Anodic Alumina-Based Sensor for MiR-99a-5p Detection as an Effective Early Breast Cancer Diagnostic Tool. *ACS Sensors*. 2021**;**6(3):1022–1029.

23. Long, X.; Shi, Y.; Ye, P.; Guo, J.; Zhou, Q.; Tang, Y. MicroRNA-99a Suppresses Breast Cancer Progression by Targeting FGFR3. *Front. Oncol.* 2020**;**9:1473.

24. Hu, Y.; Zhu, Q.; Tang, L. MiR-99a Antitumor Activity in Human Breast Cancer Cells through Targeting of MTOR Expression. *PLoS One*. 2014;9(3):e92099.

25. Yang, Z.; Han, Y.; Cheng, K.; Zhang, G.; Wang, X. MiR-99a Directly Targets the MTOR Signalling Pathway in Breast Cancer Side Population Cells. *Cell Prolif.* 2014;47(6):587–595.

26. Qin, H.; Liu, W. MicroRNA-99a-5p Suppresses Breast Cancer Progression and Cell-Cycle Pathway through Downregulating CDC25A. *J. Cell. Physiol.* 2018;1–12.

27. Wang, X.; Li, Y.; Qi, W.; Zhang, N.; Sun, M.; Huo, Q.; Cai, C.; Lv, S.; Yang, Q. MicroRNA-99a Inhibits Tumor Aggressive Phenotypes through Regulating HOXA1 in Breast Cancer Cells. *Oncotarget*. 2015;6(32):32737–32747.

28. Xia, M.; Li, H.; Wang, J.-J.; Zeng, H.-J.; Wang, S.-H. MiR-99a Suppress Proliferation, Migration and Invasion through Regulating Insulin-like Growth Factor 1 Receptor in Breast Cancer. *Eur. Rev. Med. Pharmacol. Sci.* 2016;20(9):1755–1763.

29. Mueller, A.C.; Sun, D.; Dutta, A. The MiR-99 Family Regulates the DNA Damage Response through Its Target SNF2H. *Oncogene*. 2013;32(9):1164–1172.

30. Yin, H.; Ma, J.; Chen, L.; Piao, S.; Zhang, Y.; Zhang, S.; Ma, H.; Li, Y.; Qu, Y.; Wang, X.; et al. MIR-99a Enhances the Radiation Sensitivity of Non-Small Cell Lung Cancer by Targeting MTOR. *Cell. Physiol. Biochem.* 2018;46(2):471–481.

31. Zhang, Y.; Xu, W.; Ni, P.; Li, A.; Zhou, J.; Xu, S. MiR-99a and MiR-491 Regulate Cisplatin Resistance in Human Gastric Cancer Cells by Targeting CAPNS1. *Int. J. Biol. Sci.* 2016;12(12):1437–1447.

32. Symmans, W.F.; Wei, C.; Gould, R.; Yu, X.; Zhang, Y.; Liu, M.; Walls, A.; Bousamra, A.; Ramineni, M.; Sinn, B.; et al. Long-Term Prognostic Risk After Neoadjuvant Chemotherapy Associated With Residual Cancer Burden and Breast Cancer Subtype. *J. Clin. Oncol.* 2017;35(10):1049–1060.

33. Gasparini, G.; Longo, R.; Sarmiento, R.; Morabito, A. Inhibitors of Cyclo-Oxygenase 2: A New Class of Anticancer Agents? *Lancet Oncol.* 2003;4(10):605–615.

34. Tong, D.; Liu, Q.; Wang, L. ang; Xie, Q.; Pang, J.; Huang, Y.; Wang, L.; Liu, G.; Zhang, D.; Lan, W.; et al. The Roles of the COX2/PGE2/EP Axis in Therapeutic Resistance. *Cancer Metastasis Rev.* 2018;37(2–3):355–368.

35. Tian, J.; Hachim, M.Y.; Hachim, I.Y.; Dai, M.; Lo, C.; Raffa, F. Al; Ali, S.; Lebrun, J.J. Cyclooxygenase-2 Regulates TGFβ-Induced Cancer Stemness in Triple-Negative Breast Cancer. *Sci. Rep.* 2017;7:40258.

36. Majumder, M.; Xin, X.; Liu, L.; Tutunea-Fatan, E.; Rodriguez-Torres, M.; Vincent, K.; Postovit, L.M.; Hess, D.; Lala, P.K. COX-2 Induces Breast Cancer Stem Cells via EP4/PI3K/AKT/NOTCH/WNT Axis. *Stem Cells*. 2016**;**34(9):2290–2305.

37. Singh, B.; Cook, K.R.; Vincent, L.; Hall, C.S.; Berry, J.A.; Multani, A.S.; Lucci, A. Cyclooxygenase-2 Induces Genomic Instability, BCL2 Expression, Doxorubicin Resistance, and Altered Cancer-Initiating Cell Phenotype in MCF7 Breast Cancer Cells. *J. Surg. Res.* 2008**;**147(2):240–246.

38. Chen, C.; Shen, H.L.; Yang, J.; Chen, Q.Y.; Xu, W.L. Preventing Chemoresistance of Human Breast Cancer Cell Line, MCF-7 with Celecoxib. *J. Cancer Res. Clin. Oncol.* 2011**;**137(1):9–17.

39. van Wijngaarden, J.; van Beek, E.; van Rossum, G.; van der Bent, C.; Hoekman, K.; van der Pluijm, G.; van der Pol, M.A.; Broxterman, H.J.; van Hinsbergh, V.W.M.; Löwik, C.W.G.M. Celecoxib Enhances Doxorubicin-Induced Cytotoxicity in MDA-MB231 Cells by NF-KB-Mediated Increase of Intracellular Doxorubicin Accumulation. *Eur. J. Cancer*. 2007**;**43(2):433–442.

40. Robledo-Cadena, D.X.; Gallardo-Pérez, J.C.; Dávila-Borja, V.; Pacheco-Velázquez, S.C.; Belmont-Díaz, J.A.; Ralph, S.J.; Blanco-Carpintero, B.A.; Moreno-Sánchez, R.; Rodríguez-Enríquez, S. Non-Steroidal Anti-Inflammatory Drugs Increase Cisplatin, Paclitaxel, and Doxorubicin Efficacy against Human Cervix Cancer Cells. *Pharmaceuticals*. 2020**;**13(12):463.

41. Surowiak, P.; Pawełczyk, K.; Maciejczyk, A.; Pudełko, M.; Kołodziej, J.; Zabel, M.; Murawa, D.; Drag, M.; Gansukh, T.; Dietel, M.; et al. Positive Correlation between Cyclooxygenase 2 and the Expression of ABC Transporters in Non-Small Cell Lung Cancer. *Anticancer Res.* 2008**;**28(5B):2967–2974.

42. Szczuraszek, K.; Materna, V.; Halon, A.; Mazur, G.; Wróbel, T.; Kuliczkowski, K.; Maciejczyk, A.; Zabel, M.; Drag, M.; Dietel, M.; et al. Positive Correlation between Cyclooxygenase-2 and ABC-Transporter Expression in Non-Hodgkin's Lymphomas. *Oncol. Rep.* 2009**;**22(6):1315–1323.

43. Liu, X. ABC Family Transporters. *Adv. Exp. Med. Biol.* 2019**;**1141:13–100.

44. Boca, S.; Gulei, D.; Zimta, A.A.; Onaciu, A.; Magdo, L.; Tigu, A.B.; Ionescu, C.; Irimie, A.; Buiga, R.; Berindan-Neagoe, I. Nanoscale Delivery Systems for MicroRNAs in Cancer Therapy. *Cell. Mol. Life Sci.* 2020**;**77(6):1059–1086.

45. Labatut, A.E.; Mattheolabakis, G. Non-Viral Based MiR Delivery and Recent Developments. *Eur. J. Pharm. Biopharm.* 2018**;**128:82–90.

46. Li, Z.; Barnes, J.C.; Bosoy, A.; Stoddart, J.F.; Zink, J.I. Mesoporous Silica Nanoparticles in Biomedical Applications. *Chem. Soc. Rev.* 2012**;**41(7):2590–2605.

47. Garrido-Cano, I.; Candela-Noguera, V.; Herrera, G.; Cejalvo, J.M.; Lluch, A.; Marcos, M.D.; Sancenon, F.; Eroles, P.; Martínez-Máñez, R. Biocompatibility and Internalization Assessment of Bare and Functionalised Mesoporous Silica Nanoparticles. *Microporous Mesoporous Mater.* 2021;310:110593.

48. Cha, W.; Fan, R.; Miao, Y.; Zhou, Y.; Qin, C.; Shan, X.; Wan, X.; Li, J. Mesoporous Silica Nanoparticles as Carriers for Intracellular Delivery of Nucleic Acids and Subsequent Therapeutic Applications. *Molecules*. 2017;22(5):782.

49. Boussif, O.; LezoualC'H, F.; Zanta, M.A.; Mergny, M.D.; Scherman, D.; Demeneix, B.; Behr, J.P. A Versatile Vector for Gene and Oligonucleotide Transfer into Cells in Culture and in Vivo: Polyethylenimine. *Proc. Natl. Acad. Sci. U. S. A.* 1995;92(16):7297–7301.

50. Varkouhi, A.K.; Scholte, M.; Storm, G.; Haisma, H.J. Endosomal Escape Pathways for Delivery of Biologicals. *J. Control. Release*. 2011;151(3):220–228.

51. Misra, S.; Heldin, P.; Hascall, V.C.; Karamanos, N.K.; Skandalis, S.S.; Markwald, R.R.; Ghatak, S. Hyaluronan-CD44 Interactions as Potential Targets for Cancer Therapy. *Fed. Eur. Biochem. Soc.* 2011;278(9):1429–1443.

52. De Angelis, M.L.; Francescangeli, F.; Zeuner, A. Breast Cancer Stem Cells as Drivers of Tumor Chemoresistance, Dormancy and Relapse: New Challenges and Therapeutic Opportunities. *Cancers (Basel).* 2019;11(10):1569.

53. Zeng, X.; Liu, C.; Yao, J.; Wan, H.; Wan, G.; Li, Y.; Chen, N. Breast Cancer Stem Cells, Heterogeneity, Targeting Therapies and Therapeutic Implications. *Pharmacol. Res.* 2021;163:105320.

54. Morrison, B.J.; Schmidt, C.W.; Lakhani, S.R.; Reynolds, B.A.; Lopez, J.A. Breast Cancer Stem Cells: Implications for Therapy of Breast Cancer. *Breast Cancer Res.* 2008;10(4):210.

55. Ji, X.; Lu, Y.; Tian, H.; Meng, X.; Wei, M.; Cho, W.C. Chemoresistance Mechanisms of Breast Cancer and Their Countermeasures. *Biomed. Pharmacother.* 2019;114:108800.

56. Jain, R.K.; Stylianopoulos, T. Delivering Nanomedicine to Solid Tumors. *Nat. Rev. Clin. Oncol.* 2010;7(11):653–664.

57. Danhier, F.; Feron, O.; Préat, V. To Exploit the Tumor Microenvironment: Passive and Active Tumor Targeting of Nanocarriers for Anti-Cancer Drug Delivery. *J. Control. Release*. 2010;148(2):135–146.

58. Wei, Y.; Quan, L.; Zhou, C.; Zhan, Q. Factors Relating to the Biodistribution & Clearance of Nanoparticles & Their Effects on in Vivo Application. *https://doi.org/10.2217/nnm-2018-0040*. 2018;13(12):1495–1512.

3.8 Supporting information

Supplementary Table S1. List of predicted targets of miR-99a-5p which correspond to genes significantly overexpressed in MDA-MB-231R cells compared to MDA-MB-231 (Fold Change > 2).

Gene symbol	Description	Transcript Cluster ID	Fold Change	p-value
PTGS2	prostaglandin-endoperoxide synthase 2 (prostaglandin G/H synthase and cyclooxygenase)	TC0100016715.hg.1	-4,94	0,001321
SLC7A11	solute carrier family 7 (anionic amino acid transporter light chain, xc- system), member 11	TC0400011920.hg.1	-4	0,004751
SEL1L3	sel-1 suppressor of lin-12-like 3 (C. elegans)	TC0400010282.hg.1	-3,34	0,007619
LAMP3	lysosomal-associated membrane protein 3	TC0300013336.hg.1	-2,58	0,014239
CXCL3	chemokine (C-X-C motif) ligand 3	TC0400011015.hg.1	-2,52	0,003436
FAM101B	family with sequence similarity 101, member B	TC1700009318.hg.1	-2,43	0,0016
HYOU1	hypoxia up-regulated 1	TSUnmapped00000517.hg.1	-2,32	0,000261
SLC33A1	solute carrier family 33 (acetyl-CoA transporter), member 1	TC0300012881.hg.1	-2,27	0,042048
POU2F2	POU class 2 homeobox 2	TC1900010789.hg.1	-2,25	0,007484
HYOU1	hypoxia up-regulated 1	TSUnmapped00000777.hg.1	-2,24	0,003772

Supplementary Table S1 (continued).

HYOU1	hypoxia up-regulated 1	TSUnmapped00000440.hg.1	-2,21	0,000582
HYOU1	hypoxia up-regulated 1	TSUnmapped00000067.hg.1	-2,17	0,00866
HYOU1	hypoxia up-regulated 1	TSUnmapped00000138.hg.1	-2,14	0,003763
PARM1	prostate androgen-regulated mucin-like protein 1	TC0400007868.hg.1	-2,09	0,005737
HYOU1	hypoxia up-regulated 1	TSUnmapped00000233.hg.1	-2,09	0,007523
HYOU1	hypoxia up-regulated 1	TSUnmapped00000300.hg.1	-2,08	0,000712
TFRC	transferrin receptor	TC0300013684.hg.1	-2,07	0,028857
HYOU1	hypoxia up-regulated 1	TSUnmapped00000281.hg.1	-2,06	0,003294
SDF2L1	stromal cell-derived factor 2-like 1	TC2200006718.hg.1	-2,05	0,012899
HYOU1	hypoxia up-regulated 1	TSUnmapped00000558.hg.1	-2,04	0,005336
CTSV	cathepsin V	TC0900010933.hg.1	-2,01	0,032546
PDE4D	phosphodiesterase 4D, cAMP-specific	TC0500010842.hg.1	-2,01	0,04129

Table S2. Particle size distribution obtained by DLS measurements for nanoparticles at 25ºC on previously sonicated suspensions at a concentration of 0.5 mg/mL.

Nanoparticle	Size (nm) ± SD
MSN scaffold	96.36 ± 1.23
NP-dox	119.55 ± 3.46
NP-dox-miR99a	126.33 ± 1.86
Control NP	127.28 ± 0.78
NP- miR99a	126.33 ± 1.86

Table S3. ζ potential of nanoparticles. PEI: polyethileneimine; HA: hyaluronic acid.

Nanoparticle	ζ potential ± SD
MSN scaffold	-34.36 ± 1.45
NP-dox	27.87 ± 0.21
NP-dox-miR99a	24.60 ± 0.78
Control NP	33.63 ± 0.51
NP- miR99a	32.83 ± 0.55

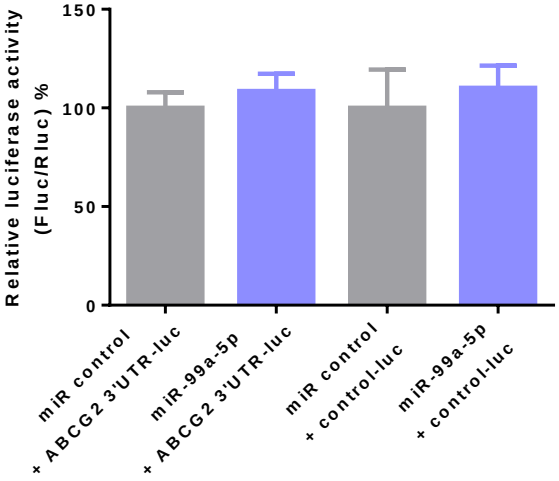

Figure S1. ABCG2 is not a direct target of miR-99a-5p. Luciferase activity assays of HEK293T cells co-transfected with miR-99a-5p or scrambled control and the luciferase vector containing 3'UTR of ABCG2 or control luciferase vector.

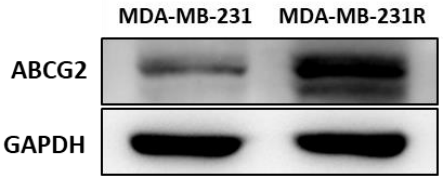

Figure S2. ABCG2 expression measured by Western blot in MDA-MB-231 and MDA-MB-231R.

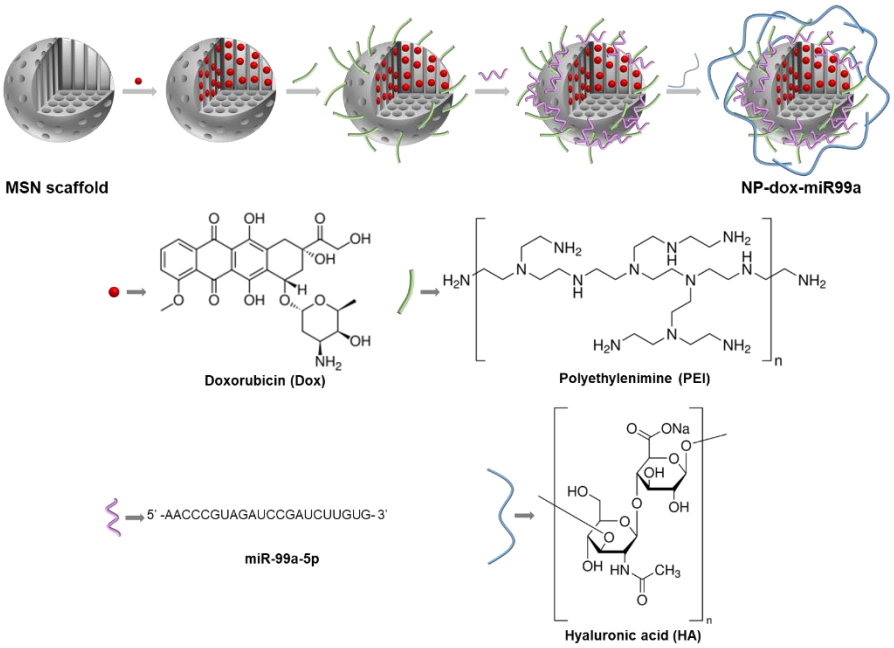

Figure S3. Schematic synthesis procedure of MSN-dox-miR99a. Doxorubicin (Dox) was loaded into pores of MSN scaffolds. Nanoparticles were coated with PEI. miR-99a-5p was then adsorbed to the surface, and nanodevices were finally coated with HA yelding the final solid NP-dox-miR99a.

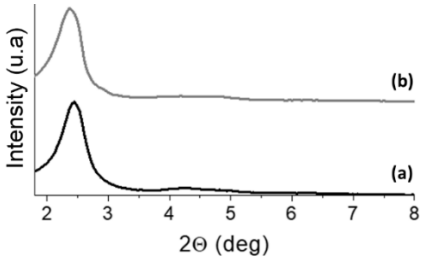

Figure S4. A. Powder X-ray diffraction (PXRD) patterns of (a) as-synthesized MCM-41, (b) MSN scaffolds. Typical of a hexagonal-ordered pore array that can be indexed as (100), (110), and (200) Bragg reflections.

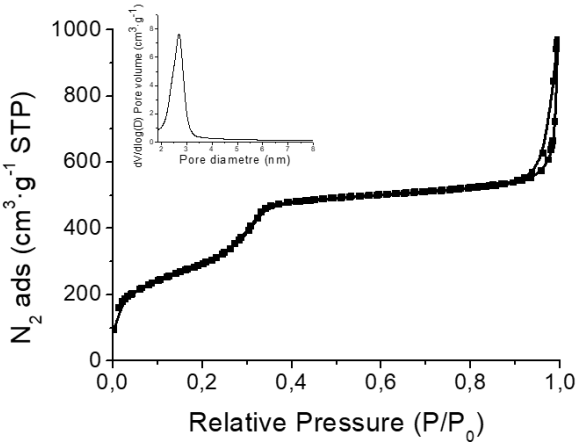

Figure S5. Nitrogen adsorption−desorption isotherms of MSN scaffold (inset: pore-size distribution). The adsorption step between P/P_0 values of 0.2 and 0.4 is typical of this type of mesoporous solids, and corresponds to a type IV isotherm due to nitrogen condensation inside the pores. Furthermore, the absence of hysteresis in this interval indicates that pores are uniform cylinders. The application of the Barrett−Joyner−Halenda (BJH) model resulted in a pore size of 2.93 nm and a pore volume of 1.06 cm3/g. By applying the Brunauer−Emmett−Teller (BET) model, a surface area of 1245.39 m^2/g was calculated.

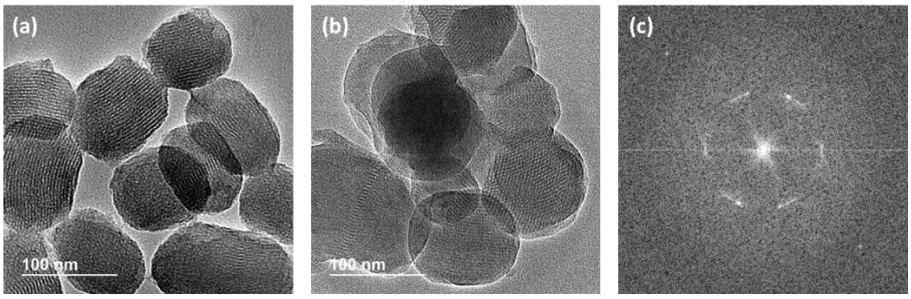

Figure S6. Transmission electron microscopy (TEM) images of MSN scaffold (a), and NP-dox-miR99a (b). Selected area electron diffraction SAED image focused on a MSN scaffold showing the presence of hexagonal domain in the structure is shown in (c).

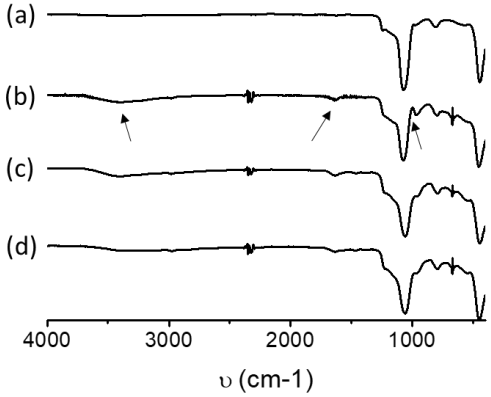

Figure S7. Attenuated total reflectance (ATR) spectra of MSN scaffold (a), MSNs loaded with doxorubicin (b), MSNs loaded with doxorubicin and coated with PEI (c), and final NP-dox-miR99a (d) loaded with doxorubicin and coated with PEI, miR-99a, and HA. All the materials present the typical peak at 1095 cm^{-1}, corresponding to vibration of Si-O-Si group. After loading with doxorubicin, the prepared nanoparticles present bands at 3550 cm^{-1}, 1626 cm^{-1}, and 960 cm^{-1}, corresponding to O-H, N-H, and C-OH bonds vibration, respectively (arrows).

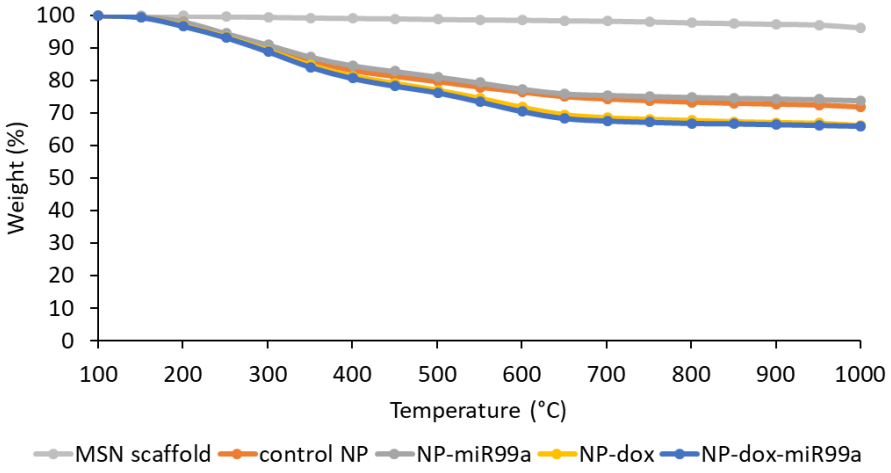

Figure S8. Thermogravimetric curves of nanoparticles. Thermogravimetric analysis (TGA) allowed to calculate the organic content in final nanoparticles, and loaded doxorubicin (6.7 % in weight).

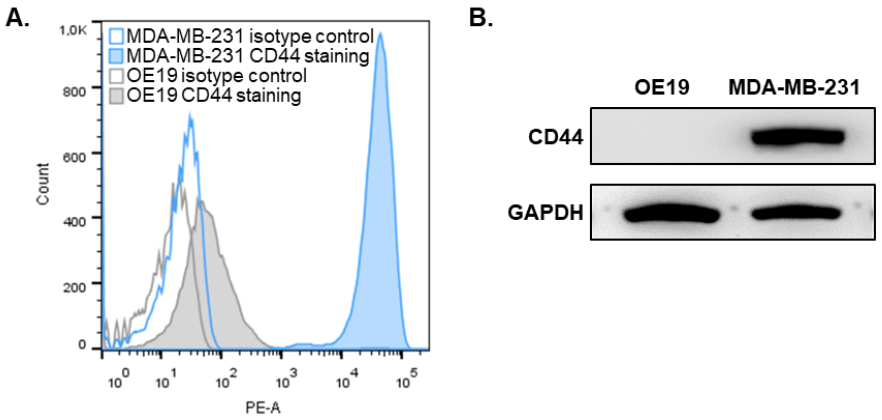

Figure S9. CD44 expression determined in OE19 and MDA-MB-231. A. Flow cytometry results. Histograms of CD44 (filled) and isotype control (empty) stained OE19 (grey) and MDA-MB-231 (blue) cells. B. Western blot results.

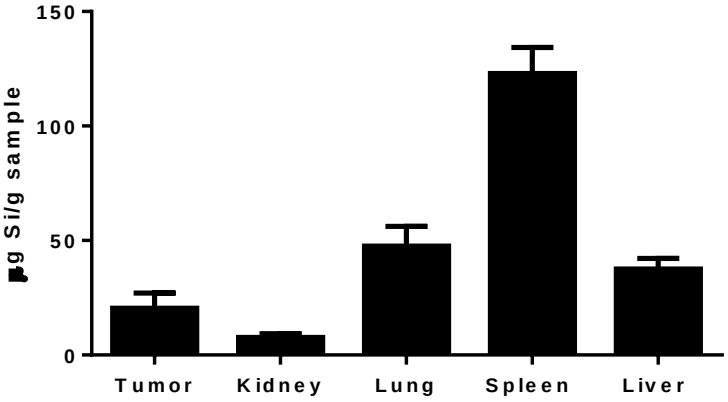

Figure S10. Biodistribution of NP-dox-miR99a nanoparticles 48 hours after last treatment. Silicon levels analyzed by ICP-MS. Data expressed as mean ± SEM (n=6) and represented as µg Si per g of sample.

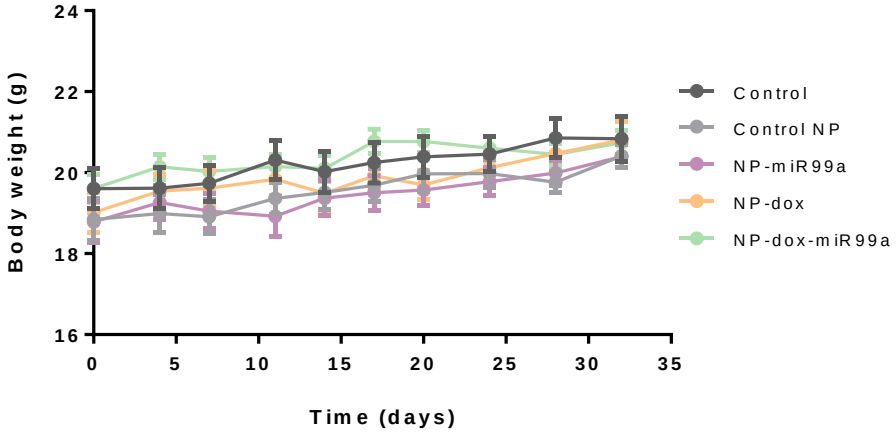

Figure S11. Changes in body weight of xenograft-bearing mice. Mean ± SD.

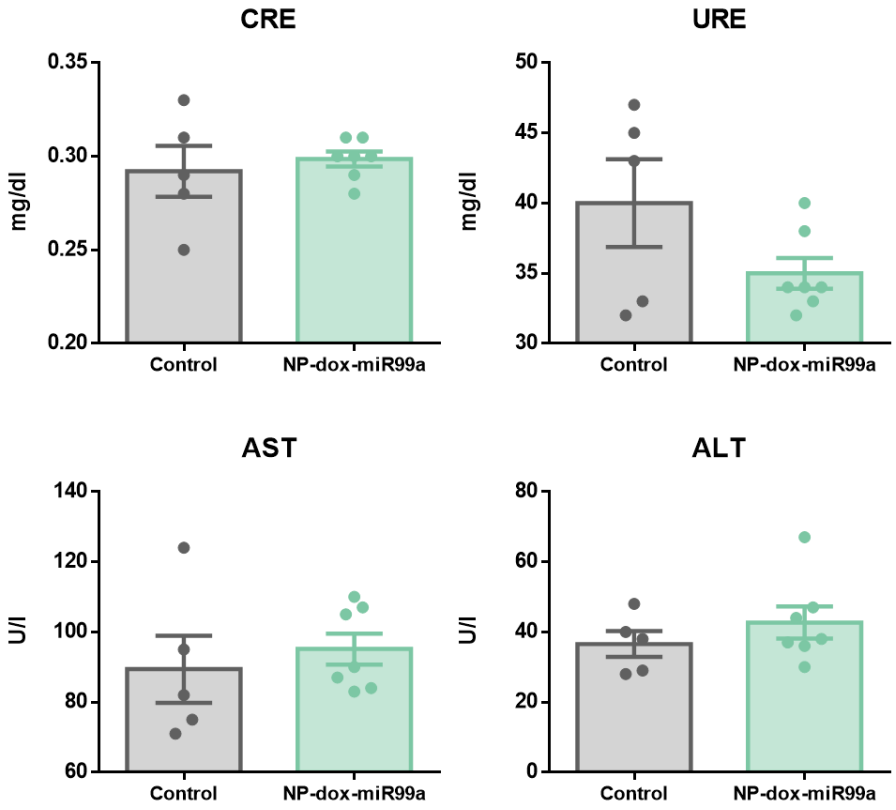

Figure S12. Serum levels of of creatinine (CRE), urea (URE), aspartate aminotransferase (AST), and alanine transaminase (ALT) are in the normal range 48 hours after last dose of treatment. Mean ± SEM.

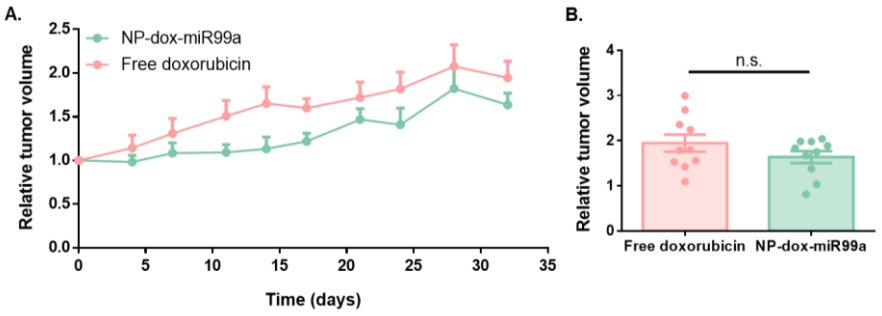

Figure S13. MDA-MB-231 were injected into the mammary fat pad of BALB/C mice. When the tumor size reached approximately 50 mm^3, mice (n=10 per group) were treated 3 times per week with 10 mg/kg of nanoparticles, or 1.6 mg/kg of free doxorubicin for one month. Tumor growth curve (A) and final tumor volume (B).

CHAPTER 4 |

miR-99a-5p as biomarker

Circulating miR-99a-5p expression in plasma: a potential biomarker for early diagnosis of breast cancer

Iris Garrido-Cano[1,2], Vera Constâncio[2], Anna Adam-Artigues[1], Ana Lameirinhas[1], Soraya Simón[1,3], Belen Ortega[1,3], María Teresa Martínez[1,3], Cristina Hernando[1,3],Begoña Bermejo[1,3], Ana Lluch[3,4,5], Paula Lopes[2,6], Rui Henrique[2,6,7], Carmen Jerónimo[2,7*], Juan Miguel Cejalvo[1,3*], Pilar Eroles[1,4,6*].

[1]Biomedical Research Institute INCLIVA, 46010 Valencia, Spain.

[2]Cancer Biology and Epigenetics Group–Research Center, Portuguese Oncology Institute of Porto (CI-IPOP), 4200-072 Porto, Portugal.

[3]Clinical Oncology Department, Hospital Clínico Universitario de Valencia, 46010 Valencia, Spain.

[4]Centro de Investigación Biomédica en Red de Cáncer (CIBERONC), 28029 Madrid, Spain.

[5]Department of Medicine, Universitat de València, 46010 Valencia, Spain.

[6]Department of Pathology, Portuguese Oncology Institute of Porto, 4200-072 Porto, Portugal.

[7]Department of Pathology and Molecular Immunology, Institute of Biomedical Sciences Abel Salazar-University of Porto (ICBAS-UP), 4050-313 Porto, Portugal.

[8]COST Action CA15204, 1210 Brussels, Belgium.

[9]Department of Physiology, Universitat de València, 46010 Valencia, Spain.

Int. J. Mol. Sci. **2020;21(19):7427.**

4.1 Abstract

MicroRNAs have emerged as new diagnostic and therapeutic biomarkers for breast cancer. Herein, we analysed miR-99a-5p expression levels in primary tumors and plasma of breast cancer patients to evaluate its usefulness as a minimally invasive diagnostic biomarker. miR-99a-5p expression levels were determined by quantitative real-time PCR in three independent cohorts of patients: (I) Discovery cohort: breast cancer tissues (n = 103) and healthy breast tissues (n = 26); (II) Testing cohort: plasma samples from 105 patients and 98 healthy donors; (III) Validation cohort: plasma samples from 89 patients and 85 healthy donors. Our results demonstrated that miR-99a-5p was significantly downregulated in breast cancer tissues compared to healthy breast tissues. Conversely, miR-99a-5p levels were significantly higher in breast cancer patients than in healthy controls in plasma samples from both testing and validation cohorts, and ROC curve analysis revealed that miR-99a-5p has good diagnostic potential even to detect early breast cancer. In conclusion, miR-99a-5p's deregulated expression distinguished healthy patients from breast cancer patients in two different types of samples (tissues and plasma). Interestingly, expression levels in plasma were significantly lower in healthy controls than in early-stage breast cancer patients. Our findings suggest circulating miR-99a-5p as a novel promising non-invasive biomarker for breast cancer detection.

4.2 Introduction

Breast cancer (BC) is one of the most common malignant diseases in the world. In 2018, more than 2 million new cases were diagnosed, also being the leading cause of cancer-related death in women in over 100 countries [1]. Indeed, although a 100% 5-year survival rate is observed for BC patients diagnosed at stage I, it dramatically decreases to 26% for those diagnosed at stage IV [2–4]. Hence, new BC effective early-diagnosis methods are urgently needed to reduce its mortality rate. Currently, mammography is still considered the gold-standard method for the detection of BC. However, the sensitivity and specificity of mammography can be low in young women and women with dense breast tissue [5]. Additionally, because BC tumors are very heterogeneous, a tissue biopsy is mandatory to obtain the molecular classification of each tumor, that is based on the expression of several biomarkers, such as estrogen receptor (ER), progesterone receptor (PR), HER2 (human epidermal growth factor receptor 2) overexpression, or Ki-67, which determine the treatment choice [4,6,7].

Recently, microRNAs (miRNAs) have emerged as new diagnostic and therapeutic biomarkers for BC [3,8,9]. miRNAs are small non-coding RNAs of 19–25 nucleotides in length, which are key regulators of post-transcriptional gene expression through the silencing of messenger RNAs (mRNAs) by different mechanisms [10]. miRNAs are involved in a wide variety of biological processes, such as proliferation, apoptosis, or cell cycle [9,11–13]. Therefore, the dysregulation of miRNA expression has been shown to have important effects on several diseases, such as autoimmune disorders, bone diseases, or cancer. Recently, due to their ability to regulate tumor initiation,

progression, and metastasis, miRNAs have become promising BC biomarkers [3,8].

Indeed, several miRNAs were shown to be differentially expressed in breast tumors and healthy counterparts, and their expression levels have been related to immunohistochemical profiles, prognosis, response to treatment, or clinical outcomes [8,14].

miRNAs are detectable in biological fluids that can be collected with minimally invasive techniques. Thus, the diagnostic and prognostic value of circulating miRNAs might be of great interest [9]. Several studies have been assessing the potential use of circulating miRNAs in plasma as biomarkers for different types of cancers and, nowadays, they are considered promising markers for diagnosis, prognosis, and treatment response [7,15–18]. In BC, it has been proven that circulating miRNAs differ between cancer patients and healthy volunteers [9,19,20]. Therefore, miRNAs could be used as effective minimally invasive biomarkers for the diagnosis and monitoring of BC patients.

miR-99a-5p, which functions as a tumor suppressor gene by inhibiting proliferation, migration, and invasion, has been found dysregulated in several tumors [21,22]. Specifically, in BC tissues miR-99a-5p has been consistently reported to be downregulated [23–26]. Hence, herein we sought to investigate the applicability of miR-99a-5p expression levels as a minimally invasive BC diagnostic biomarker.

4.3 Materials and methods

4.3.1 Clinical samples

This retrospective study included non-consecutive female patients over the age of 18 years. Samples were collected from two independent institutions: Portuguese Oncology Institute of Porto (IPO-Porto, Portugal) and Biomedical Research Institute INCLIVA (Spain).

A discovery cohort included a total of 103 BC tissue samples available at the Biobank of the Department of Pathology from IPO-Porto (cohort #1). Furthermore, 26 healthy breast tissue samples collected from reduction mammoplasties of the contralateral breast from BC patients were also included for our purposes. All these specimens were obtained from patients without BC hereditary syndrome and no evidence of preneoplastic/neoplastic lesions. After surgical resection, samples were immediately frozen at −80 ◦C. Five micrometer frozen sections were cut and stained with hematoxylin-eosin for confirmation of BC by an experienced pathologist, ensuring that samples contained at least 70% of tumor cells, and confirming that tissues obtained from reduction mammoplasties harbored normal epithelial cells.

The testing cohort included a total of 105 patients with BC diagnosed at the IPO-Porto, for which plasma samples were available (cohort # 2). All samples were collected before any treatment. For control purposes, plasma samples were collected from 98 healthy donors from the same institution. After the collection of peripheral blood into EDTA-containing tubes, plasma was obtained by centrifugation at 2000 rpm for 10 min at 4 ◦C and was stored at -80 ◦C until further use.

The validation cohort (cohort #3), included 89 BC patients from INCLIVA with plasma samples collected before treatment, and control plasma samples collected from 85 healthy donors from the same institution and Valencian Biobanking Network. After the collection of peripheral blood into EDTA-containing tubes, plasma was obtained and stored as described for cohort #2.

This study was approved by the institutional ethical committees of IPO-Porto (CES-IPOFG-120/015) and INCLIVA (2019/196). Informed consent was obtained from all patients and donors included in the study. Sample collection was performed in accordance with the Declaration of Helsinki.

4.3.2 RNA extraction from tissue and plasma

Total RNA from tissue using TRIzol Reagent (Invitrogen, Carlsbad, CA, USA) according to the manufacturer's recommendations. RNA concentrations and purity ratios were determined using a NanoDrop Lite spectrophotometer (NanoDrop Technologies, Wilmington, DE, USA). MiRNAs were extracted from plasma samples using miRNeasy Serum/Plasma Kit (Qiagen, Hilden, Germany), according to manufacturer's instructions. RNA samples were stored at −80°C.

4.3.3 cDNA synthesis

For coding DNA (cDNA) synthesis, 500 ng of total RNA from tissue or 9.16 µL of miRNA from plasma were used. TaqMan MicroRNA Reverse Transcription Kit (Thermo Fisher Scientific, Waltham, Massachusetts, USA) was employed, according to the manufacturer's protocol in a total volume of

15 µL. For the synthesis of cDNA, reaction mixtures were incubated in a thermal cycler at 16°C for 30 min, at 42°C for 30 min, and at 85°C for 5 min.

4.3.4 miRNA expression analysis

Expression levels of miR-99a-5p (Assay ID 000435) and the reference gene RNU38B (Assay ID 001004) were analysed in triplicate via quantitative real-time PCR (qRT-PCR) using the human TaqMan microRNA Assay kit (Thermo Fisher Scientific Waltham, Massachusetts, USA). Then, 2 µL of cDNA solution were amplified with 5 µL of Xpert Fast Probe 2x MasterMix (GRiSP, Portugal), 0.5 µL of gene-specific primers/probe, and 2.5 µL of nuclease-free water in a final volume of 10 µL. qRT-PCR of cohort #1 and cohort #2 were run in a LightCycler 480 Instrument (Roche Diagnostics, Manheim, Germany), and cohort #3 was run in a QuantStudio 5 Real-Time PCR System (Thermo Fisher Scientific Waltham, Massachusetts, USA). Reaction mixtures were incubated at 98°C for 3 min, followed by 45 cycles of 95°C for 10 s, 60°C for 30 s, and 37°C for 30 s. Five serial 10X dilutions of positive control were run in each plate to generate a standard curve, which was used to calculate the expression level of miRNAs.

4.3.5 TCGA database validation

The expression levels of miR-99a-5p were validated in the The Cancer Genome Atlas (TCGA) dataset. miRNA expression data were downloaded from OncoMir Cancer Database (OMCD) (https://www.oncomir.umn.edu/omcd/basic_search.php).

4.3.6 Statistical analysis

To evaluate differences in the miRNA expression levels and associations between miRNA expression and clinical variables, Mann–Whitney U and Kruskal–Wallis tests were used. Receiver-operating characteristic (ROC) curves were constructed by plotting the true positive (sensitivity) against the false-positive (1-specificity) rate, and area under the curve (AUC) was calculated. Optimal cut-off values were established based on the highest value obtained in ROC curve analysis according to Youden's J index [45,46]. Then, specificity, sensitivity, and accuracy were determined. In cohort #3 (validation cohort), specificity, sensitivity, and accuracy were determined by applying cut-off obtained in cohort #2 (testing cohort). Statistical analyses were performed using GraphPad Prism 6.01 software for Windows (GraphPad Software, La Jolla, California, USA). Results were considered statistically significant when the *p*-value was <0.05.

4.4 Results

4.4.1. Study design to develop a novel mirna biomarker

Herein, we tested miR-99a-5p as a candidate biomarker to diagnose BC. This study was divided into three parts: (1) Assessment of miR-99a-5p expression levels in BC and healthy breast tissue; (2) Evaluation of the miR-99a-5p expression levels in plasma of BC patients and healthy controls; (3) Validation of miR-99a-5p expression levels as a diagnostic biomarker for BC (**Figure 1**).

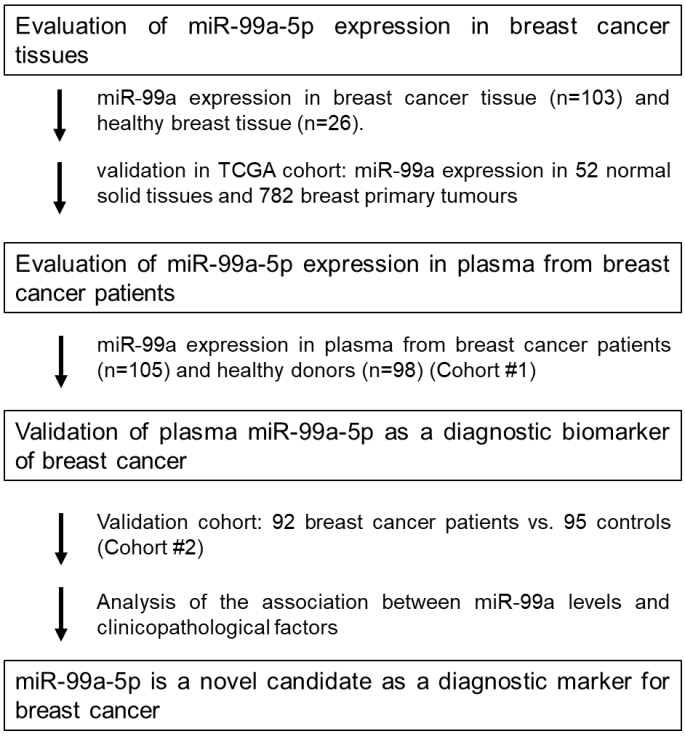

Figure 1. Study design to develop a novel miRNA biomarker.

4.4.2. miR-99a-5p expression in tissue

4.4.2.1 Cohort #1: Discovery cohort

miR-99a-5p expression was determined in 103 BC tissues and 26 healthy breast tissues by qRT-PCR. Detailed clinical and pathological data are depicted in **Table 1**. Overall, the median age of controls was significantly lower than that of patients (p = 0.0228). Nonetheless, no correlation between miR-99a-5p levels and age was observed (data not shown). miR-99a-5p expression levels were significantly lower in BC tissue (median, 95% CI: 32.72, 18.46–38.76) than in healthy breast tissues (median, 95% CI: 190, 85.20–317.80) (**Figure 2A**). miR-99a-5p expression levels were able to

discriminate BC from healthy breast tissues with an AUC of 0.8458 (95% CI: 0.7441–0.9474; $p < 0.0001$) (**Figure 2B**). Importantly, using the best cut-off value (78.17), 87.38% sensitivity, 76.92% specificity, and 85.27% accuracy were obtained. No significant associations were found between tissue miR-99a-5p levels and clinicopathological features (BC subtypes, histological grade, stage, pathological T stage, and regional lymph node metastasis) (**Table 2**).

Moreover, we also verified the expression of miR-99a-5p in the TCGA cohort. Data from 52 normal solid tissues and 782 breast primary tumors confirmed that miR-99a-5p expression was higher in normal tissues than in tumor tissues ($p < 0.0001$) (**Figure 2C**).

Table 1. Clinicopathological characteristics of breast cancer patients and controls in discovery cohort (cohort #1). [a]

Characteristics	Tissue Samples	
	Breast Cancer Patients	**Controls**
Number	103	26
Median age, years (range)	59.7 (57–62)	54.6 (47–63)
Molecular subtype, *n* (%)		
Luminal	59 (57.3%)	
TNBC	30 (29.1%)	n.a.
Her-2	14 (13.6%)	
Grade group, *n* (%)		
1	9 (8.7%)	
2	36 (35%)	n.a.
3	46 (44.7%)	
Unknown	12 (11.6%)	
Stage, *n* (%)		
I	12 (11.7%)	
II	63 (61.2%)	n.a.
III	13 (12.6%)	
Unknown	15 (14.6%)	

Table 1 (continued).

Pathological T stage, *n* (%)		
pT1	24 (23.3%)	
pT2	57 (55.3%)	
pT3	6 (5.8%)	n.a.
pT4	1 (1%)	
Unknown	15 (14.6%)	
Regional lymph node metastasis, *n* (%)		
No	39 (37.9%)	
Yes	50 (48.5%)	n.a.
Unknown	14 (13.6)	
Distant metastasis, *n* (%)		
No	89 (86.4%)	
Yes	0 (0%)	n.a.
Unknown	14 (13.6%)	

[a]TNBC, triple-negative breast cancer; n.a., not applicable

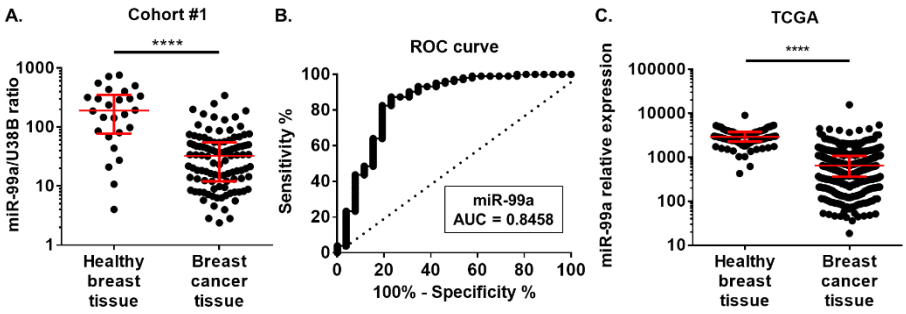

Figure 2. (A) MiR-99a expression levels in breast cancer tissues from cohort #1. Differential miR-99a expression levels in 103 breast cancer tissues were compared with 26 normal breast tissues. Red horizontal line: median with interquartile range. Mann–Whitney U, ****$p < 0.0001$.(B) ROC curve analysis for miR-99a expression levels in breast cancer tissue samples. (C) TCGA data for the expression of miR-99a-5p in normal solid tissue (n = 52) and breast primary tumour (n = 782). Expression is represented as reads per million miRNA mapped. Horizontal line: median with interquartile range. Mann–Whitney U, ****$p < 0.0001$.

Table 2. Association between tissue miR-99a-5p levels and clinicopathological features of breast cancer patients (cohort #1). [a]

	Number (%)	Median (95% CI)	*p* value
Histological subtype, *n* (%)			
Luminal	59 (57.3%)	27.00 (31.25–55.26)	
TNBC	30 (29.1%)	33.65 (25.62–44.83)	0.9783
Her 2-enriched	14 (13.6%)	18.51 (8.64–93.79)	
Unknown	n.a.		
Grade group, *n* (%)			
1	9 (8.7%)	38.76 (9.45–110.10)	
2	36 (35.0%)	18.18 (25.27–56.10)	0.7869
3	46 (44.7%)	32.33 (25.31–57.65)	
Unknown	12 (11.6%)		
Stage			
Early (I and II)	75 (72.8%)	21.38 (29.78–54.31)	0.8250
Late (III and IV)	13 (12.6%)	35.87 (19.85–43.36)	
Unknown	15 (14.6%)		
Pathological T stage, *n* (%)			
pT1	24 (23.3%)	23.40 (18.43–52.7)	
pT2	57 (55.3%)	23.05 (28.32–48.89)	0.687
pT3	6 (5.8%)	24.57 (-61.25–213.1)	
pT4	1 (1%)	54.97	
Unknown	15 (14.6%)		
Regional lymph node metastasis, *n* (%)			
No	39 (37.9%)	18.51 (23.08–64.21)	0.6279
Yes	50 (48.5%)	33.90 (28.52–49.03)	
Unknown	14 (13.6)		

[a]TNBC, triple-negative breast cancer; n.a., not applicable

4.4.3 miR-99a-5p expression in plasma

4.4.3.1 Cohort #2: Testing cohort

Considering the promising results obtained in tissue samples, we proceeded to explore the diagnostic value of miR-99a-5p in liquid biopsies. Indeed, miR-99a-5p was evaluated in plasma samples from BC patients (n = 105) and healthy controls (n = 98) (cohort #2). Clinicopathological data are detailed in **Table 3**. No significant differences in median age between groups

were observed. Herein, miR-99a-5p expression levels were significantly higher in plasma from BC patients (median, 95% CI: 21.02, 15.26 – 28.79) than in healthy volunteers (median, 95% CI: 7.09, 5.03 – 9.65) (p < 0.0001)(**Figure 3A**).

To assess the potential value of the miR-99a-5p expression in plasma for the diagnosis of BC, we computed the ROC curve for differentiating between BC patients and asymptomatic controls (**Figure 3B**). The obtained AUC was 0.7555 (95% CI: 0.69–0.82; p < 0.0001). At the optimal cut-off value of 15.04, 63.81% sensitivity, 79.59% specificity, and 71.43% accuracy were obtained.

Table 3. Clinicopathological characteristics of breast cancer patients and controls of testing and validation cohorts: cohort #2 and cohort #3.[a]

	Cohort #2		**Cohort #3**	
	Breast cancer patients	**Controls**	**Breast cancer patients**	**Controls**
Number	105	98	89	85
Median age, years (range)	52 (29–82)	50 (40–64)	54(32–92)	55 (32–90)
Histological subtype, *n* (%)				
Luminal	92 (87.6%)	n.a.	54 (60.7%)	n.a.
TNBC	7 (6.7%)		15 (16.9%)	
Her 2-enriched	5 (4.8%)		18 (20.2%)	
Unknown	1 (1%)		2 (2.2%)	
Grade group, n (%)				
1	8 (7.6%)	n.a.	19 (21.3%)	n.a.
2	54 (51.4%)		44 (49.4%)	
3	39 (37.1%)		25 (28.1%)	
Unknown	4 (3.8%)		1 (1.1%)	
Stage, *n* (%)				
I	42 (40%)	n.a.	24 (27.0%)	n.a.
II	18 (17.1%)		41 (46.1%)	
III	32 (30.5%)		15 (16.3%)	
IV	13 (12.4%)		5 (5.4%)	
Unknown			4 (4.3%)	

Table 3 (continued).

Pathological T stage, *n* (%)				
pT1	46 (43.8%)		36 (40.4%)	
pT2	29 (27.6%)		37 (41.6%)	
pT3	18 (17.1%)	n.a.	9 (10.1%)	n.a.
pT4	10 (9.5%)		1 (1.1%)	
Unknown	2 (1.9%)		6 (6.7%)	
Regional lymph node metastasis, *n* (%)				
No	53 (50.5%)		47 (52.8%)	
Yes	50 (47.6%)	n.a.	36 (40.4%)	n.a.
Unknown	2 (1.9%)		6 (6.7%)	
Distant metastasis, *n* (%)				
No	92 (87.6%)		80 (89.9%)	
Yes	13 (12.4%)	n.a.	7 (7.9%)	n.a.
Unknown			2 (2.2%)	

[a]TNBC, triple-negative breast cancer; n.a., not applicable

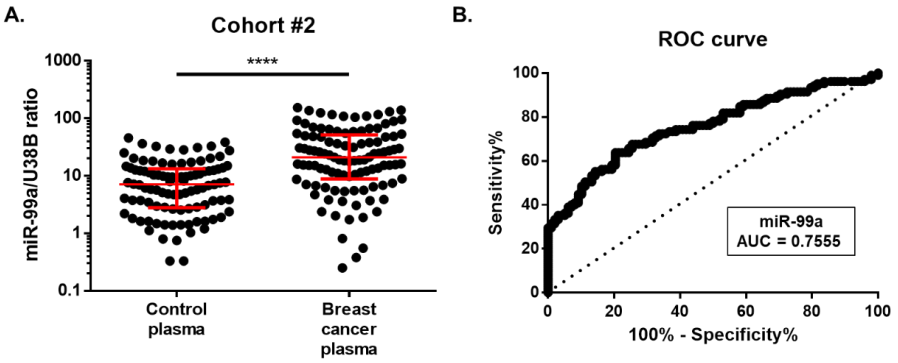

Figure 3. (A) Circulating miR-99a levels in cohort #2. Differential miR-99a levels in 105 plasma of breast cancer patients were compared with those of 98 healthy controls. Expression levels were significantly lower in healthy controls than in breast cancer patients. Red horizontal line: median with interquartile range. Mann–Whitney U, ****$p < 0.0001$. (B) ROC curve analysis for circulating miR-99a levels in cohort #2.

4.4.3.2. Cohort #3: Validation cohort

The value of circulating miR-99a-5p levels as a BC biomarker was further assessed in an independent cohort (cohort #3: validation cohort) comprising plasmas of 89 BC patients and 85 asymptomatic controls (Table 3). No significant differences were observed between the median age of both groups. miR-99a-5p levels were significantly overexpressed in the plasma of BC patients (median, 95% CI: 33.09, 12.95–54.40) than in controls (median, 95% CI: 9.11, 4.73–11.86) ($p < 0.0001$) (**Figure 4A**), in agreement with the results obtained for the testing cohort (cohort #2). Furthermore, using the cut-off value obtained from cohort #2 (15.04), miR-99a-5p was able to identify BC with 57.30% sensitivity, 67.06% specificity, and 62.07% accuracy. Nonetheless, a 0.6732 AUC (95% CI: 0.59–0.75; $p < 0.0001$) was observed for this set of samples (**Figure 4B**).

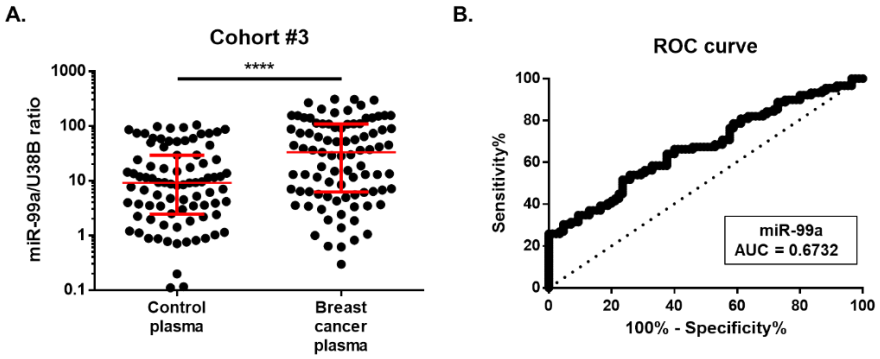

Figure 4. (A) Circulating miR-99a levels in cohort #3. Differential miR-99a levels in plasma of 89 breast cancer patients were compared with those of 85 healthy controls. Expression levels were significantly lower in healthy controls than in breast cancer patients. Red horizontal line: median with interquartile range. Mann–Whitney U, ****$p < 0.0001$. (B) ROC curve analysis for circulating miR-99a levels in cohort #3.

4.3.4. miR-99a-5p as a biomarker for early BC detection

We further hypothesized that circulating miR-99a-5p might be used as a biomarker for non-invasive early BC detection. Patients from cohort #2 and cohort #3 were put together (194 plasma samples), as there were no statistical differences in miR-99a-5p expression between cohorts (p = 0.22, data not shown). No significant associations were found between circulating miR-99a-5p levels and clinicopathological features (BC subtypes, histological grade, stage, pathological T stage, regional lymph node metastasis, and distant metastasis) (**Table 4**). Interestingly, circulating miR-99a-5p levels were up-regulated in early BC patients (stage I and II) compared with asymptomatic controls (p < 0.0001) (**Figure 5A**). Moreover, using the optimal cut-off value of 12.75, circulating miR-99a-5p levels were able to discriminate early BC from healthy controls with a 66.67% accuracy, 68.80% sensitivity, 65.28% specificity, and an AUC of 0.6913 (95% CI: 0.63 – 0.75; p < 0.0001; **Figure 5B**).

Overall, these results provide evidence that circulating miR-99a-5p levels may be used to detect early BC patients.

Table 4. Association between circulating miR-99a levels and clinicopathological features of breast cancer patients (cohorts #2 and #3)[a].

	Number (%)	Median (95% CI)	*p* value
Histological subtype, *n* (%)			
Luminal	146 (75.3%)	24.42 (16.00–36.14)	
TNBC	22 (11.3%)	9.50 (3.46–33.22)	0.0590
Her 2-enriched	23 (11.9%)	29.93 (13.53–89.41)	
Unknown	3 (1.5%)		
Grade group, *n* (%)			
1	27 (13.9%)	14.86 (5.61–36.9)	
2	98 (50.5%)	28.29 (18.05–44.09)	0.4594
3	64 (33.0%)	18.06 (12.88–36.14)	
Unknown	5 (2.6%)		

Table 4 (continue).

Stage			
Early (I and II)	125 (64.4%)	24.26 (15.98–36.90)	0.2382
Late (III and IV)	65 (33.5%)	21.02 (12.08–35.81)	
Unknown	4 (2.1%)		
Pathological T stage, *n* (%)			
pT1	82 (42.3%)	24.23 (15.98–38.61)	0.4119
pT2	66 (34.0%)	27.26 (12.91–44.91)	
pT3	27 (13.9%)	10.99 (3.54–49.49)	
pT4	11 (5.6%)	35.81 (5.34–48.45)	
Unknown	8 (4.1%)		
Regional lymph node metastasis, *n* (%)			
No	100 (51.5%)	24.23 (15.98–38.61)	0.3232
Yes	86 (44.3%)	19.54 (12.91–35.84)	
Unknown	8 (4.1%)		
Distant metastasis, *n* (%)			
No	172 (88.7%)	20.03 (15.18–29.70)	0.1810
Yes	20 (10.3%)	35.82 (16.2–91.99)	
Unknown	2 (1.0%)		

[a]TNBC, triple-negative breast cancer; n.a., not applicable

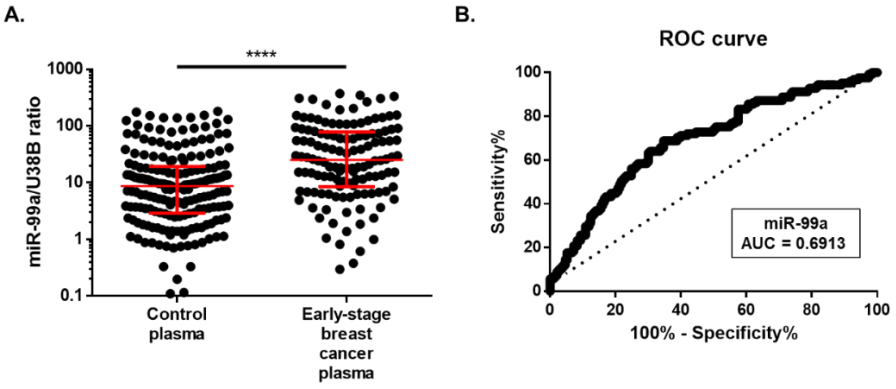

Figure 5. (A) Expression of miR-99a in early-stage breast cancer plasma. Distribution of circulating miR-99a levels in 125 plasma of early-stage breast cancer patients (stage I and II) and 193 healthy controls. Expression levels were significantly lower in healthy controls than in early-stage breast cancer patients. Horizontal line: median with interquartile range. Mann–Whitney U, ****$p < 0.0001$.(B) ROC curve analysis for circulating miR-99a levels in early-stage breast cancer patients.

4.5 Discussion

Breast cancer is the most common malignant tumor in the female population [1]. The importance of early detection of BC through the use of mammography and other techniques is fundamental as they change the prognosis of the disease. Therefore, the identification of biomarkers providing more accurate diagnostic information for BC patients is urgently needed.

In order to find new strategies for early diagnosis, several studies have been focused on miRNAs. These are a group of small non-coding RNAs that are involved in regulating a range of developmental and physiological processes, and their dysregulation has been associated with cancer. Specifically, circulating miRNAs have been proposed as being useful biomarkers for different cancer types' detection. Indeed, miRNAs present advantages that make them interesting to be used as diagnostic tools. These include being stable molecules that can be easily detected in body fluids such as plasma and the fact that their expression has been correlated with clinicopathological features, being promising as prognostic and predictive biomarkers [9].

Several authors assessed miR-99a expression in BC tissues and demonstrated its downregulation when compared to healthy tissues [23–26]. In this respect, miR-99a has been confirmed to be a tumor suppressor and its overexpression was associated with proliferation, invasion, and migration inhibition in BC cells *in vitro* and *in vivo* [23,27]. Moreover, that effect has been suggested to be mediated by several confirmed targets, such as mTOR [23,28], HOXA1 [24], IGF-1R [27], CDC25A [25], or FGFR3 [29].

Additionally, it is important to underline that miR-99a is significantly downregulated in several tumors, including glioma [30], oral squamous cell carcinoma [31], head and neck squamous cell carcinoma [22], endometrioid endometrial carcinoma [32], bladder cancer [21], non-small cell lung cancer [33], anaplastic thyroid cancer [34] or hepatocellular carcinoma [35]. All these findings suggest that miR-99a might be a potential cancer biomarker. In this study, we aimed to explore the value of circulating miR-99a-5p levels as a BC diagnostic biomarker.

Firstly, we evaluated miR-99a-5p expression in tissue samples from 26 healthy patients and 103 BC patients. The downregulation of miR-99a-5p in BC tissue was confirmed, in agreement with previous studies [23–26]. Besides, our result was also validated in the TCGA cohort.

Using plasma samples for diagnosis and follow-up of patients presents some advantages, as its extraction is less invasive than tissue biopsies. Many previous studies demonstrated the applicability of miRNAs in plasma as novel biomarkers for cancer diagnosis and prognosis [3,6,7]. Herein, we assessed circulating miR-99a-5p levels in two independent cohorts of BC patients and healthy volunteers from two different hospitals (testing and validation, respectively, cohorts # 2 and #3).

Surprisingly, contrary to the discovery cohort (cohort #1), in the testing cohort (cohort #2) from IPO-Porto, circulating miR-99a-5p expression levels were significantly higher in patients than in healthy controls. Then, our results were blindly validated in the validation cohort (cohort #3) from INCLIVA. Significant differences between groups were confirmed, suggesting

that circulating miR-99a-5p concentrations may be a useful biomarker for the detection of BC.

Importantly, to validate the application of circulating miR-99a-5p levels as a diagnostic biomarker, optimal cut-off from cohort #2 was applied in cohort #3, and the value of circulating miR-99a-5p levels in discriminating BC patients from controls was confirmed. Moreover, we tested the capacity of miR-99a-5p to detect early BC (stages I and II), and our results suggest that circulating miR-99a-5p concentrations might accurately detect BC patients in early stages of the disease.

Although it was somewhat unexpected to find opposite trends in tissue and plasma samples, similar results have been already reported for this miRNA and others in different tumor models [36]. Specifically regarding miR-99a, Torres *et al*. found similar results in endometrial endometrioid cancer, miR-99a expression being downregulated in the tissue of patients compared with tissue controls, whereas it was overexpressed in patients' plasma when compared to healthy samples [32,36]. Moreover, in the context of BC, several other microRNAs were demonstrated by other researchers to have opposite expression patterns in tissue and peripheral blood [19,20,37,38].

The processes by which miRNAs enter the bloodstream remain poorly understood. Nevertheless, several reasons might underlie the differential circulating expression profiles found: (I) miRNAs might be released by cancerous cells in an active manner [39]; (II) miRNAs are passively released by apoptotic or necrotic cells [40]; (III) miRNAs may derive from tumor microenvironments [37]. Pigati *et al*. reported that released miRNAs may

not, indeed, reflect the miRNA profile in the cell of origin, and demonstrated that the amount of released miRNA significantly differs between cell lines with similar death rates [39]. Hence, these results reinforce the concept of selective release, which may explain the expression profile's differences also observed in the current study.

Intriguingly, several authors that determined miR-99a levels in serum samples from BC patients found opposite results compared to ours. First, Li *et al*. obtained serum from 72 BC patients and 40 healthy volunteers and found that miR-99a-5p was downregulated in patients [41]. Then, Yu and co-workers determined miR-99a expression in serum samples of 113 BC patients and 47 healthy controls and found the same trend [42]. Nevertheless, several authors have already reported the lack of correlation between miRNAs expression in serum and plasma samples [43,44]. For instance, Li *et al*. found a negative correlation between plasma and serum of BC patients for some miRNAs [44]. The explanation for these findings might be that, before serum collection, blood is allowed to clot before obtaining the supernatant. Several authors consider that coagulation could cause cell lysis and blood cells would release miRNAs as a consequence, as well as loss of some vesicles that may be trapped in the coagulum [43,44]. Therefore, it is not possible to compare results from serum and plasma.

To our best knowledge, this is the first study to evaluate the value of circulating miR-99a-5p in plasma as a BC detection biomarker. Our results provide the evidence to consider plasma miR-99a-5p as a non-invasive biomarker for early BC, which might contribute to improving early detection and consequently reduce BC-related mortality.

4.6 Conclusions

Overall, our results show that circulating miR-99a-5p levels in plasma might be clinically useful as a non-invasive BC cancer detection biomarker, namely in the early stages of the disease. Importantly, similar results were obtained in two independent cohorts of BC patients from two different hospitals. Nonetheless, validation in larger multi-institutional cohorts are necessary to confirm these results.

Author Contributions

I.G.-C.: Conceptualization, methodology, data analysis, writing—original draft preparation. V.C., A.A.-A., A.L. (Ana Lameirinhas), S.S.: Methodology, data analysis. B.O., M.T.M., C.H., B.B.: patient´s data collection and analysis, writing—reviewing. A.L. (Ana Lluch): Conceptualization, funding acquisition. P.L., R.H.: data acquisition and analysis. C.J.: Supervision, conceptualization, writing—reviewing and editing, funding acquisition. J.M.C.: Conceptualization, methodology, reviewing and editing. P.E.: Supervision, conceptualization, writing—reviewing and editing, funding acquisition. *Corresponding authors. All authors have read and agreed to the published version of the manuscript.

Funding

This work was supported by Spanish Government PI18/01219 (ISCIII), CIBERONC (CB16/12/00481), and Grant PI 74-CBEG-CI-IPOP-19-2015 from Research Center—Portuguese Oncology Institute of Porto. I.G.-C. was funded by Generalitat Valenciana (ACIF/2016/030. V.C. was funded by Liga Portuguesa Contra o Cancro/Fundação P.T. A.A. and A.L. were funded by

Asociación Española Contra el Cancer. J.M.C. was funded by Sociedad Española de Oncología Médica (Río Hortega-SEOM).

Conflicts of Interest

The authors declare no conflict of interest.

4.7 Bibliography

1. Bray, F.; Ferlay, J.; Soerjomataram, I.; Siegel, R.L.; Torre, L.A.; Jemal, A. Global Cancer Statistics 2018: GLOBOCAN Estimates of Incidence and Mortality Worldwide for 36 Cancers in 185 Countries. *CA. Cancer J. Clin.* 2018;68(6):394–424.

2. Miller, K.D.; Nogueira, L.; Mariotto, A.B.; Rowland, J.H.; Yabroff, K.R.; Alfano, C.M.; Jemal, A.; Kramer, J.L.; Siegel, R.L. Cancer Treatment and Survivorship Statistics, 2019. *CA. Cancer J. Clin.* 2019;69(5):363–385.

3. Jafari, S.H.; Saadatpour, Z.; Salmaninejad, A.; Momeni, F.; Mokhtari, M.; Nahand, J.S.; Rahmati, M.; Mirzaei, H.; Kianmehr, M. Breast Cancer Diagnosis: Imaging Techniques and Biochemical Markers. *J. Cell. Physiol.* 2018;233(7):5200–5213.

4. Kashyap, D.; Kaur, H. Cell-Free MiRNAs as Non-Invasive Biomarkers in Breast Cancer: Significance in Early Diagnosis and Metastasis Prediction. *Life Sci.* 2020;246:117417.

5. Ng, E.K.O.; Li, R.; Shin, V.Y.; Jin, H.C.; Leung, C.P.H.; Ma, E.S.K.; Pang, R.; Chua, D.; Chu, K.M.; Law, W.L.; et al. Circulating MicroRNAs as Specific Biomarkers for Breast Cancer Detection. *PLoS One.* 2013;8(1):e53141.

6. Hamam, R.; Hamam, D.; Alsaleh, K.A.; Kassem, M.; Zaher, W.; Alfayez, M.; Aldahmash, A.; Alajez, N.M. Circulating MicroRNAs in Breast Cancer: Novel Diagnostic and Prognostic Biomarkers. *Cell Death Dis.* 2017;8(9):e3045.

7. Bottani, M.; Banfi, G.; Lombardi, G. Circulating MiRNAs as Diagnostic and Prognostic Biomarkers in Common Solid Tumors: Focus on Lung, Breast, Prostate Cancers, and Osteosarcoma. *J. Clin. Med.* 2019;8(10):1661.

8. Loh, H.Y.; Norman, B.P.; Lai, K.S.; Rahman, N.M.A.N.A.; Alitheen, N.B.M.; Osman, M.A. The Regulatory Role of MicroRNAs in Breast Cancer. *Int. J. Mol. Sci.* 2019;20(19):4940.

9. Cortez, M.A.; Welsh, J.J.; Calin, G.A. Circulating MicroRNAs as Noninvasive Biomarkers in Breast Cancer. *Recent Results Cancer Res.* 2012;195:151–161.

10. Bartel, D.P. MicroRNAs: Genomics, Biogenesis, Mechanism, and Function. *Cell.* 2004;116(2):281–297.

11. He, L.; Hannon, G.J. MicroRNAs: Small RNAs with a Big Role in Gene Regulation. *Nat. Rev. Genet.* 2004;5(7):522–531.

12. Tormo, E.; Adam-Artigues, A.; Ballester, S.; Pineda, B.; Zazo, S.; González-Alonso, P.; Albanell, J.; Rovira, A.; Rojo, F.; Lluch, A.; et al. The Role of MiR-26a and MiR-30b in HER2+ Breast Cancer Trastuzumab Resistance and Regulation of the CCNE2 Gene. *Sci. Rep.* 2017;7:41309.

13. Tormo, E.; Ballester, S.; Adam-Artigues, A.; Burgués, O.; Alonso, E.; Bermejo, B.; Menéndez, S.; Zazo, S.; Madoz-Gúrpide, J.; Rovira, A.; et al. The MiRNA-449 Family Mediates Doxorubicin Resistance in Triple-Negative Breast Cancer by Regulating Cell Cycle Factors. *Sci. Rep.* 2019;9(1):5316.

14. Iorio, M. V.; Ferracin, M.; Liu, C.G.; Veronese, A.; Spizzo, R.; Sabbioni, S.; Magri, E.; Pedriali, M.; Fabbri, M.; Campiglio, M.; et al. MicroRNA Gene Expression Deregulation in Human Breast Cancer. *Cancer Res.* 2005;65(16):7065–7070.

15. Mitchell, P.S.; Parkin, R.K.; Kroh, E.M.; Fritz, B.R.; Wyman, S.K.; Pogosova-agadjanyan, E.L.; Peterson, A.; Noteboom, J.; Briant, K.C.O.; Allen, A.; et al. Circulating MicroRNAs as Stable Blood-Based Markers for Cancer Detection. *PNAS.* 2008;105(30):10513–10518.

16. Ng, E.K.O.; Chong, W.W.S.; Jin, H.; Lam, E.K.Y.; Shin, V.Y.; Yu, J.; Poon, T.C.W.; Ng, S.S.M.; Sung, J.J.Y. Differential Expression of MicroRNAs in Plasma of Patients with Colorectal Cancer: A Potential Marker for Colorectal Cancer Screening. *Gut.* 2009;58(10):1375–81.

17. Bidarra, D.; Constâncio, V.; Barros-Silva, D.; Ramalho-Carvalho, J.; Moreira-Barbosa, C.; Antunes, L.; Maurício, J.; Oliveira, J.; Henrique, R.; Jerónimo, C. Circulating MicroRNAs as Biomarkers for Prostate Cancer Detection and Metastasis Development Prediction. *Front. Oncol.* 2019;9(September):1–8.

18. Estevão-Pereira, H.; Lobo, J.; Salta, S.; Amorim, M.; Lopes, P.; Cantante, M.; Reis, B.; Antunes, L.; Castro, F.; Palma De Sousa, S.; et al. Overexpression of Circulating MiR-30b-5p Identifies Advanced Breast Cancer. *J. Transl. Med.* 2019;17(435):.

19. van Schooneveld, E.; Wouters, M.C.A.; Van der Auwera, I.; Peeters, D.J.; Wildiers, H.; Van Dam, P.A.; Vergote, I.; Vermeulen, P.B.; Dirix, L.Y.; Van Laere, S.J. Expression Profiling of Cancerous and Normal Breast Tissues Identifies MicroRNAs That Are Differentially Expressed in Serum from Patients with (Metastatic) Breast Cancer and Healthy Volunteers. *Breast Cancer Res.* 2012;14(1):R34.

20. Matamala, N.; Vargas, M.T.; González-Cámpora, R.; Miñambres, R.; Arias, J.; Menéndez, P.; Andrés-León, E.; Mez-López, G.G.; Yanowsky, K.; Calvete-Candenas, J.; et al. Tumor MicroRNA Expression Profiling Identifies Circulating MicroRNAs for Early Breast Cancer Detection. *Clin. Chem.* 2015;61(8):1098–1106.

21. Feng, Y.; Kang, Y.; He, Y.; Liu, J.; Liang, B.; Yang, P.; Yu, Z. MicroRNA-99a Acts as a Tumor Suppressor and Is down-Regulated in Bladder Cancer. *BMC Urol.* 2014;14(50):.

22. Hou, B.; Ishinaga, H.; Midorikawa, K.; Shah, S.A.; Nakamura, S.; Hiraku, Y.; Oikawa, S.; Murata, M.; Takeuchi, K. Circulating MicroRNAs as Novel Prognosis Biomarkers for Head and Neck Squamous Cell Carcinoma. *Cancer Biol. Ther.* 2015;16(7):1042–1046.

23. Hu, Y.; Zhu, Q.; Tang, L. MiR-99a Antitumor Activity in Human Breast Cancer Cells through Targeting of MTOR Expression. *PLoS One.* 2014;9(3):e92099.

24. Wang, X.; Li, Y.; Qi, W.; Zhang, N.; Sun, M.; Huo, Q.; Cai, C.; Lv, S.; Yang, Q. MicroRNA-99a Inhibits Tumor Aggressive Phenotypes through Regulating HOXA1 in Breast Cancer Cells. *Oncotarget.* 2015;6(32):32737–32747.

25. Qin, H.; Liu, W. MicroRNA-99a-5p Suppresses Breast Cancer Progression and Cell-Cycle Pathway through Downregulating CDC25A. *J. Cell. Physiol.* 2018;1–12.

26. Toda, H.; Seki, N.; Kurozumi, S.; Shinden, Y.; Yamada, Y.; Nohata, N.; Moriya, S.; Idichi, T.; Maemura, K.; Fujii, T.; et al. RNA-Sequence-Based MicroRNA Expression Signature in Breast Cancer: Tumor-Suppressive MiR-101-5p Regulates Molecular Pathogenesis. *Mol. Oncol.* 2020;14(2):426–446.

27. Xia, M.; Li, H.; Wang, J.-J.; Zeng, H.-J.; Wang, S.-H. MiR-99a Suppress Proliferation, Migration and Invasion through Regulating Insulin-like Growth Factor 1 Receptor in Breast Cancer. Eur. Rev. Med. *Pharmacol. Sci.* 2016;20(9):1755–63.

28. Turcatel, G.; Rubin, N.; El-Hashash, A.; Warburton, D. MIR-99a and MIR-99b Modulate TGF-β Induced Epithelial to Mesenchymal Plasticity in Normal Murine Mammary Gland Cells. *PLoS One.* 2012;7(1):e31032.

29. Long, X.; Shi, Y.; Ye, P.; Guo, J.; Zhou, Q.; Tang, Y. MicroRNA-99a Suppresses Breast Cancer Progression by Targeting FGFR3. *Front. Oncol.* 2020;9:1473.

30. Ning, S.; Liu, H.; Gao, B.; Wei, W.; Yang, A.; Li, J.; Zhang, L. MiR-155, MiR-96 and MiR-99a as Potential Diagnostic and Prognostic Tools for the Clinical Management of Hepatocellular Carcinoma. *Oncol. Lett.* 2019;18(3):3381–3387.

31. He, K.; Tong, D.; Zhang, S.; Cai, D.; Wang, L.; Yang, Y.; Gao, L.; Chang, S.; Guo, B.; Song, T.; et al. MiRNA-99b-3p Functions as a Potential Tumor Suppressor by

Targeting Glycogen Synthase Kinase-3β in Oral Squamous Cell Carcinoma Tca-8113 Cells. *Int. J. Oncol.* 2015;47(4):1536.

32. Torres, A.; Torres, K.; Pesci, A.; Ceccaroni, M.; Paszkowski, T.; Cassandrini, P.; Zamboni, G.; Maciejewski, R. Deregulation of MiR-100, MiR-99a and MiR-199b in Tissues and Plasma Coexists with Increased Expression of MTOR Kinase in Endometrioid Endometrial Carcinoma. *BMC Cancer.* 2012;12:369.

33. Yu, S.; Zhang, C.; Dong, F.; Zhang, Y. MiR-99a Suppresses the Metastasis of Human Non-Small Cell Lung Cancer Cells by Targeting AKT1 Signaling Pathway. *J. Cell. Biochem.* 2015;116(2):276.

34. Huang, H.-G.; Luo, X.; Wu, S.; Jian, B. MiR-99a Inhibits Cell Proliferation and Tumorigenesis through Targeting MTOR in Human Anaplastic Thyroid Cancer. *Asian Pac. J. Cancer Prev.* 2015;16(12):4937–44.

35. Li, D.; Liu, X.; Lin, L.; Hou, J.; Li, N.; Wang, C.; Wang, P.; Zhang, Q.; Zhang, P.; Zhou, W.; et al. MicroRNA-99a Inhibits Hepatocellular Carcinoma Growth and Correlates with Prognosis of Patients with Hepatocellular Carcinoma. *J. Biol. Chem.* 2011;286(42):36677–36685.

36. Tanaka, M.; Oikawa, K.; Takanashi, M.; Kudo, M.; Ohyashiki, J.; Ohyashiki, K.; Kuroda, M. Down-Regulation of MiR-92 in Human Plasma Is a Novel Marker for Acute Leukemia Patients. *PLoS One.* 2009;4(5):e5532.

37. Cuk, K.; Zucknick, M.; Heil, J.; Madhavan, D.; Schott, S.; Turchinovich, A.; Arlt, D.; Rath, M.; Sohn, C.; Benner, A.; et al. Circulating MicroRNAs in Plasma as Early Detection Markers for Breast Cancer. *Int. J. Cancer.* 2013;132(7):1602–1612.

38. Chan, M.; Liaw, C.S.; Ji, S.M.; Tan, H.H.; Wong, C.Y.; Thike, A.A.; Tan, P.H.; Ho, G.H.; Lee, A.S.G. Identification of Circulating MicroRNA Signatures for Breast Cancer Detection. *Clin. Cancer Res.* 2013;19(16):4477–4487.

39. Pigati, L.; Yaddanapudi, S.C.S.; Iyengar, R.; Kim, D.J.; Hearn, S.A.; Danforth, D.; Hastings, M.L.; Duelli, D.M. Selective Release of MicroRNA Species from Normal and Malignant Mammary Epithelial Cells. *PLoS One.* 2010;5(10):.

40. Turchinovich, A.; Weiz, L.; Langheinz, A.; Burwinkel, B. Characterization of Extracellular Circulating MicroRNA. *Nucleic Acids Res.* 2011;39(16):7223–33.

41. Li, J.; Song, Z.J.J.; Wang, Y.Y.Y.; Yin, Y.; Liu, Y.; Nan, X. Low Levels of Serum MiR-99a Is a Predictor of Poor Prognosis in Breast Cancer. *Genet. Mol. Res.* 2016;15(3):.

42. Yu, X.; Liang, J.; Xu, J.; Li, X.; Xing, S.; Li, H.; Liu, W.; Liu, D.; Xu, J.; Huang, L.; et al. Identification and Validation of Circulating MicroRNA Signatures for Breascancer

Early Detection Based on Large Scale Tissue-Derived Data. *J. Breast Cancer.* 2018;21(4):363–370.

43. Heegaard, N.H.H.; Schetter, A.J.; Welsh, J.A.; Yoneda, M.; Bowman, E.D.; Harris, C.C. Circulating MicroRNA Expression Profiles in Early Stage Non- Small Cell Lung Cancer. *Int. J. Cancer.* 2012;130(6):1378–1386.

44. Li, M.; Zhou, Y.; Xia, T.; Zhou, X.; Huang, Z.; Zhang, H.; Zhu, W.; Ding, Q.; Wang, S. Circulating MicroRNAs from the MiR-106a–363 Cluster on Chromosome X as Novel Diagnostic Biomarkers for Breast Cancer. *Breast Cancer Res. Treat.* 2018;170(2):257–270.

45. Youden, W.J. Index for Rating Diagnostic Tests. *Cancer.* 1950;3(1):32–35.

46. Schisterman, E.F.; Perkins, N.J.; Liu, A.; Bondell, H. Optimal Cut-Point and Its Corresponding Youden Index to Discriminate Individuals Using Pooled Blood Samples. *Epidemiology.* 2005;16(1):73–81.

CHAPTER 5 |

Biosensor for detection of circulating miR-99a-5p

Nanoporous anodic alumina-based sensor for miR-99a-5p detection as an effective early breast cancer diagnostic tool

Iris Garrido-Cano[1,2‡], Luis Pla[2,3,4,‡], Sara Santiago-Felipe[2,3,4,*], Soraya Simón[1,5], Belen Ortega[1,5], Begoña Bermejo[1,5], Ana Lluch[1,5,6,7], Juan Miguel Cejalvo[1,5,6], Pilar Eroles[1,6,8] and Ramón Martínez-Máñez[2,3,4,9,*]

[1] Biomedical Research Institute INCLIVA,46010 Valencia, Spain

[2] CIBER de Bioingeniería, Biomateriales y Nanomedicina (CIBER-BBN), 28029 Madrid, Spain

[3] Unidad Mixta de Investigación en Nanomedicina y Sensores, Universitat Politècnica de València, Instituto de Investigación Sanitaria La Fe, 46026 Valencia, Spain

[4] Instituto Interuniversitario de Investigación de Reconocimiento Molecular y Desarrollo Tecnológico (IDM), Universitat Politècnica de València, Universitat de València, 46010 Valencia, Spain

[5] Clinical Oncology Department, Hospital Clínico Universitario de Valencia, 46010 Valencia, Spain

[6] Centro de Investigación Biomédica en Red de Cáncer (CIBERONC), 46010 Valencia, Spain

[7] Universitat de València, 46010 Valencia, Spain

[8] COST Action CA15204, 1210 Brussels, Belgium

[9] Unidad Mixta UPV-CIPF de Investigación en Mecanismos de Enfermedades y Nanomedicina. Universitat Politècnica de València, Centro de Investigación Príncipe, 46012 València, Spain.

ACS Sensors. **2021;6(3):1022–1029.**

5.1 Abstract

Circulating microRNAs have emerged as potential diagnostic biomarkers. The deregulation of the microRNA miR-99a-5p has been previously described as an effective biomarker of early breast cancer. Herein, we present a new nanoporous anodic alumina (NAA)-based biosensor that can detect plasma miR-99a-5p with high sensitivity and selectivity. NAA pores were loaded with rhodamine B and capped with a specific oligonucleotide able to block cargo release until the target is present. In the presence of miR-99a-5p, the capping oligonucleotide recognizes the miR-99a-5p sequence and displaces allowing the release of the encapsulated dye. This method was able to successfully distinguish healthy controls from breast cancer patients, even at early stages with high efficiency, showing the presented system as a promising tool for breast cancer detection.

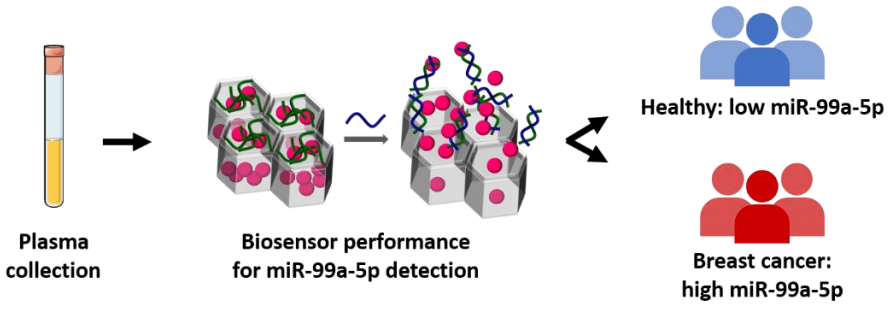

Graphical abstract.

5.2 Introduction

Breast cancer (BC) is one of the most common types of cancer in the world and one of the leading causes of cancer-related death in women [1]. Early BC diagnosis has been proven to significantly improve the patient's survival rates. The five-year survival rate for BC patients diagnosed at stage I is 98% and falls until 25% for those diagnosed at stage IV [2−4]. Currently, mammography is the gold-standard technique for diagnosis, but it presents some limitations such as radiation exposure, as well as low sensitivity and specificity in young women with dense breast tissue [5]. Therefore, the development of new diagnostic tools for early BC detection is needed.

Interest in microRNAs (miRNAs) has recently emerged due to their potential application as diagnostic biomarkers [3,6,7]. They consist of small non-coding ribonucleic acids (RNAs) of 19−25 nucleotides that regulate gene expression through different mechanisms [8]. Their deregulation has been described in many diseases including BC, where they have been associated with tumor aggressiveness, prognosis, response to treatment, and clinical outcome [6,9−11]. Indeed, several authors evidenced the relevance of circulating miRNAs in plasma as minimally invasive biomarkers for the prognosis and diagnosis of different types of cancers [7,12,13]. Nowadays, the detection of circulating miRNAs is mainly assessed in laboratories through quantitative real-time PCR (qRT-PCR), microarrays, northern blotting, and RNA sequencing, which are time-consuming and complex techniques. As a result, the detection of miRNAs as a diagnosis tool falls outside the clinical context.

Implementing circulating miRNAs for diagnosis requires the development of effective, rapid, simple, and low-cost analytical methods. In this context, nanomaterials and, in particular, nanoporous anodic alumina (NAA), have emerged as optimal supports for the design of several biosensors for numerous sensing applications [14]. To provide specificity, nanoporous entrances are blocked with molecular gates (also known as gatekeepers or nanovalves) of different natures (such as proteins, enzymes, antibodies, metallic nanoparticles, organic molecules, polymeric structures, and deoxyribonucleic acid (DNA) sequences) that can control cargo delivery depending on the presence or absence of a stimulus [15−17]. In these systems, NAA was loaded with a chromo-fluorogenic reporter and capped with selective molecules that are able to recognize a specific analyte. Therefore, the dye remains inside the pores until capping molecules recognize the target (bio)molecule, triggering its displacement and inducing payload release. Based on this approach, it is possible to detect cations, anions, and biomolecules [18−24]. As a particularity of this sensing concept, host−guest interaction is independent of the signaling subunit and, besides, an amplifying effect is provided since few stimuli units are able to release a large quantity of entrapped signaling molecules.

Herein, we present a new DNA-gated mesoporous biosensor for the detection of circulating miR-99a-5p, which has been previously described as an effective biomarker for BC [25]. Our proposed system is based on NAA supports whose pores are loaded with rhodamine B and capped with an oligonucleotide that specifically hybridizes with the miR-99a-5p sequence. Therefore, in the absence of the target miRNA, the capping oligonucleotide continues blocking the pores, inhibiting the dye release. In contrast, in the

presence of the miR-99a-5p, there is a favorable DNA−RNA interaction between the microRNA and the capping oligonucleotide that induces the uncapping of the pores, giving rise to dye delivery. High selectivity and sensibility were accomplished, and, after confirming the potential of our system *in vitro*, its diagnosis applicability was validated in plasmas from healthy controls and BC patients.

5.3 Materials and methods

5.3.1 General techniques

Field emission scanning electron microscopy (FESEM) experiments, including energy-dispersive X-ray spectroscopy (EDX), were performed on a ZEISS Ultra 55 microscope. Fluorescence spectra were measured on a microplate reader (Synergy H1, BioTek, Winooski, VT).

5.3.2 Chemicals

(3-Aminopropyl)triethoxysilane (APTES), hydrochloric acid, rhodamine B, and tris(hydroxymethyl)aminomethane (TRIS) were purchased from Sigma-Aldrich (Spain). NAA supports were provided by InRedox Company (Longmont, CO). O1 sequence 5'-CAC AAG ATC GGA TCT ACG GGT T-3' was designed as the complementary sequence of miR-99a-5p (obtained from mirbase.org) and was obtained from Thermo Fisher Scientific (Waltham, MA). MirVana mimics of miR-99a-5p, miR-200c-3p, miR-449c-3p, miR- 221-3p, miR-21-5p, and the mirVana miRNA Mimic Negative Control no.1 were obtained from Thermo Fisher Scientific (Waltham, MA).

5.3.3 Synthesis of solids

To prepare S1, NAA supports of 2 mm diameter were immersed in 8 mL of rhodamine B solution in acetonitrile (1 mM, ACN) and stirred for 24 h to ensure its entrance inside the pores. Then, the mesoporous surface was functionalized by the addition of APTES (1.32 mmol, 328 µL) and stirred at room temperature for 6 h. Afterward, the obtained S1 supports were washed dropwise with a rhodamine B-ACN solution and dried overnight at room temperature.

Then, the final solid S2 was obtained by submerging S1 in a solution of the capping oligonucleotide O1 in TRIS hybridization buffer (20 mM Tris−HCl, 37.5 mM MgCl2, pH 7.5). After the corresponding optimization, capping conditions were established in 20 µL of O1 (100 µM) in a 250 µL final volume of TRIS hybridization buffer for two S1 supports agitated at 37 °C during 1 h. Finally, the as-prepared S2 solids were washed with TRIS hybridization buffer to remove the leftover O1.

5.3.4 Cargo quantification

To determine the quantity of the loaded rhodamine B inside the pores, two S2 supports were immersed in the hybridization buffer (1 mL). Then, one of the supports was stirred for 1 h at 90 °C to induce maximum cargo delivery. As a control, the other support was stirred for 1 h at 25 °C. To quantify the released fluorophore, fluorescence was measured (λexc = 555 nm, λem = 575 nm), and the released dye was determined using a calibration curve. The experiment was carried out in triplicate.

5.3.5 Detection protocol

The S2 ability for recognition and detection of miR-99a-5p was determined by fluorescence spectroscopy measurements of the delivered fluorescence indicator entrapped into the nanostructure of the supports in the absence and the presence of the miR-99a-5p sequence. In a typical experiment, two different and independent S2 solids were submerged in separate solutions containing 900 µL of TRIS hybridization buffer. Then, 100 µL of miR-99a-5p (1 µM) or TRIS hybridization buffer (control) were inoculated into the solids and stirred for 1 h at 37 °C. Aliquots were collected every 15 min. The released rhodamine B was monitored by measuring the fluorescence at 575 nm (λexc = 555 nm). The experiment was carried out in triplicate.

5.3.6 Amplification assay

To determine the signal amplification, two S2 solids were immersed in 900 µL of TRIS hybridization buffer. Then, 100 µL of miR-99a-5p (1 µM) was added to one support. As a control, 100 µL of the hybridization buffer was added to the second support. Solids were incubated for 1 h at 37 °C, and the released fluorophore was measured at 575 nm (λexc = 555 nm). Finally, the amount of released dye was determined by using a calibration curve.

5.3.7 Selectivity assessment

To evaluate the selectivity of the synthesized sensor, seven individual and separate S2 supports were submitted to the presence of target mRNA-99 as well as other miRNA sequences such as miR-200c-3p, miR-449c-3p, miR-221-3p, miR-21- 5p, and the mirVana miRNA Mimic Negative Control no.

1, all of them at a final concentration of 10^{-1} µM in 1 mL of TRIS hybridization buffer, and stirred for 1 h at 37 °C. The response to the bare TRIS hybridization buffer was also evaluated as a negative control experiment. The delivered rhodamine B was determined by fluorescence (λexc = 555 nm, λem = 585 nm). The experiment was carried out in triplicate with an average of 21 S2 supports.

5.3.8 Determination of sensitivity of mir-99a-5p in real competitive media

The response of S2 to decreasing concentrations of miR-99a-5p was evaluated in human plasma media. For that, eight S2 materials prepared were separately immersed in 200 µL of plasma from non-BC patients. Then, 200 µL of 10-fold dilutions of miRNA-99a-5p were added to reach a final concentration between 0 and 500 nM. Mixtures were stirred for 60 min at room temperature and aliquots were obtained at 0 and 60 min. Finally, the diffused rhodamine B was determined by fluorescence emission at 575 nm (λexc = 555 nm). The experiment was carried out in triplicate with an average of 24 S2 supports.

5.3.9 Validation in clinical samples

Plasma samples from 47 BC patients were collected before treatment from Biomedical Research Institute INCLIVA (Spain). Plasma samples from 47 healthy volunteers were obtained from the same institution and the Valencian Biobanking Network. Ethylenediaminetetraacetic acid (EDTA)-containing blood tubes were centrifuged at 2000 rpm for 10 min at 4 °C. The superior phase corresponding to the plasma was stored at−80 °C until further use.

To carry out the validation analysis, 250 µL of plasma were added to S2 supports and diluted in 150 µL of TRIS hybridization buffer (final assay volume, 400 µL). Supports were stirred for 1 h at 37 °C. Then, fluorescence emission was measured at 575 nm (λexc = 555 nm) at 0 and 60 min to determine the amount of diffused rhodamine B. TRIS buffer was used as a negative control.

5.3.10 Ethical committee

Informed consent was obtained from all subjects included in this work, and the study was approved by the Ethics Committee of INCLIVA (2019/196) in accordance with the ethical standards of the Declaration of Helsinki.

5.3.11 Statistical analysis

Differences between groups were evaluated by Mann−Whitney U or Kruskal Wallis nonparametric tests. The receiver-operating characteristic (ROC) curves were applied to determine the diagnostic value of our nanodevice, and the area under the curve (AUC) was calculated. The optimal sensitivity, specificity, and accuracy were obtained according to Youden's J index (sensitivity + specificity − 1) [31,32]. Statistical analyses were carried out with GraphPad Prism 6.01 (GraphPad Software). Results were considered statistically significant when P-value was <0.05.

5.4 Results and discussion

5.4.1 Design, synthesis, and characterization of the functional nanodevice

The aim of this work was to develop an effective, rapid, and easy to handle tool to detect circulating miR-99a-5p in clinical samples. To achieve

it, pores of NAA support were loaded with the fluorescent dye rhodamine B. Then, the external surface was functionalized with APTES to obtain S1. Subsequently, oligonucleotide O1, which was designed as a complementary sequence of miR-99a-5p, was anchored to APTES through electrostatic interactions between positively charged amino moieties provided by APTES functionalization and negative charges from the nucleotide sequence, affording the final S2 sensing material. This system was designed to trigger a specific pore opening in the presence of miR-99a-5p, allowing the delivery of the entrapped rhodamine B (**Figure 1**).

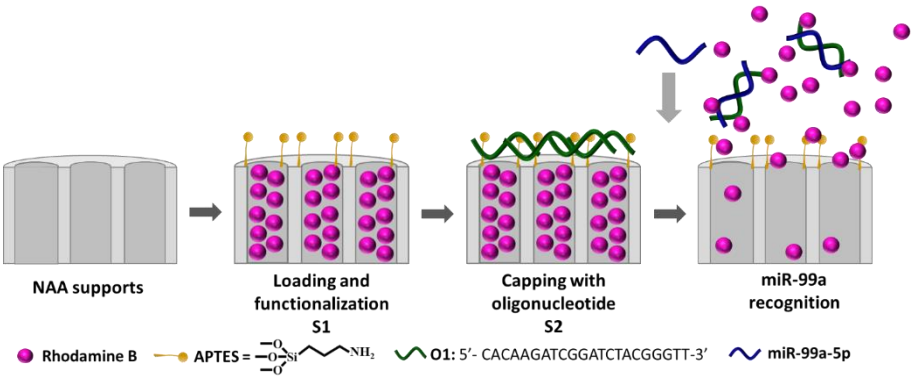

Figure 1. Schematic representation of the preparation and sensing process of S2 material. Nanoporous anodic alumina (NAA) support was loaded with rhodamine B and functionalized with APTES to obtain solid S1. Solid S2 was obtained after capping with an oligonucleotide with binding affinity for miR-99a-5p. Delivery of the entrapped rhodamine B is selectively achieved in the presence of miR-99a-5p with high-signal amplification.

Characterization of the raw NAA material (S0), S1, and S2 was undertaken by FESEM and EDX analyses. Commercially available NAA supports are composed of a matrix of alumina with funnel-like pores with a diameter that varies between 20 and 30 nm at the top and 5 nm at the bottom, and an average pore density of 9×10^{11} pores·cm^{-2}. The pore profundity reaches ca. 15 nm, and below this depth, the pore configuration becomes uniform along 10 µm. According to the obtained data, this pore morphology allows, approximately, a maximum loading of 4 ng of rhodamine B per µg of NAA. FESEM images of the NAA scaffold and the S2 solid confirmed the porous structure and evidenced structure maintenance after subsequent chemical processes required for system preparation (**Figure 2**).

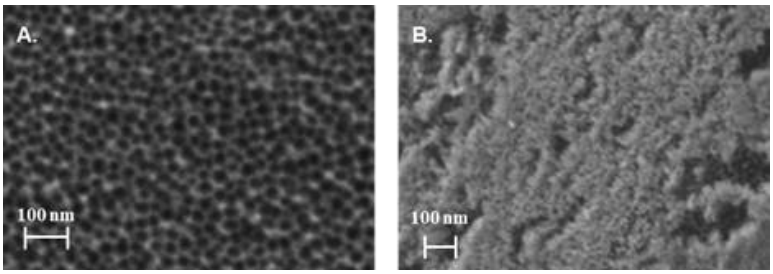

Figure 2. FESEM images of (A) NAA support and (B) S2.

The organic content of the successive prepared materials (S0, S1, and S2) was followed by energy-dispersive X-ray spectroscopy (**Table 1**). High carbon (C/Al: 2.28) and nitrogen (N/Al: 0.38) content was observed in S1 due to the rhodamine B dye loading and APTES functionalization. However, these amounts decreased for S2 because of some unspecific dye leakage during the capping process with O1 and as a result of not complete blockage of the pores. The amount of capping oligonucleotide O1 was evidenced by the

presence of phosphorus in the final material S2 (P/Al 0.01) as it was not observed in the NAA support or in S1.

Table 1. Atomic elemental ratios in the different solids prepared.

	C/Al	N/Al	P/Al
S1	2.28	0.38	-
S2	0.74	0.49	0.01

5.4.2 Controlled delivery studies

First, *in vitro* detection of miR-99a-5p was carried out employing our system. In a typical experiment, two separated S2 solids were immersed either in a solution of 10^{-1} μM miRNA in TRIS buffer or in bare TRIS buffer as a control solution. They were incubated for 1 h, and rhodamine B release was determined by fluorescence measurement at selected times. Our results showed that in the absence of miR-99a-5p, dye diffusion from the pores was negligible, with an average dye delivery of less than 20% (**Figure 3**). In contrast, after the addition of miR-99a-5p, as a result of the complementary hybridization between both miRNA and O1, capping sequences were displaced, pores opened, and dye diffused from the inner structure to the outer solution, as depicted in **Figure 1**. The observed enhancement in fluorescence emission was attributed to the favorable interaction between the capping oligonucleotide and the miR-99a-5p sequence as well as the intrinsic signal amplification that is observed when gated materials are used. In this context, recent works based on these gated systems have demonstrated that a unique DNA molecule can lead to the delivery of approximately 10^4–10^{11} dye molecules when the pores are opened [19,20].

In this work, it has been determined that 1 nM of miRNA was able to induce the release of an average of 2×10^{11} molecules of rhodamine B, confirming a high-signal amplification capacity.

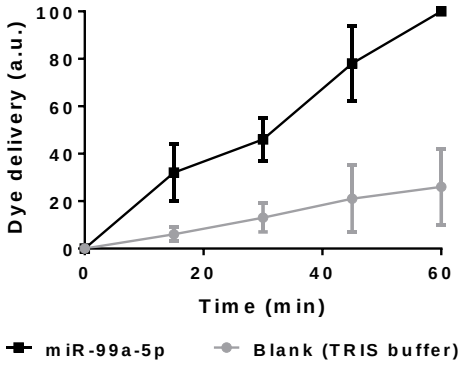

Figure 3. Rhodamine B delivery from the pores of the S2 material in the absence (gray) or in the presence of miR-99a-5p (10^{-1} µM)(black). Mean ± SD.

In a second step, we further evaluated the response of our system to different concentrations of miR-99a-5p. Human plasma solutions containing different spiked concentrations of miRNA were added to several S2 solids, and the dye release was determined after 60 min. We confirmed the correlation between the released rhodamine B and the concentration of miR-99a-5p (**Figure 4**), which is in agreement with the uncapping protocol, based on the displacement of O1 by complementary hybridization with miR-99a-5p. In these conditions, a linear response in the 0.5−25.0 nM concentration range was observed and a limit of detection (LOD) of 0.5 nM was calculated. It is worth mentioning that this value is in the concentration range of the circulating miRNAs present in the human plasma, which usually varies from

femtomolar to nanomolar, suggesting the potential use of the proposed system for the miRNA detection [28].

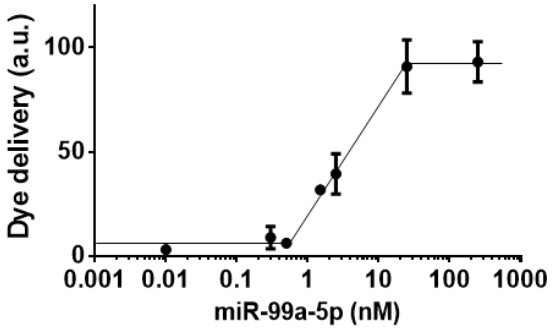

Figure 4. Release of rhodamine B in TRIS buffer (pH 7.4) from support S2 in the presence of different concentrations of miR-99a-5p. Mean ± SD.

In addition, the selectivity of the prepared gated material was tested. For this purpose, we evaluated the response of our system in the presence of 10^{-1} μM miR-200c-3p, miR-449c-3p, miR-221-3p, miR-21-5p, and a miRNA negative control that consists of a random sequence. We compared the dye delivery induced by those biomolecules with the response to miR-99a-5p. After 60 min of incubation, fluorescence emission was determined for each one of the tests. The results indicated that the diffusion of rhodamine B in the presence of other miRNAs was similar to the cargo release in the bare TRIS buffer (**Figure 5**). By contrast, in the presence of the specific miR-99a-5p sequence, support S2 induced a significant cargo delivery. These results demonstrate that S2 selectively recognizes the miR-99a-5p sequence.

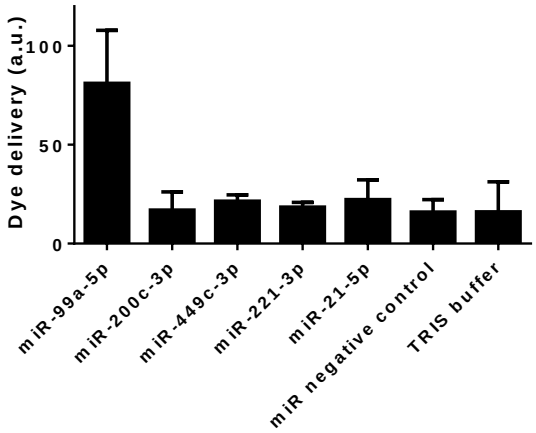

Figure 5. Selectivity of the proposed method. Release of rhodamine B from S2 support in the presence of 10^{-1} µM miR-99a-5p, miR-200c- 3p, miR-449c-3p, miR-221-3p, miR-21-5p, miRNA negative control (random sequence), and TRIS buffer. Mean ± SD.

5.4.3 Validation in clinical samples

Next, encouraged by the promising results previously obtained, we proceeded to validate the applicability of the nanodevices in real clinical samples. For this purpose, miR-99a-5p was assessed in plasma from 47 healthy controls and 47 BC patients (**Table 2**). Our results revealed that the levels of released rhodamine B were significantly higher in patients than in healthy controls. The median was 15343 (95% CI, 8706−23182) and 3629 (95% CI, 2487−6495) ($p < 0.0001$), respectively (**Figure 6A**). These results clearly agreed with our previous work, where we performed qRT-PCR to determine circulating levels of miR-99a-5p in plasma of BC patients and controls and concluded that miR-99a is overexpressed in plasma from BC patients [25].

Table 2. Association between clinicopathological features of breast cancer patients and circulating mir-99a-5p levels. [a]

	Number (%)	Median (95% CI)	P value
Hystological subtype, *n* (%)			
Luminal	29 (61.7 %)	11527 (7318 - 27759)	0.444
TNBC	6 (12.8 %)	8782 (2457 - 49145)	
Her 2-enriched	11 (23.4 %)	21791 (8231 - 42082)	
Unknown	1 (2.1 %)		
Grade group, *n* (%)			
1	11 (23.4 %)	11527 (2985 - 47462)	0.720
2	23 (48.9 %)	19677 (7605 - 27759)	
3	13 (27.6 %)	22562 (7318 - 42082)	
Stage, *n* (%)			
I	9 (19.1 %)	15768 (7605 - 42082)	0.0770
II	25 (53.2 %)	8772 (5432 - 22735)	
III	8 (17.0 %)	22177 (8792 - 50246)	
IV	4 (8.5 %)	37980 (22479 - 52086)	
Unknown	1 (2.1 %)		
Tumour size, *n* (%)			
≤ 50 mm	40 (85.1 %)	11168 (7933 - 23955)	0.3681
> 50 mm	5 (10.6 %)	22562 (9164 - 37389)	
Unknown	2 (4.3 %)		
Regional lymph node metastasis, *n* (%)			
No	23 (48.9 %)	9164 (7605 - 35514)	0.8074
Yes	22 (46.8 %)	17723 (7933 - 23182)	
Unknown	2 (4.3 %)		
Distant metastasis, *n* (%)			
No	42 (89.4 %)	11168 (8231 - 22735)	0.85853
Yes	4 (8.5 %)	29934 (2457 - 38571)	
Unknown	1 (2.1%)		

[a]TNBC, triple-negative breast cancer

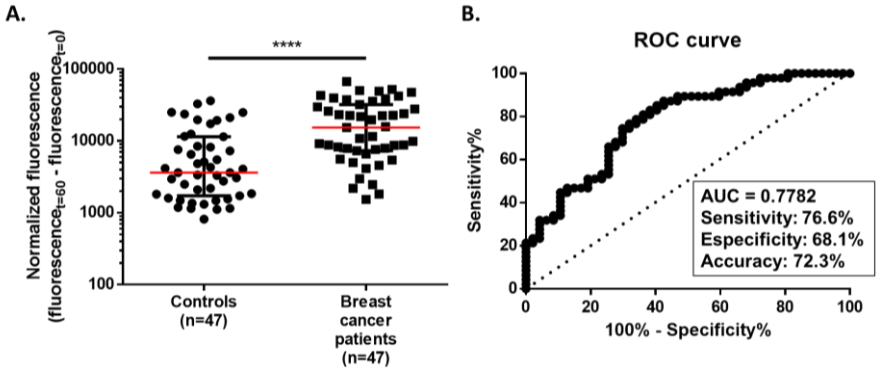

Figure 6. Measurement of miR-99a-5p in human plasma. (A) Expression levels were significantly lower in healthy controls (n = 47) than in breast cancer patients (n = 47). Median (red) ± interquartile range. Mann−Whitney U, ****p < 0.0001. (B) The receiver-operating characteristic (ROC) analysis displays the specificity and sensitivity of the developed sensor to discriminate between breast cancer patients and healthy controls.

To assess the value of the nanosensor as a diagnostic tool, we computed the ROC curve to discriminate between BC patients and controls. Our system was able to discriminate between BC patients and healthy controls with an AUC of 0.78 (95% CI: 0.69−0.87; $p < 0.0001$) (**Figure 6B**). The optimal cut-off value was identified based on the highest value obtained in the ROC curve analysis according to Youden's J index. Using the optimal cut-off value (7285), 76.6% sensitivity, 68.09% specificity, and 72.34% accuracy were obtained. These data provide evidence that the tested nanomaterial may be considered a diagnostic tool for BC.

We also hypothesized that our system could be useful to diagnose BC at a very early stage (stages I and II). We compared the levels of delivered rhodamine B in healthy controls (n = 47) and early-stage BC patients (n = 34).

Our data revealed that the levels of released fluorophore were higher in early-stage BC patients (median, 95% CI: 9315, 7318−23955) than in controls (median, 95% CI: 3629, 2487− 6495) (**Figure 7A**). Moreover, our biosensor was able to discriminate between controls and early-stage BC patients with 85.29% sensitivity, 57.45% specificity, and 69.14% accuracy, using the optimal cut-off value of 4426. Nonetheless, AUC was 0.7516 (95% CI: 0.65−0.86; $p < 0.0001$) for this set of samples (**Figure 7B**).

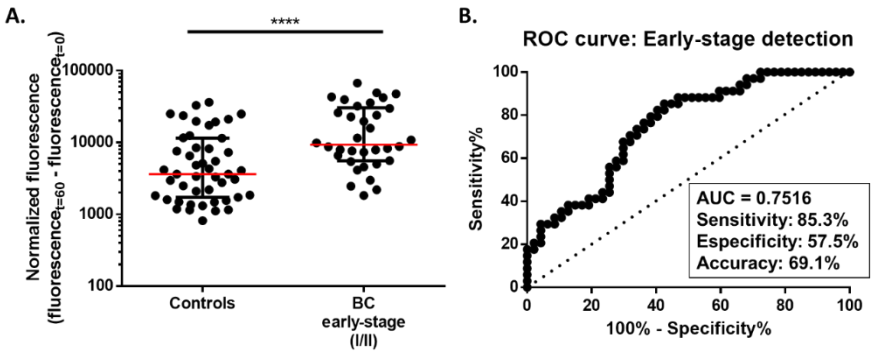

Figure 7. (A) Expression of miR-99a-5p in healthy controls (n = 47) and early-stage breast cancer (BC) (n = 34). Median (red) ± interquartile range. Mann−Whitney U, ****p < 0.0001. (B) The receiver-operating characteristic (ROC) analysis displays the specificity and sensitivity of the developed sensor to discriminate between early-stage BC patients and healthy controls.

Other miRNA biosensors based on different strategies have been developed previously by other authors. Some examples include the system developed by Qavi *et al*., which was based on photonic resonance in silicon microrings, giving a LOD near 1 nM [29], or the silver nanocluster DNA probe designed by Yang *et al*. with a LOD of 20 nM [30]. There is a vast list of different approaches to detect circulating microRNAs, and some authors also

validated those systems in biological samples; e.g., Hizir *et al*. used nanographene oxide for the detection of miR-21 and miR-141 in serum (LOD 1.2 nM) and confirmed their detection in some serum samples [31]. Li *et al*. used hairpin probe-based rolling circle amplification to detect serum miR-486-5p for the diagnosis of lung cancer and tested the system in six healthy controls and six lung cancer patients [32]. Remarkably, to the best of our knowledge, our system is the first NAA-based system designed for the detection of miRNAs. We provided evidence that the proposed method can be performed by directly applying the serum without the involvement of either miRNA isolation or retrotranscription processes, thus being faster than conventional techniques. Moreover, this is a more cost-efficient system, and the required equipment is considered to be of low cost. Besides, the presented strategy may be extrapolated for the development of gated and nanostructured devices for the detection of other circulating miRNAs. Our results evidenced the potential of the presented biosensor for the detection of circulating miR-99a-5p as a tool to diagnose early BC. Detection of BC at the initial stages may improve the overall survival. At this moment, mammography screening programs are proven to decrease disease-specific mortality as well as the occurrence of advanced disease. Furthermore, early detection can result in less radical treatment and less expensive with substantial resource savings.

5.5 Conclusions

Overall, our work provides a promising strategy to diagnose BC patients based on the miR-99a-5p detection in plasma. We have developed a biosensor supported on mesoporous NAA films loaded with rhodamine B and capped with an oligonucleotide that is able to specifically recognize miR-

99a-5p. Our results demonstrated that the developed system was able to quantify miRNA expression with high sensitivity and specificity. Moreover, the designed material is simple to prepare, easy to handle, and can discriminate between healthy controls and BC patients, even at very early stages, providing high accuracy. We validated the developed gated system in a total of 94 plasma samples, and our results confirmed that our system might hold great potential for further applications in the clinical diagnosis of BC.

Author Contributions

‡These authors contributed equally. Conceptualization, I.G-C., L.P. and S.S-F; methodology, L.P. and S.S-F.; validation, I.G-C., L.P. and S.S-F.; formal analysis, I.G-C., L.P. and S.S-F.; investigation, I.G.C., L.P., S.S-F., S.S, B.O and B.B.; resources, JM.C., P.E, R.M-M; writing—original draft preparation, I.G-C., L.P.; writing—review and editing, S.S-F, A.L, JM.C., P.E and R.M-M.; supervision, S.S-F.; project administration, S.S-F, JM.C, P.E and R.M-M; funding acquisition, R.M-M. *Corresponding author. All authors have read and agreed to the published version of the manuscript. All authors have given approval to the final version of the manuscript.

Funding Sources

This work was supported by, CIBERONC (CB16/12/00481), CIBER-BBN (CB07/01/2012), Spanish Government PI18/01219 (ISCIII), project RTI2018-100910-B-C41 (MCUI/AEI/FEDER, UE) and the Generalitat Valenciana (PROMETEO/2018/024) for support. IG-C was funded by Generalitat Valenciana (ACIF/2016/030). LP was funded by Ministerio de Econo-mia, Industria y Competitividad (FPI grant). SS was funded by Instituto de Salud

Carlos III and the European Social Fund for the financial support “Sara Borrell” (CD16/000237). JMC was funded by Sociedad Española de Oncología Médica (Río Hortega-SEOM).

Acknowledgments

The authors would like to thank the INCLIVA Biobank (PT17/0015/0049; B.000768 ISCIII) and the Valencian Biobanking Network integrated into the Spanish National Biobanks Network for providing the human biological samples. We would also like to thank the plasma donors and the nursing staff that accepted to participate in this study.

5.6 Bibliography

1. Bray, F.; Ferlay, J.; Soerjomataram, I.; Siegel, R.L.; Torre, L.A.; Jemal, A. Global Cancer Statistics 2018: GLOBOCAN Estimates of Incidence and Mortality Worldwide for 36 Cancers in 185 Countries. *CA. Cancer J. Clin.* 2018;68(6):394–424.
2. Miller, K.D.; Nogueira, L.; Mariotto, A.B.; Rowland, J.H.; Yabroff, K.R.; Alfano, C.M.; Jemal, A.; Kramer, J.L.; Siegel, R.L. Cancer Treatment and Survivorship Statistics, 2019. *CA. Cancer J. Clin.* 2019;69(5):363–385.
3. Jafari, S.H.; Saadatpour, Z.; Salmaninejad, A.; Momeni, F.; Mokhtari, M.; Nahand, J.S.; Rahmati, M.; Mirzaei, H.; Kianmehr, M. Breast Cancer Diagnosis: Imaging Techniques and Biochemical Markers. *J. Cell. Physiol.* 2018;233(7):5200–5213.
4. Kashyap, D.; Kaur, H. Cell-Free MiRNAs as Non-Invasive Biomarkers in Breast Cancer: Significance in Early Diagnosis and Metastasis Prediction. *Life Sci.* 2020;246:117417.
5. Ng, E.K.O.; Li, R.; Shin, V.Y.; Jin, H.C.; Leung, C.P.H.; Ma, E.S.K.; Pang, R.; Chua, D.; Chu, K.M.; Law, W.L.; et al. Circulating MicroRNAs as Specific Biomarkers for Breast Cancer Detection. *PLoS One.* 2013;8(1):e53141.

6. Loh, H.Y.; Norman, B.P.; Lai, K.S.; Rahman, N.M.A.N.A.; Alitheen, N.B.M.; Osman, M.A. The Regulatory Role of MicroRNAs in Breast Cancer. *Int. J. Mol. Sci.* 2019;20(19):4940.

7. Cortez, M.A.; Welsh, J.J.; Calin, G.A. Circulating MicroRNAs as Noninvasive Biomarkers in Breast Cancer. *Recent Results Cancer Res.* 2012;195:151–161.

8. Bartel, D.P. MicroRNAs: Genomics, Biogenesis, Mechanism, and Function. *Cell.* 2004;116(2):281–297.

9. Kent, O.A.; Mendell, J.T. A Small Piece in the Cancer Puzzle : MicroRNAs as Tumor Suppressors and Oncogenes. *Oncogene.* 2006;25:6188–6196.

10. Tormo, E.; Ballester, S.; Adam-Artigues, A.; Burgués, O.; Alonso, E.; Bermejo, B.; Menéndez, S.; Zazo, S.; Madoz-Gúrpide, J.; Rovira, A.; et al. The MiRNA-449 Family Mediates Doxorubicin Resistance in Triple-Negative Breast Cancer by Regulating Cell Cycle Factors. *Sci. Rep.* 2019;9(1):5316.

11. Tormo, E.; Adam-Artigues, A.; Ballester, S.; Pineda, B.; Zazo, S.; González-Alonso, P.; Albanell, J.; Rovira, A.; Rojo, F.; Lluch, A.; et al. The Role of MiR-26a and MiR-30b in HER2+ Breast Cancer Trastuzumab Resistance and Regulation of the CCNE2 Gene. *Sci. Rep.* 2017;7:41309.

12. van Schooneveld, E.; Wouters, M.C.A.; Van der Auwera, I.; Peeters, D.J.; Wildiers, H.; Van Dam, P.A.; Vergote, I.; Vermeulen, P.B.; Dirix, L.Y.; Van Laere, S.J. Expression Profiling of Cancerous and Normal Breast Tissues Identifies MicroRNAs That Are Differentially Expressed in Serum from Patients with (Metastatic) Breast Cancer and Healthy Volunteers. *Breast Cancer Res.* 2012;14(1):R34.

13. Matamala, N.; Vargas, M.T.; González-Cámpora, R.; Miñambres, R.; Arias, J.; Menéndez, P.; Andrés-León, E.; Mez-López, G.G.; Yanowsky, K.; Calvete-Candenas, J.; et al. Tumor MicroRNA Expression Profiling Identifies Circulating MicroRNAs for Early Breast Cancer Detection. *Clin. Chem.* 2015;61(8):1098–1106.

14. Chen, Y.; Santos, A.; Wang, Y.; Kumeria, T.; Li, J.; Wang, C.; Losic, D. Biomimetic Nanoporous Anodic Alumina Distributed Bragg Reflectors in the Form of Films and Microsized Particles for Sensing Applications. *ACS Appl. Mater. Interfaces.* 2015;7(35):19816–19824.

15. Hofmann, C.; Duerkop, A.; Baeumner, A.J. Nanocontainers for Analytical Applications. *Angew. chem.* 2019;58(37):12840–12860.

16. García-Fernández, A.; Aznar, E.; Martínez-Máñez, R.; Sancenón, F. New Advances in In Vivo Applications of Gated Mesoporous Silica as Drug Delivery Nanocarriers. *Small.* 2020;16:1902242.

17. Aznar, E.; Oroval, M.; Pascual, L.; Murguía, J.R.; Martínez-Máñez, R.; Sancenón, F. Gated Materials for On-Command Release of Guest Molecules. *Chem. Rev.* 2016;116(2):561–718.

18. Ribes, À.; Xifré-Pérez, E.; Aznar, E.; Sancenón, F.; Pardo, T.; Marsal, L.F.; Martínez-Máñez, R. Molecular Gated Nanoporous Anodic Alumina for the Detection of Cocaine. *Sci. Rep.* 2016;6(August):1–9.

19. Ribes, À.; Aznar, E.; Santiago-Felipe, S.; Xifre-Perez, E.; Tormo-Mas, M. ángeles; Pemán, J.; Marsal, L.F.; Martínez-Mántild;ez, R. Selective and Sensitive Probe Based in Oligonucleotide-Capped Nanoporous Alumina for the Rapid Screening of Infection Produced by Candida Albicans. *ACS Sensors.* 2019;4(5):1291–1298.

20. Pla, L.; Santiago-Felipe, S.; Tormo-Más, M.Á.; Pemán, J.; Sancenón, F.; Aznar, E.; Martínez-Máñez, R. Aptamer-Capped Nanoporous Anodic Alumina for Staphylococcus Aureus Detection. *Sensors Actuators B Chem.* 2020;128281.

21. Pla, L.; Xifré-Pérez, E.; Ribes, À.; Aznar, E.; Marcos, M.D.; Marsal, L.F.; Martínez-Máñez, R.; Sancenón, F. A Mycoplasma Genomic DNA Probe Using Gated Nanoporous Anodic Alumina. *ChemPlusChem.* 2017;82(3):337–341.

22. Sancenon, F.; Pascual, L.; Oroval, M.; Aznar, E.; Martínez-Máñez, R. Gated Silica Mesoporous Materials in Sensing Applications. *ChemistryOpen.* 2015;4(4):418–437.

23. Llopis-Lorente, A.; Lozano-Torres, B.; Bernardos, A.; Martínez-Máñez, R.; Sancenón, F. Mesoporous Silica Materials for Controlled Delivery Based on Enzymes. *J. Mater. Chem. B.* 2017;5(17):3069–3083.

24. Oroval, M.; Coll, C.; Bernardos, A.; Marcos, M.D.; Martínez-Máñez, R.; Shchukin, D.G.; Sancenón, F. Selective Fluorogenic Sensing of As(III) Using Aptamer-Capped Nanomaterials. *ACS Appl. Mater. Interfaces.* 2017;9(13):11332–11336.

25. Garrido-Cano, I.; Constâncio, V.; Adam-Artigues, A.; Lameirinhas, A.; Simón, S.; Ortega, B.; Martínez, M.T.; Hernando, C.; Bermejo, B.; Lluch, A.; et al. Circulating MiR-99a-5p Expression in Plasma: A Potential Biomarker for Early Diagnosis of Breast Cancer. *Int. J. Mol. Sci.* 2020;21(19):7427.

26. Youden, W.J. Index for Rating Diagnostic Tests. *Cancer.* 1950;3(1):32–35.

27. Schisterman, E.F.; Perkins, N.J.; Liu, A.; Bondell, H. Optimal Cut-Point and Its Corresponding Youden Index to Discriminate Individuals Using Pooled Blood Samples. *Epidemiology.* 2005;16(1):73–81.

28. Ragan, C.; Zuker, M.; Ragan, M.A. Quantitative Prediction of MiRNA-MRNA Interaction Based on Equilibrium Concentrations. *PLoS Comput. Biol.* 2011;7(2):e1001090.

29. Qavi, A.J.; Bailey, R.C. Multiplexed Detection and Label-Free Quantitation of MicroRNAs Using Arrays of Silicon Photonic Microring Resonators. *Angew. Chemie - Int. Ed.* 2010;49(27):4608–4611.

30. Yang, S.W.; Vosch, T. Rapid Detection of MicroRNA by a Silver Nanocluster DNA Probe. *Anal. Chem.* 2011;83(18):6935–6939.

31. Hizir, M.S.; Balcioglu, M.; Rana, M.; Robertson, N.M.; Yigit, M. V. Simultaneous Detection of Circulating OncomiRs from Body Fluids for Prostate Cancer Staging Using Nanographene Oxide. *ACS Appl. Mater. Interfaces.* 2014;6(17):14772–14778.

32. Li, Y.; Liang, L.; Zhang, C.Y. Isothermally Sensitive Detection of Serum Circulating Mirnas for Lung Cancer Diagnosis. Anal. Chem. 2013;85(23):11174–11179.

CHAPTER 6 |

General discussion

Despite the advances in BC clinical management, it is the first cause of cancer-related death in women. Targeted therapies notably improved the outcome of patients, but cytotoxic chemotherapy remains one of the most important therapeutic strategies for BC. Therefore, chemoresistance is a major problem. In this context, microRNAs have elicited great interest as these molecules regulate numerous targets involved in drug resistance. Based on the above, in the third chapter, miRNAs expression profiles of breast cancer cells sensitive and resistant to doxorubicin were compared. miR-99a-5p was identified as the most downregulated miRNA in resistant cells and we found a positive correlation between expression levels of miR-99a-5p and DRFS and OS in BC patients, suggesting the implication of the miRNA in treatment response. Moreover, we revealed in our study a new mechanism of action of miR-99a-5p, which increases sensitivity to doxorubicin through directly targeting COX-2, which induces the downregulation of the drug transporter ABCG2 that has been previously related to drug resistance. However, the use of miRNAs for treatment applications presents important limitations. Thus as free molecules, miRNAs have a short half-life in circulation, low efficiency to reach the tumor, and are poorly internalized by cells. To overcome these limitations, nanoparticles have attracted great interest as vectors for the delivery of nucleic acids. Therefore, we focused in chapter three on the use of MSNs as carriers of miR-99a-5p due to their unique properties such as high stability, biocompatibility, and the possibility to be functionalized to obtain systems able to release their content on-demand. Besides, MSNs can passively target tumors through the EPR effect, but it is also possible to include specific ligands that allow an active targeting of tumors in order to enhance the therapeutic effect while minimizing undesired side effects of drugs. Therefore, nanodevices based on

MSNs for combined delivery of miR-99a-5p and doxorubicin were designed. Hyaluronic acid and PEI were included to target the CD44 receptor overexpressed in BCSCs, and to ensure the lysosomal escape required for the proper function of the miRNA, respectively. The *in vitro* experiments confirmed the targeting to CD44, as well as the delivery of encapsulated drugs once nanoparticles are internalized. The efficacy of the developed therapeutic strategy to reduce tumor growth, cellular proliferation, and doxorubicin-induced cardiotoxicity was confirmed in an *in vivo* model of BC. The nanodevice allows controlled delivery of the cargos in tumors, thus avoiding adverse effects and ensuring the efficient transport of the miRNA. The developed nanosystem is a suitable tool to deliver efficiently miRNAs alone or in combination with other therapeutic agents *in vivo*.

From another point of view, early detection of BC is also crucial to improve the outcomes of patients. Consequently, based on the findings detailed above, the potential of miR-99a-5p as a biomarker was assessed in chapter four. First, the expression levels in the breast tissue of BC patients and healthy volunteers were determined. In agreement with previous results, miR-99a-5p was found downregulated in patients' samples. In order to determine the potential of miR-99a-5p as a minimally invasive biomarker, circulating levels of the miRNA were determined in plasma in two independent cohorts of BC patients and healthy controls. miR-99a-5p was found upregulated in plasma from BC patients when compared to controls in both cohorts. Although there were opposite trends in tissue and plasma samples, the obtained results evidenced the potential of plasma miR-99a-5p as a diagnostic biomarker BC even at early stages. Besides, there are several hypotheses that could explain the opposite expression patterns between

tissue and plasma, such as an active secretion from tumor cells, or the passive release of miRNAs from apoptotic or necrotic cells that are abundant in tumors, but further studies are still needed to better understand the origin of circulating miRNAs.

Following with the interest in the use of circulating miR-99a-5p as a potential diagnostic biomarker of BC, a NAA-based biosensor for the detection of miR-99a-5p was developed in chapter five. The system was demonstrated to be useful to detect miR-99a-5p with high sensitivity and specificity, and allowed to discriminate between healthy controls and BC patients even at very early stages providing high accuracy. Nowadays, techniques such as qRT-PCR, northern blot, sequencing, and microarrays are employed to determine circulating levels of miRNAs. Our work provides a new strategy that is faster, cost-effective, and less complex than actual methods. The biosensor developed holds great potential for the diagnosis of BC and could be useful as a model to detect other circulating miRNAs.

In summary, the results obtained in this thesis aim to translate molecular findings into clinical tools that may have a positive impact on breast cancer patients. Despite the use of nanomaterials in clinical practice is still limited, our results reinforce the applicability of nanomaterials for clinical management (for both detection and treatment). It is expected that these or similar nanomaterials will reach the bedside to improve the outcomes of cancer patients in the near future. Nevertheless, more validations studies are needed to additionally determine potential side effects and to ensure safety issues. Hopefully, the results derived from this PhD thesis will give rise to new research projects applicable not only to BC but also to other diseases.

CHAPTER 7 |

Conclusions

1. miR-99a-5p is downregulated in doxorubicin-resistant breast cancer cells and associates with better clinical prognosis in breast cancer patients.
2. Upregulation of miR-99a-5p increases sensitivity to doxorubicin through directly targeting COX-2, which induces the downregulation of ABCG2.
3. MSNs-based nanodevices for combined delivery of miR-99a-5p and doxorubicin are efficient to reduce tumor growth, cellular proliferation, and doxorubicin-induced cardiotoxicity in a murine orthotopic breast cancer model.
4. miR-99a-5p is an efficient diagnostic biomarker of breast cancer in tissue and plasma samples.
5. The developed nanoporous anodic alumina based-biosensor for the detection of miR-99a-5p in plasma is a sensitive, specific, and efficient tool for breast cancer diagnosis even at early stages.